AFRL-RY-WP-TR-2022-0056

THE DESIGN, FABRICATION, AND APPLICATIONS OF 3D PRINTED CAPACATROS (Preprint)

Brandon Andrew Phillips
University of Dayton

MARCH 2022
Final Report

STINFO COPY

AIR FORCE RESEARCH LABORATORY
SENSORS DIRECTORATE
WRIGHT-PATTERSON AIR FORCE BASE, OH 45433-7320
AIR FORCE MATERIEL COMMAND
UNITED STATES AIR FORCE

REPORT DOCUMENTATION PAGE

PLEASE DO NOT RETURN YOUR FORM TO THE ABOVE ORGANIZATION.

1. REPORT DATE	2. REPORT TYPE	3. DATES COVERED	
		START DATE	END DATE
March 2022	Thesis Preprint	11 January 2022	11 January 2022

4. TITLE AND SUBTITLE

THE DESIGN, FABRICATION, AND APPLICATIONS OF 3D PRINTED CAPACATROS (Preprint)

5a. CONTRACT NUMBER	5b. GRANT NUMBER	5c. PROGRAM ELEMENT NUMBER
N/A	N/A	N/A
5d. PROJECT NUMBER	**5e. TASK NUMBER**	**5f. WORK UNIT NUMBER**
N/A	N/A	N/A

6. AUTHOR(S)

Brandon Andrew Phillips

7. PERFORMING ORGANIZATION NAME(S) AND ADDRESS(ES)

University of Dayton
300 College Park
Dayton, OH 45469

8. PERFORMING ORGANIZATION REPORT NUMBER

9. SPONSORING/MONITORING AGENCY NAME(S) AND ADDRESS(ES)	10. SPONSOR/MONITOR'S ACRONYM(S)	11. SPONSOR/MONITOR'SREPORT NUMBER(S)
Air Force Research Laboratory Sensors Directorate Wright-Patterson Air Force Base, OH 45433-7320 Air Force Materiel Command United States Air Forces	AFRL/RYDI	AFRL-RY-WP-TR-2022-0056

12. DISTRIBUTION/AVAILABILITY STATEMENT

DISTRIBUTION STATEMENT A. Approved for public release; distribution is unlimited.

13. SUPPLEMENTARY NOTES

PAO case number AFRL-2022-0102, Clearance Date 11 January 2022. To be Submitted to The School of Engineering of the University of Dayton in partial fulfillment of the requirements for the degree of Master of Science in Electrical Engineering. This work was funded in whole or in part by Department of the Air Force contract. The U.S. Government has for itself and others acting on its behalf an unlimited, paid-up, nonexclusive, irrevocable worldwide license to use, modify, reproduce, release, perform, display, or disclose the work by or on behalf of the U. S. Government. Report contains color.

14. ABSTRACT

Over the past decade, Additive Manufacturing (AM) has advanced as a novel manufacturing technique used to develop rapid prototypes for custom and complex geometries and multilayer devices in many different industries. Recent advances in emerging technologies such as dual-extrusion FDM 3D printing, along with newly introduced conductive polymer filament materials, have created the potential to use low-cost, readily available 3D printing methods to fabricate electronic devices on-the-fly in remote environments. This study explores the use of Protopasta conductive filament and various common thermoplastic filament materials (PLA, PP, PC) and an Ultimaker s5 Pro dual-extrusion FDM printer with high-resolution 0.25 mm diameter print nozzles to fabricate a fully-fused 50mm x 50mm plate capacitor. A maximum capacitance of 328 pF was measured with a 0.25 mm thick dielectric layer of extruded PLA. This demonstrates a 215% increase in capacitance when compared to measurements for a similar plate capacitor constructed with wrought sheet aluminum (104 pF) using the same dielectric material and thickness. An EVAL-AD5940 impedance analyzer was used to measure the capacitance with PLA, PP, and PC dielectric layers at 1 kHz, 5 kHz, 7.5 kHz, and 10 kHz. From these measurements, the dielectric constant of each material was calculated for a dielectric thickness of 1 mm, as follows: 1 kHz (PLA: 3.00, PP: 2.96, PC: 3.00); 5 kHz (PLA: 2.83, PP: 2.74, PC: 2.83); 7.5 kHz (PLA: 2.82, PP: 2.76, PC: 2.910; and 10 kHz (PLA: 2.39, PP: 2.63, PC: is 2.99).

15. SUBJECT TERMS

3D printing, capacitor(s)

16. SECURITY CLASSIFICATION OF:			17. LIMITATION OF ABSTRACT	18. NUMBER OF PAGES
a. REPORT	b. ABSTRACT	C. THIS PAGE		
Unclassified	Unclassified	Unclassified	SAR	138

19a. NAME OF RESPONSIBLE PERSON	19b. PHONE NUMBER *(Include area code)*
Carrie Bartsch	

THE DESIGN, FABRICATION, AND APPLICATIONS OF 3D PRINTED CAPACITORS

Thesis

Submitted to

The School of Engineering of the

UNIVERSITY OF DAYTON

In Partial Fulfillment of the Requirements for

The Degree of

Master of Science in Electrical Engineering

By

Brandon Andrew Phillips, B.S

Dayton, Ohio

December 2021

THE DESIGN, FABRICATION, AND APPLICATIONS OF

3D PRINTED CAPACITORS

Name: Phillips, Brandon Andrew

APPROVED BY:

Amy T. Neidhard-Doll, Ph.D., P.E. Advisory Committee Chairperson Associate Professor Electrical and Computer Engineering University of Dayton	Carrie M. Bartsch, Ph.D. Committee Member Senior Research Electronics Engineer Air Force Research Laboratory
Guru Subramanyam, Ph.D. Committee Member Professor Electrical and Computer Engineering University of Dayton	Vamsy P. Chodavarapu, Ph.D., P.E. Committee Member Professor Electrical and Computer Engineering University of Dayton
Robert J. Wilkens, Ph.D., P.E. Associate Dean for Research and Innovation Professor School of Engineering	Margaret F. Pinnell, Ph.D. Interim Dean Professor School of Engineering

ABSTRACT

THE DESIGN, FABRICATION, AND APPLICATIONS OF

3D PRINTED CAPACITORS

Name: Phillips, Brandon Andrew
University of Dayton

Advisor: Dr. Amy Neidhard-Doll

Over the past decade, Additive Manufacturing (AM) has advanced as a novel manufacturing technique used to develop rapid prototypes for custom and complex geometries and multilayer devices in many different industries. Recent advances in emerging technologies such as dual-extrusion FDM 3D printing, along with newly introduced conductive polymer filament materials, have created the potential to use low-cost, readily available 3D printing methods to fabricate electronic devices on-the-fly in remote environments.

This study explores the use of Protopasta conductive filament and various common thermoplastic filament materials (PLA, PP, PC) and an Ultimaker s5 Pro dual-extrusion FDM printer with high-resolution 0.25 mm diameter print nozzles to fabricate a fully-fused 50mm x 50mm plate capacitor. A maximum capacitance of 328 pF was measured with a 0.25 mm thick dielectric layer of extruded PLA. This demonstrates a 215% increase in capacitance when compared to measurements for a similar plate capacitor constructed with wrought sheet aluminum (104 pF) using the same dielectric material and thickness. An

EVAL-AD5940 impedance analyzer was used to measure the capacitance with PLA, PP, and PC dielectric layers at 1 kHz, 5 kHz, 7.5 kHz, and 10 kHz. From these measurements, the dielectric constant of each material was calculated for a dielectric thickness of 1 mm, as follows: 1 kHz (PLA: 3.00, PP: 2.96, PC: 3.00); 5 kHz (PLA: 2.83, PP: 2.74, PC: 2.83); 7.5 kHz (PLA: 2.82, PP: 2.76, PC: 2.910; and 10 kHz (PLA: 2.39, PP: 2.63, PC: is 2.99).

Dedicated to my family, friends, and those who helped me get this far, and those who will help me in the future.

ACKNOWLEDGMENTS

I would like to thank both of my Master's Thesis advisors; my University of Dayton advisor, Dr. Amy Neidhard-Doll, and Dr. Carrie Bartsch, my Air Force Base advisor, both of whom were instrumental, not only in my research but helped me to become a better person in general. I would also like to acknowledge the Air Force Research Laboratory at Wright Patterson Air Force Base and the University of Dayton for providing funding to support my research through a DAGSI Fellowship. I would also like to thank Dr. Guru Subramanyam for providing guidance with my research and for serving on my Master's Thesis Committee, along with Dr. Vamsy Chodavarapu. In addition, I would like to thank Mr. Birhanu Alemayehu for his assistance with setting up test instrumentation for initial impedance measurements.

TABLE OF CONTENTS

LIST OF FIGURES

LIST OF TABLES

LIST OF ABBREVIATIONS AND NOTATIONS

ABS	Acrylonitrile Butadiene Styrene
AL	Aluminum
AM	Additive Manufacturing
FDM	Fused Deposition Modeling
SLA	Stereolithography
SLM	Selective Laser Melting
PLA	Polylactic Acid
PP	Polypropylene
PCB	Printed Circuit Board
PC	Polycarbonate
UV	Ultraviolet
PET	Polyethylene Terephthalate
E	Energy Density
EDLC	Electric Double Layer Capacitor
ε	Dielectric Permittivity
C	Capacitance
A	Area of Electrodes
k	Dielectric Constant
X_c	Capacitive Reactance
f	Frequency (Hz)
d	Distance between electrodes plates

Q	Charge
V	Voltage

CHAPTER 1

INTRODUCTION

1.1 Overview and Benefits of Additive Manufacturing in the Modern World

Over the past decade, Additive Manufacturing (AM) has advanced as a novel manufacturing technique used to develop rapid prototypes for custom and complex geometries and multilayer devices in many different industries. In the field of electrical engineering, AM methods have emerged as an innovative technology for the fabrication of electronic components, such as capacitors, resistors, and antennas. One of the advantages of 3D printed electronics is that prototype devices can be designed and fabricated in-house, on-demand, and with very low production costs. This dramatically improves the progression of new technology by reducing the time in between design iterations and the overall logistics of the supply chain with industry.

Within the field of Additive Manufacturing, there are many different types of 3D printing techniques, which have developed over time for specific applications. For this thesis, several common 3D printing techniques were explored for potential use in the design and fabrication of a low-cost, on-the-fly 3D printed capacitor using equipment that was readily available in-house at the University of Dayton, including Fused Deposition Modeling (FDM), Selective Laser Melting (SLM), and Stereolithography (SLA).

1.2 Problem Statement

While existing non-traditional fabrication methods have employed aerosol jet printing and inkjet deposition for a myriad of electronics applications such as capacitors,

antennas, sensors, and thin-film transistors [1], these techniques have historically been very expensive due to the high cost of the printer and materials. In addition, the conductive inks dispensed through these methods are difficult to formulate in-house, costly to purchase, exhibit a relatively short shelf-life, and may require cleanroom facilities and safety precautions due to potential toxicity to humans. In addition, while the print resolution for components printed using these methods is typically high, the maximum print height and ability to print complex geometries is limited when compared to other additive manufacturing methods.

Recent advances in emerging technologies such as dual-extrusion FDM 3D printing, along with newly introduced conductive polymer filament materials, have created the potential to use low-cost, readily available 3D printing methods to fabricate electronic devices on-the-fly in remote environments. For example, this approach could be implemented in different emergency situations the military faces during wartime or rescue missions to fabricate replacement electrical components or portable power supplies *in theater*. Since FDM 3D printing technology does not require a large footprint and utilizes rugged materials with a long shelf-life that can withstand extreme environments, this 3D printing technique has game-changing potential for remote military operations. The use of low-cost, in-house additive manufacturing techniques also provides an inexpensive and novel method to incorporate proprietary security markers within the build job that can be used to ensure an encrypted supply chain for trusted electronics. In addition, this approach provides a potential solution for the severe recent global IC chip shortage that has resulted from newly enforced international trade tariffs and taxes and the lack of manufacturing resources (including the availability of personnel) secondary to the coronavirus epidemic.

1.3 Research Objectives

In response to the opportunities previously outlined for the potential use of emerging technology in the design and fabrication of a low-cost, on-the-fly 3D printed capacitor, the following research objectives were identified:

1. To determine the feasibility of new-to-market FDM conductive filament materials that can be implemented for the electrodes of a 3D printed plate capacitor;
2. To determine the dielectric constant of common FDM polymer filament materials (PLA, PP, PC) that can be implemented for the insulator layer of a 3D printed plate capacitor;
3. To determine the feasibility of dual-extrusion FDM as a low-cost, on-the-fly 3D printing technique for manufacturing fully fused plate capacitors through the analysis of measured capacitance from this novel approach versus other fabrication methods established in the literature.

CHAPTER 2

BACKGROUND

The chapter provides an overview of the different technologies, materials, and terminology associated with various common 3D printing techniques that were explored for potential use in the design and fabrication of a low-cost, on-the-fly 3D printed capacitor, including Fused Deposition Modeling (FDM), Selective Laser Melting (SLM), and Stereolithography (SLA). The advantages and disadvantages of these 3D printing technologies were compared to existing non-traditional 2.5D electronics fabrication methods such as aerosol printing and inkjet deposition. In addition, this chapter investigates the various types of capacitors and materials commonly used to manufacture them and a review of the current state-of-the-art for 3D printed capacitors, as published in the literature.

2.1 Additive Manufacturing

Additive manufacturing has played a vital role in the future of engineering technology over the past 40 years, especially for rapid prototyping applications [2]. The terms ‘AM’ and ‘3D printing’ are often used interchangeably, especially in the industrial setting. One of the first methods of 3D printing was developed in the 1980s and was similar to the modern-day Fused Deposition Modeling (FDM) system wherein parts were created using subsequent “multiple layers of thermoplastics” [3] rather than traditional cast molds. Within the past decade, multiple types of 3D printing systems have been developed, and

more recently, the unique field of '3D printed electronics' has emerged as an innovative fabrication method for electronic circuit components within the field of electrical engineering.

3D printing techniques are commonly implemented for rapid prototyping since the successive design iterations can be processed quickly and inexpensively, resulting in improved efficiency in the supply chain. This rapid turnaround during the design process can also result in improved performance specifications and faster time-to-market when commercializing a product. 3D printing techniques also provide a cost-effective mechanism for custom and complex geometries and micro-structured multilayer electronic devices such as Printed Circuit Boards (PCBs), capacitors, transistors, and antennas.

2.1.1 Fused Deposition Modeling

Fused Deposition Modeling (FDM) is one of the most readily available and affordable types of 3D printing currently used in the industry. FDM is an additive process in which a thermoplastic polymer filament material is dispensed through a heated nozzle that melts the material and deposits it onto a build plate, layer-by-layer, corresponding to a CAD model in three-dimensional space. The availability of a wide variety of inexpensive polymer and composite filament materials that can be 3D printed with a relatively standard set of build parameters has contributed to the popularity of FDM. Two popular FDM filament materials frequently implemented for strength and durability in finished parts are PLA (Polythetic Acid) and Acrylonitrile Butadiene Styrene (ABS). Over the past several years, many new types of filaments have entered the market, most recently including conductive filaments (e.g., Electrifi, Black Magic 3D, and Protopasta) that consist of

polymer materials such as PLA infused with nanoparticle conductors such as copper, silver, and carbon. These newly available materials combined with current advances in simultaneous dual-extrusion FDM nozzle technology have afforded new and emerging frontiers in 3D printed electronics.

The general process of FDM printing includes approximately five steps, as illustrated in Figure 1 below. The first step (1) entails the use of slicer software that translates measurements from a corresponding CAD drawing into x, y, and z coordinates, which maps out a path for the movement of the print nozzle [4]. The next step (2) involves the insertion of the chosen filament, which is fed through a heated nozzle and melts as it is deposited as a thin layer onto the build plate below (3). As each successive layer of melted filament material is deposited, it bonds to the layer beneath it (4). Finally, as the material cools, it hardens and takes the shape of the finished part (5), which corresponds to the dimensions and geometry specified in the accompanying CAD model. Between layers, the build plate adjusts in height, and the process repeats itself.

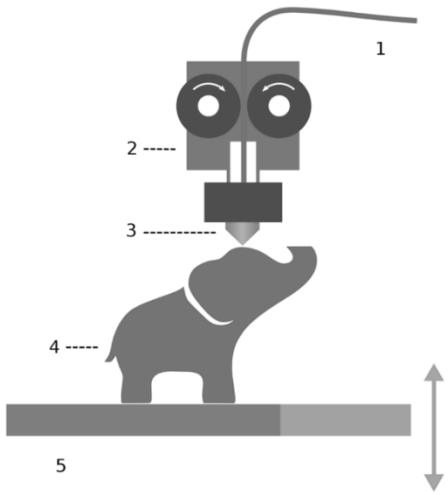

Figure 1: FDM 3D Printer Diagram [5]

2.1.2 Selective Laser Melting

Selective Laser Melting (SLM) is a relatively new additive manufacturing technique used to build custom metal parts from metallic powder, which is deposited and melted, layer-by-layer, using a high power laser that moves in three-dimensional space in accordance with a CAD model, as illustrated in Figure 2. As subsequent layers of powder are deposited and melted, a thin film layer of new material fuses with previous layers. As the melted material cools, it hardens and assumes its final shape corresponding to the original CAD model. Between layers, the build plate is adjusted in height and recoated with powder.

SLM has many applications in commercial industries such as aerospace and medicine [6]. This method is advantageous for high-risk applications such as replacement aircraft parts or orthopedic implants, which require high yield strength and durability under extreme environmental conditions. Common materials used in SLM include powder formulations made from metals such as aluminum, stainless steel, and titanium (and their alloys). As described in the literature, SLM has been used for 3D printed electronics such as heat sinks for microprocessors, airfoils, and heat exchange devices [7].

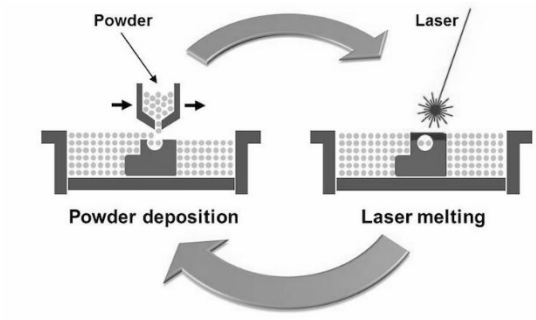

Figure 2: SLM Printing Process [8]

2.1.3 Stereolithography

Stereolithography (SLA) is a type of 3D printing that belongs to the category of additive manufacturing techniques known as "vat photopolymerization" [9]. This technique involves the use of a liquid photosensitive polymer resin, which is solidified through exposure to a light-emitting device (typically a low-power laser) that moves in three-dimensional space corresponding to a CAD model. One common configuration shown in Figure 3 entails a laser that shines through the bottom of a transparent tank containing the resin. As the laser activates specific locations in the resin that correspond to the CAD model, the resin begins to solidify. At the same time, a build platform above moves the solidified resin part upward out of the resin. This process is repeated layer-by-layer. In comparison to other types of polymer printing such as FDM, SLA can provide a sharper, higher resolution part with a smoother finish. However, resin-based printing requires a post-processing wash to remove sticky residue from the finished part, and in some cases (depending upon the type of resin used), an additional curing process under ultraviolet light.

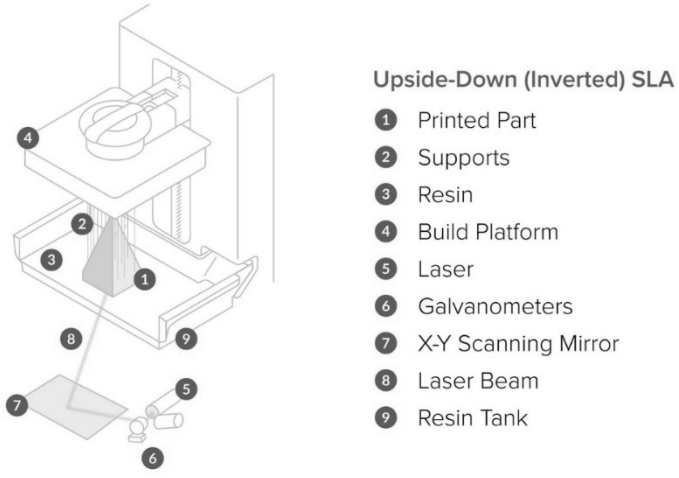

Figure 3: Schematic Diagram of SLA 3D Printer [10]

2.1.4 Comparison of 3D Printing Technologies for Electronics Applications

The design and fabrication of low-cost, on-the-fly 3D printed electronics is an emerging technology. This section provides an analysis of the advantages and disadvantages of FDM, SLM, and SLA 3D printing technologies in comparison with existing non-traditional 2.5D electronics fabrication methods such as aerosol printing and inkjet deposition.

As illustrated in Table 1, in comparison to other methods, FDM technology is the simplest to operate with little to no requirements for pre-or post-processing, has minimal space, clean-room, and safety requirements, is very inexpensive to use and is highly versatile with respect to availability of diverse polymer filament materials that could be implemented as a dielectric. However, FDM is limited in print resolution, as well as the number of commercially available filaments with conductive properties that could be used for electronics applications such as circuit traces or more advanced devices such as a capacitor.

Table 1: Comparison of 3D Printing Techniques

Type	Pros	Cons	Resolution	Companies	Example Devices
Inkjet Printing (2.5D)	Simultaneous printing with multiple materials Multiple Print Heads Resolution finishing steps are not required Printing over a large area	Limited material selection Lower mechanical strength and fracture easier Expensive	20-25 microns [11]	nScrypt, Dynamism Nano Dimension DragonFly	PCB's [11] Full-scale fabrication of complex electronics [11]
Aerosol Printing (2.5D)	Low-temperature processing [12] High-quality thin deposits 10 nm [12] Print resolution is almost 2-4 times higher than inkjet [12] Clog Resistant Nozzle	Expensive Limited material selection	5-10 microns [12]	Optomec	Flexible Displays Sensors, resistors, solder-free electronics Printed Antennae [13]
SLA (3D)	High-quality 3D models Fast process Strong pattern [14]	Expensive materials Materials have a shelf life Cleanup	30-140 microns [15]	Formlabs	Capacitors [16]
FDM (3D)	Inexpensive [17] Different variety of materials Compact design Ease of operations	Rough surface finish Nozzle clogging Layer adhesion problem	20-300 microns [18]	Ultimaker, Fusion 3	Resistors, inductors, capacitors [19]

2.2 Capacitor Background

The capacitor, which stores potential energy within an electric field, is one of the most straightforward and most essential components of an electrical circuit. The first capacitor, coined "The Leydon Jar," was invented by Pieter van Musschenbroek in 1746

and consisted of a glass jar insulated both internally and externally by a thin metal foil to store the electrical charge [20]. The general design of a capacitor consists of an arrangement of two conductive plates that are separated by a non-conductive material that is either an insulator (e.g., air, paper, glass) or a semi-conductor (dielectric). The conductors have equal but opposite charges that create a potential energy gradient (voltage) when charged by an external source. During the discharge cycle of a capacitor, energy stored in a capacitor is released to power other connected circuit elements and devices.

Capacitors are commonly in filters for electrical noise and ripple voltage in a plethora of applications including RF transmission lines, audio processing, radio reception, and power circuit conditioning [21]. The capacitor encompasses a relatively design, which allows for a smaller footprint when compared to other energy storage devices, such as batteries. Additive manufacturing provides a mechanism to further miniaturize capacitors through custom three-dimensional geometries that are not possible through other fabrication methods. Some specific types of capacitors include electrolytic capacitors, mica capacitors, paper capacitors, film capacitors, non-polarized capacitors, and ceramic capacitors.

Beginning in 1993, the capacitor worldwide market value was approximately $12.3 billion US dollars and has grown each year exponentially by 20% [22]. According to "*The Global Capacitor Market Demand,*" researchers anticipate "an increase at an extensive rate" [23] due to an increase in the production of electric vehicles. These figures indicate substantial market potential for emerging technology and novel methods such as low-cost, on-the-fly additive manufacturing for the fabrication and optimization of capacitors.

2.2.1 Parallel-Plate Capacitor

A parallel plate capacitor consists of two conductive plates of surface area *A*, which are separated by a dielectric material of thickness *d*, as show in Figure 4. The dielectric material in the capacitor impedes the flow of current between the electrodes. When a voltage is applied across a capacitor, an electric field develops across the dialectic layer, which results in the accumulation of an equal, but opposite charge *Q* on each plate of the capacitor, as shown in Figure 5 below. As indicated in Equation (1) [24], the capacitance *C* is directly dependent upon the area of the conductive plates and the thickness of the dielectric, where ε_0 is the dielectric permittivity of free space which is equal to 8.85*10^{-12} Farads/meter.

$$C = \frac{\varepsilon_0 * A}{d} \tag{1}$$

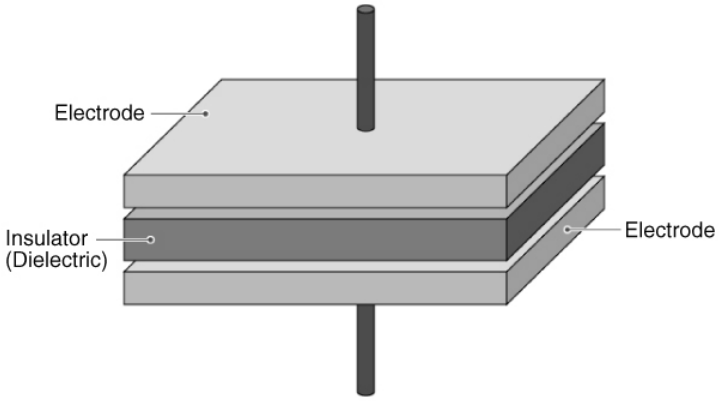

Figure 4: Capacitor Components [24]

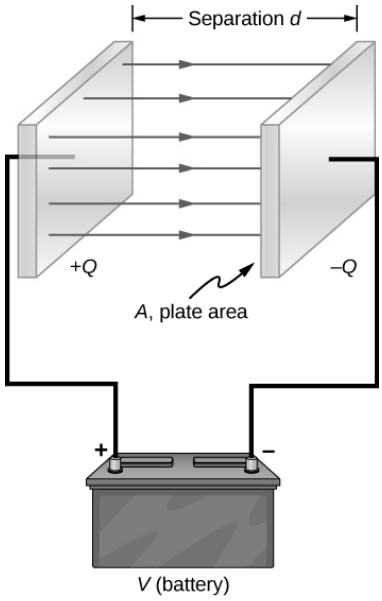

Figure 5: Parallel Plate Capacitor [25]

Over time, a voltage potential develops across the plates of the capacitor due to the accumulation of charges. Once connected to an external circuit, current from the capacitor discharges quickly along this potential energy gradient [26].

2.2.2 Electrolytic Capacitor

The electrolytic capacitor is a polarized capacitor that uses an electrolyte material as the dielectric. The electrolyte is typically a gel or liquid containing a high concentration of ions, which enables the device to achieve much higher levels of capacitance. These capacitors are utilized when large capacitance is required and implemented as the principal component in multiple power supplies. Figure 6 displays a visual diagram of the electrolytic capacitor.

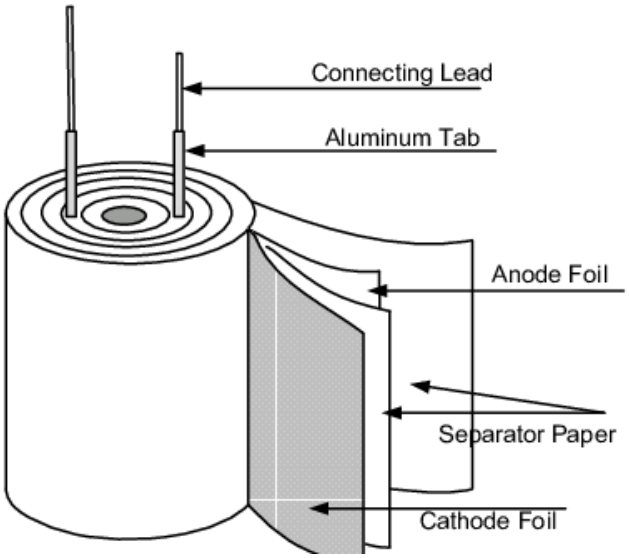

Figure 6: Electrolytic Capacitor [27]

Some of the main disadvantages for this capacitor design include different degradations based on, “thermal overstress and accelerated aging stress periods” [27].

2.2.3 Mica Capacitor

Mica capacitors fall into two groups; clamped and silver mica capacitors. The dielectrics of these capacitors consists of natural minerals. The clamped mica capacitors are typically seen as inferior to the silver capacitors because of their “precision, stability, and low losses” [28]. The silver mica capacitor consists of a sandwich layer of mica sheets that are coated in metal and encased in an epoxy outer layer. These capacitors have low loss capacitance at high frequencies. The characteristics of these capacitors allow for “stability in chemical, electrical, and mechanical applications” [28].

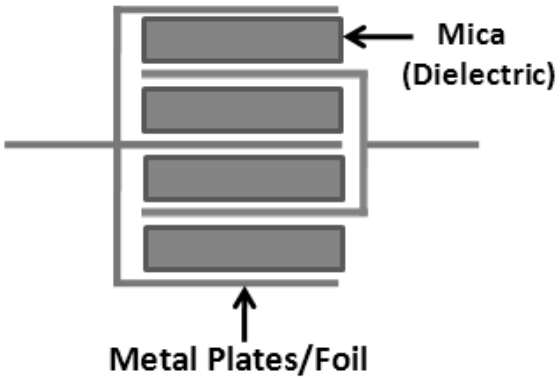

Figure 7: Mica Capacitor [28]

2.2.4 Film Capacitor

A film capacitor utilizes a thin layer of plastic for the dielectric material. This thin layer allows for several different applications due to their "low inductance, stability, and relatively low cost" [29]. There are various types of film capacitors. For example, epoxy cases are capacitors encased in a plastic material with an epoxy filling. 'Wrap-and-fill' designs consist of an oval and round plastic tape to tightly wrap the capacitor and polar ends filled with an epoxy adhesive. Film capacitors are classified into two categories: wound and stacked. A wound film capacitor reaches much higher voltage levels due to their multiple wound layer construction that is continuous rather than the abrupt edges of the stacked capacitor. Contrary to the wound capacitors, the stacked capacitors are used in higher frequency applications. The multiple layer design or "stacked" allow for a greater size efficiency while it minimizes the safety margins which provide higher capacitance per unit volume [30].

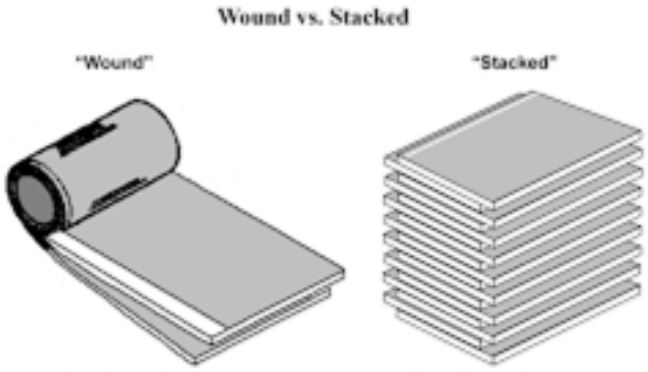

Figure 8: Wound Capacitor vs Stacked [31]

2.2.5 Paper Capacitor

This type of capacitor consists of paper as the dielectric medium between aluminum sheets. Currently, there are other materials as well that are used in place of the paper between the two plates; for example, plastics are implemented as dielectric insulators. In these capacitors, the paper is covered in wax or soaked with oil, and then these capacitors are fixed in terms of the amount of electric charge and capacitance value. One of the main disadvantages of this capacitor is that the moisture from the air could be absorbed into the paper which causes the device's dielectric resistance to decrease [32].

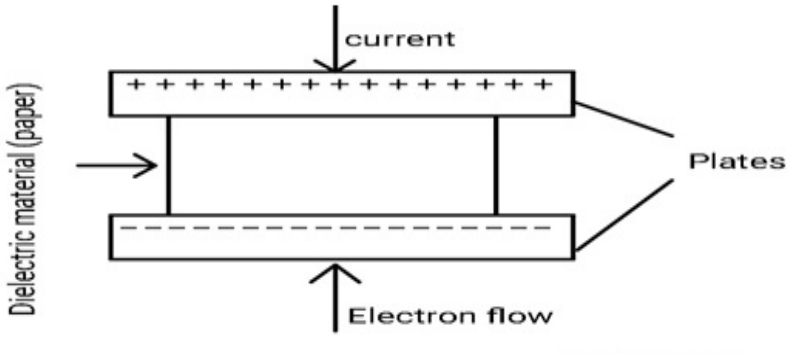

Figure 9: Paper Capacitor Construction [32]

2.2.6 Non-Polarized Capacitors

The benefits of this type of the capacitor allow for a bidirectional voltage source to flow through rather than a normal unidirectional voltage. Common materials in the construction include aluminum electrolytic capacitors and tantalum electrolytic capacitors. Some of the disadvantages include the inability to scale up for large power sources due to the small size. Benefits of this design include more materials that can be used for dielectrics rather than a single direction polarized capacitor [33].

2.2.7 Ceramic Capacitor

The ceramic capacitor implements a ceramic layer for the dielectric material. The ceramic material is reported as being one of the first dielectric materials used in the production of capacitors [34]. The most common type of ceramic capacitor is a multilayer chip capacitor (MLCC). Other shapes of this capacitor include tubular and barrier capacitors "which are obsolete today due to their size, parasitic effects, and the electrical characteristics [35]." Larger ceramic capacitors, produced as power ceramic capacitors, are designed to withstand higher voltages, providing exceptionally accurate results. The capacitance values are stable [35] with reference to the applied frequency, voltage, and temperature.

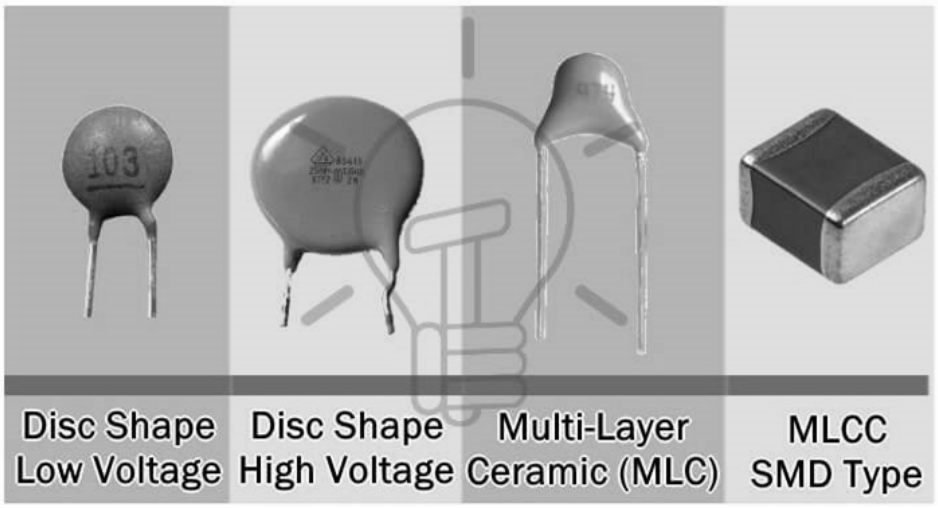

Figure 10: Different types of Ceramic Capacitors [36]

2.2.8 Supercapacitors

Another type of capacitor, the supercapacitor, is gaining in popularity for use in electric vehicles due to its ability to store large amounts of energy for a short period of time. The supercapacitor, also called the "ultra-capacitor," stores energy in an electrostatic field between two separate electrodes. The ultra-capacitor yields a lower energy density than that of the conventional Li-ion batteries. As the schematic layout in Figure 10 exhibits, this electrical double layer capacitor (EDLC) consists of two or more electrodes, a separator, and unlike the conventional capacitor: a liquid electrolyte [38].

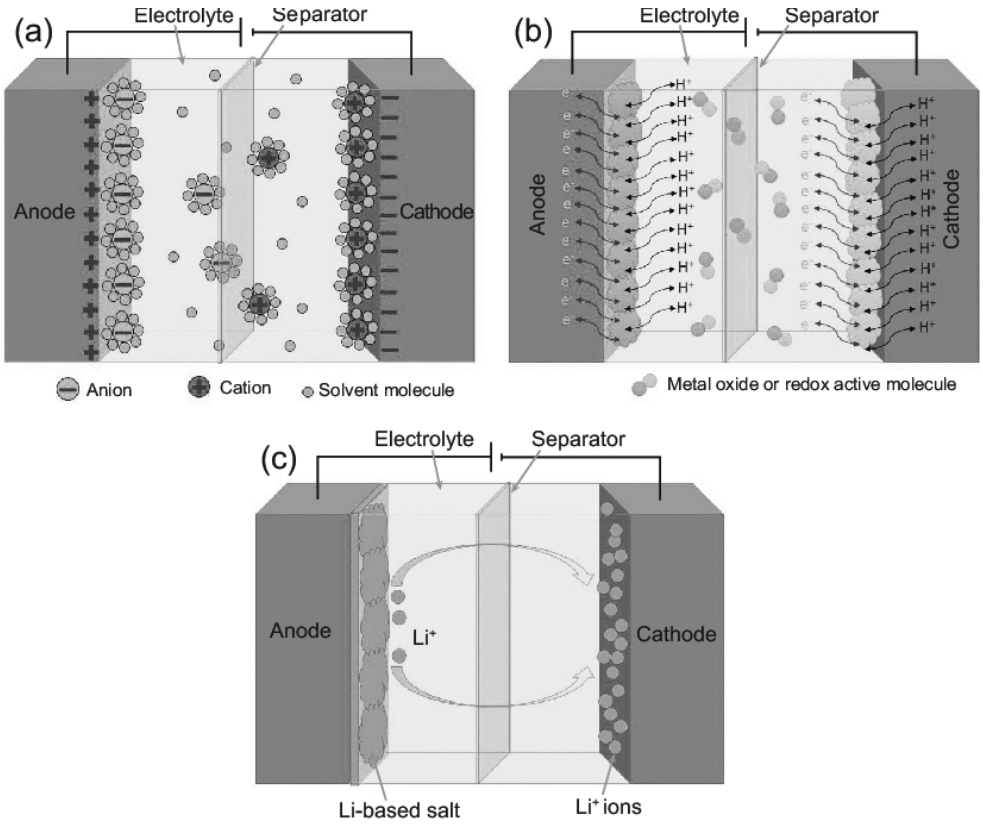

Figure 11:(a) Electrical Double Layer Capacitor (EDLC), (b) Pseudocapacitor (PC) and (c) Hybrid Supercapacitor (HSC) [39]

2.3 3D-Printed Capacitors Research

Over the past decade, a number of 3D printing technologies such as FDM have emerged as low-cost, on-the-fly methods to create rapid prototypes for custom and complex geometries and multilayer devices. The majority of research in the field of additive manufacturing focuses primarily on the material properties and the mechanical properties of the filaments on the market. However, the electrical properties are often omitted or inaccessible due to limited documentation. The following section provides an overview of the state-of-the-art in 3D printed electronics, as surveyed from a review of the literature. New-to-market conductive and dielectric thermoplastic filaments for FDM printers have

afforded new opportunities in the field of 3D printed electronics. In [40], the authors explore the benefits of dual extrusion technology for certain electrical components, but finds that cross-contamination is the most prevalent impediment for this fabrication method. As a potential solution, reverting to a single extrusion process wherein the nozzle is cleaned after each use is explored. However, it appears that this may result in longer production times and less than optimal performance specifications in the finished part.

In [41], the authors discuss several applications for 3D printed electronics (including conductor traces, an inductor, a capacitor, and a high pass filter) using Electrifi conductive filament and two different types of PLA filament (black pigmented; bronze nanoparticle) as the dielectric material with an open source D-Bot FDM printer. The electrical properties of the printed specimens (resistance, conductance, inductance) were determined and used to calculate the dielectric constant for the PLA composite filaments. One specific problem discussed in the article concerns the thermal expansion of the Electrifi filament when extruded, which can clog the print nozzle.

In [42], the authors explore the use of FDM to 3D print capacitive and resistive transducers. This research concludes that the thermal loading associated with FDM printing modifies the electromechanical properties of the printed part, including the dielectric constant.

In [43], the authors provide an extensive overview of the requirements, process, outcome and future scope of manufacturing electronic components and circuits using conductive metal-polymer filaments and PLA with FDM/FFF printers. This research discusses the fabrication of simple traces implementing the conductive filament, and then describes the methods utilized to measure the conductive traces by attaching a short piece

of melted filament, silver paste or a screw terminal to connect to the multimeter probe to better read the resistance measurements. The study found that single-extrusion techniques are preferred due to the interruption of conductive traces that can occur when dual extrusion methods are employed.

CHAPTER 3

METHODS

To test which dielectric material held the highest capacitance in each model, the dielectric constant for each material was solved for and then calculated using the EVAL device and MATLAB. The dielectric materials implemented included PLA, PP, AND PC. The next objective was to design CAD models for the parallel plate capacitors, which included the dielectric mediums with varying thicknesses (1.5 mm, 1.0 mm, 0.5 mm, and 0.25 mm). The other components of the CAD design consisted of four 50 x 50 mm electrode replicates printed using the conductive filament on the Ultimaker. Each component was created in SolidWorks, and then they were fabricated employing the Ultimaker Cura Slicer software. The final goal of this research was to test each design for highest yielded capacitance and dielectric constants to compare the results from each device and model. This process was then utilized to acquire the highest quality parallel plate capacitor design and components, including the dielectric material.

3.1 Why FDM?

The literature review highlighted that there were several variations of 3D printers and techniques used to fabricate 3D printed electronics. However, FDM was most conducive since it allowed for on-the-fly rapid prototyping and was most cost-efficient compared to the other 3D printing technologies. FDM also allotted for ease of operations as the most user-friendly printer, was highly researched, and encompassed a small footprint. The implications of this emerging technology could be utilized in various

military operations and missions since its small footprint allowed for the ease of mobility. Such a 3D device brought into fruition the printing of replacement components; rescue missions and disaster missions that necessitated replacement parts on-the-fly. The replacement printed components then could be printed with an inexpensive material (Filament). The Ultimaker S5 Pro was the FDM printer of choice, which was described in more detail below in Figure 13. This 3D printer allowed for the use of dual extrusion, which permitted the implementation of conductive and non-conductive filaments to be printed simultaneously.

3.2 Procedures

The procedure section below further explained the different types of materials used in the research and the different devices utilized to attain the collected data.

3.2.1 Plate Electrode Design

This section consisted of the procedural steps for designing the wrought aluminum plate electrode design. The design incorporated the use of 4 wrought cut aluminum plates, which was described below in greater detail.

3.2.2 Wrought Sheet Aluminum

The base model, designed as the control, consisted of 4 wrought cut aluminum plates for the electrodes combined with the 3 different dielectric mediums sandwiched in the middle of the top and bottom plates. The aluminum plates from wrought material were purchased at Home Depot to create the square aluminum sample electrodes, and each piece

was measured to be around 50 x 50 mm. This specific size was selected based on the values found in the literature [44] to measure the dielectric constant for PLA. The major variation that occurred in comparison to the literature and research was that the literature values utilized a 50-diameter circular contact pad in contrast to this research that implemented a 50 x 50 mm square. This thesis research simplified the shape to easily calculate the capacitance of a parallel plate by incorporating a square shape method. Although, some inaccuracies in the aluminum results were attributed to the variation in the actual plate size. Micrometer measurements displayed that the average thickness of the aluminum samples was 0.65 mm. The four aluminum replicates were then cut and divided to attain four samples; Al1, Al2, Al3, and Al4, as displayed below in Figure 12.

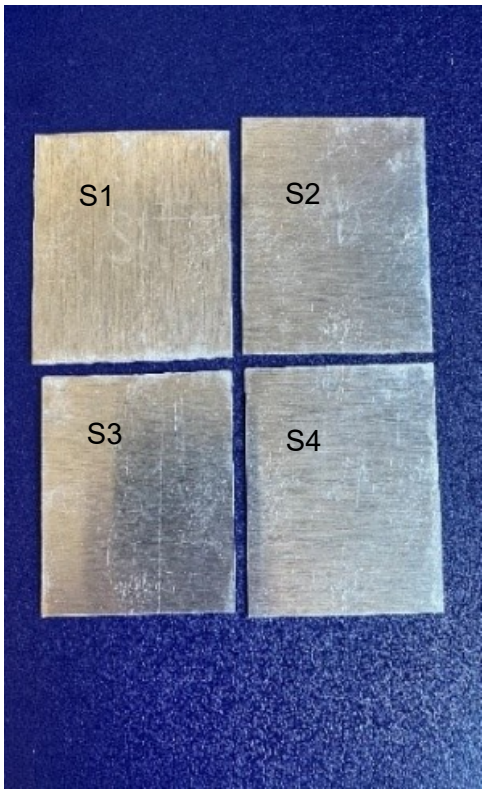

Figure 12: Aluminum Plate Cut (Four Samples 50 x 50 mm)

3.2.3 3D-Printed Electrode

As described in the first part of the Methods Section, the Ultimaker s5 Pro was utilized for this research based on the technology of dual extrusion capability and the accessibility on campus. Some other advantageous components of the Ultimaker S5 Pro were removable print nozzles, temperature controllable print nozzles, a programmable heated bed, and a large build volume. The Ultimaker S5 Pro demonstrated print nozzles of diameters ranging between 0.25 mm, and 0.8 mm. The temperature of the print nozzles was controlled and manipulated by means of the software (Cura). The bed itself was programmed to be heated, as it strengthened the adhesion properties of the filament materials to the bed. That, in turn, ultimately aided with the first layer of the print and created a smoother more uniform print. The Cura Slicer Software provided the user with default printing settings that were previously tested on other makes and models. The printing settings were further modified based on nozzle size, support material, and other printing properties. Another benefit of technology, the build volume, “was considerably larger for an FDM printer, that ranged from around 330 x 240 x 300 mm” [44]. The setup and operation of the machine was user friendly, with a vast online community of user forums for technical support.

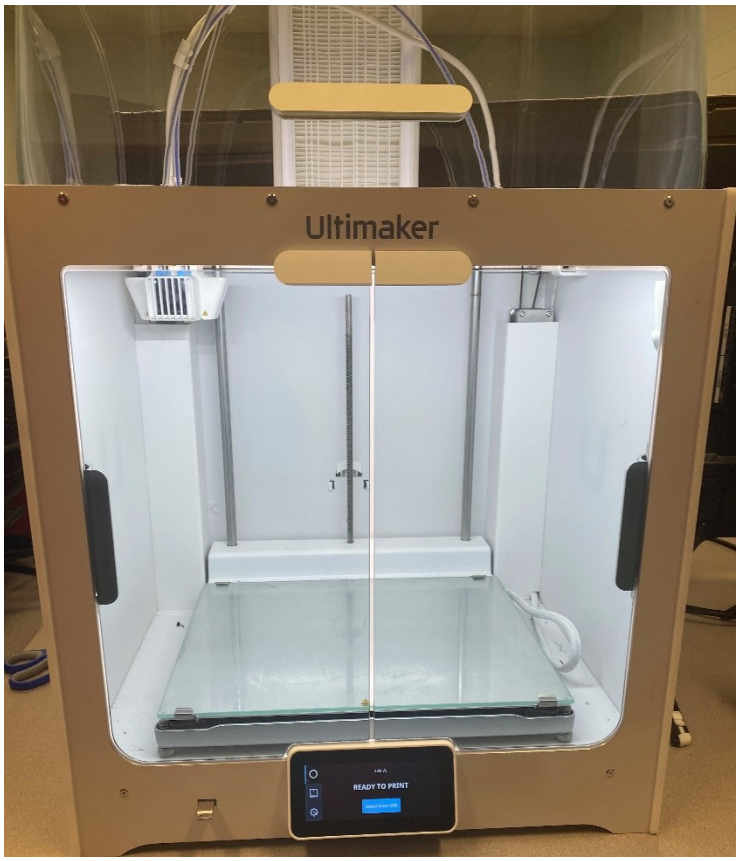

Figure 13: Ultimaker S5 Pro

3.3 Conductive FDM Filament

One possible solution to the Electrifi filament clogging issue concerned the implementation of a separate nozzle specifically for this filament. However, it was found that the Electrifi filament was not relevant to the project due to its complex printing. When the nozzle temperature was increased, then it simultaneously decreased the resistance of the printed object. Another type of filament with copper particles was printed as a proof of this concept. This material, 3D Copper, an antibacterial filament, was measured to have zero resistance due to its low copper additive components.

The following table depicted the different types of conductive and insulating/dielectric filaments utilized for this research. Table 2 presented the other filaments that were incorporated and their desirable characteristics and attributes. The two conductive filaments utilized in the experiment were Protopasta and Electrifi. The diameters measured were based on the Ultimaker printer filament diameter at 2.85 mm.

Table 2: Conductive Filament Data Sheet [46-47]

Name	Information	Tech Specs
Electrifi	Non- hazardous metal-polymer composite World's most conductive filament Stored in a dry environment	Nozzle Temperatures between [°C] 130-160 Recommend printing speed: 10-30 mm/s Resistivity 0.006 Ω cm
Protopasta Conductive PLA	Heat treatable PLA w/ high temp resistance, PLA compound of NatureWorks 4043D PLA	Nozzle Temperature [°C] 206 Printing Speed: 25-45 mm/s Bed Temp (if available, is not required): 50° C Resistance of a 10cm length of 2.85mm filament: 800-1200ohm

3.3.1 Protopasta Material Properties

Protopasta was the conductive filament that was ultimately fabricated for both electrodes of the sandwich model and the fully printed model. In the data table illustrated below, the filament was conductive, with a resistance of approximately 800-1200 ohm-cm for the 2.85 mm filament used [47]. This material was comprised of an amorphous fused carbon called carbon black, which provided its electrical properties.

Table 3: Protopasta Material Properties (Modified from Resource) [47]

Properties	Value/ Description
Base Material	Heat treatable PLA w/high temp resistance
Characteristics	Low odor, non-toxic, renewably sourced
Molecular structure	Amorphous or partially crystalline (Amorphous as printed, part crystalline when heat-treated) (Melting resets crystalline structure to amorphous state)
Additives	Minimal color added

The electrical conductivity of aluminum was then examined based on values displayed in the literature and compared to the above conductive filament Protopasta. This comparison was displayed below in Table 4. The calculation of resistivity of the Protopasta filament was displayed below. Resistivity constant ρ of the filament, was measured in ohms per cm, the length of the filament was L in cm, d was the diameter of the filament in $cm^{2,}$ and R was the resistance in ohms [46].

$$R = \frac{\rho L}{\pi\left(\frac{d}{2}\right)^2} \tag{2}$$

$$\rho = R * \frac{\pi\left(\frac{d}{2}\right)^2}{L}$$

$$\rho = 800 * \frac{\pi\left(\frac{0.285}{2}\right)^2}{10}$$

$$\rho = 5.10\ Ohms$$

A sample of a Protopasta filament measuring 10 cm long, with a resistance of 800-1200 ohm [47] based on the above calculation resistivity is ρ= 5.10-7.66 Ohms.

Table 4: Aluminum Material Resistivity vs Protopasta

Material	Resistivity (ohms per cm)
Aluminum	2.65×10^{-8} [45]
Protopasta	5.10 – 7.66

This table above exhibits that the aluminum plate material yielded a higher conductivity than the Protopasta conductive filament.

3.3.2 Printer Settings for Protopasta

The default printer settings implemented for the conductive filament in this research were depicted below. These tests incorporated a nozzle size of 0.25 mm, and the infill density was modified from the recommended infill of 20% to 100% to ensure that the material was present during each test procedure.

Table 5: Printer Setting for Protopasta

Layer Height	0.1 mm
Infill Density	100 %
Infill Pattern	Triangles
Printing Temperature	215 ℃
Build Plate Temperature	60℃
Print Speed	55 mm/s

These specifications were documented by Ultimaker as the most conducive printing and testing results. Four samples each of the same thickness (0.65 mm) were printed. The size ranged around 50 x 50 mm for each electrode sample; the final size measurements by the micrometer were displayed in the Results Section of this report.

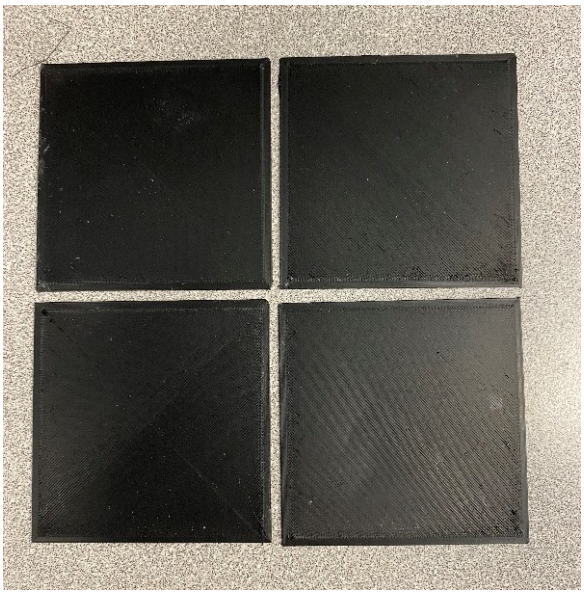

Figure 14: Protopasta 3D Printed Samples (Four Samples 50 x 50 mm)

3.3.3 Conductive Filaments Test Prints

Through the experimentation with the Protopasta filament in 3D printing, it was observed that printing with the glue stick inclusive with the Ultimaker was the most advantageous for sample removal from the print bed. This adhesion problem was then solved as Figure 15 below displayed. The glass printing board was broken down into three separate sections; the first was bare glass, the second being the glue stick, and finally the blue painter's tape section.

Figure 15: Bed Adhesion Test
(Left: Blue Painter's Tape, Middle: Glue, Right: Bare Glass)

As displayed below from the retrieved printed models, the bare glass demonstrated the slightest bend compared to the glue. Contrary to the blue painter's tape, the tape model, when removed from the plate, retained some of the tape along with the final printed model. Therefore, it can be deduced that for the entirety of the remaining samples in this research, the glue was the adhesive material implemented when printing with the Protopasta.

Figure 16: Printed Protopasta Samples on Each Different Adhesion Types (Left: Blue Painters Tape, Middle: Glue, Right: Bare Glass)

3.3.4 3D-Printed Electrodes

The next step in the experimentation process involved testing the different conductive filaments. Considering the two that were primarily tested, Protopasta's Conductive filament and Electrifi Conductive filament, each contained different micro-materials fused with thermoplastics. The Protopasta filament at 10 cm was measured with both probes attached to a multimeter with a measured resistance of approximately 2.557 k Ω, which was around a 2,557 Ω sample. After these samples were tested, then a fully printed conductive parallel plate capacitor was fabricated utilizing the conductive Protopasta PLA implemented for the conductive plates instead of the aluminum plates. These outcomes are explored and displayed in the Results Section below.

Once the prints were completed utilizing the Protopasta filament, the next step was to repeat the process with the Electrifi Filament; the results were compared, plotted, and methodically calculated. The Ultimaker S5 Pro was also incorporated in the experiment due to its dual extrusion capability, which eradicated replacing the filaments to allow the entire print job to be completed in a timelier manner. The nozzle most conducive for the experiment based on the small diameter of the nozzle head measured at the 0.25 mm model size. The nozzle was selected based on the novelty of the nozzle size itself, which yielded a more accurate and higher resolution for each trace than the larger standard nozzle sizes.

The next step was to print with the conductive filament Electrifi. Contrary to the Protopasta filament, the Electifi displayed a lower resistance per centimeter and a higher conductivity as compared to the Protopasta. Unfortunately, Electrifi filament resulted in several clogs due to its soft, supple form, and high-temperature printing. As displayed in below, Electrifi produced a clogged nozzle as the filament was printed.

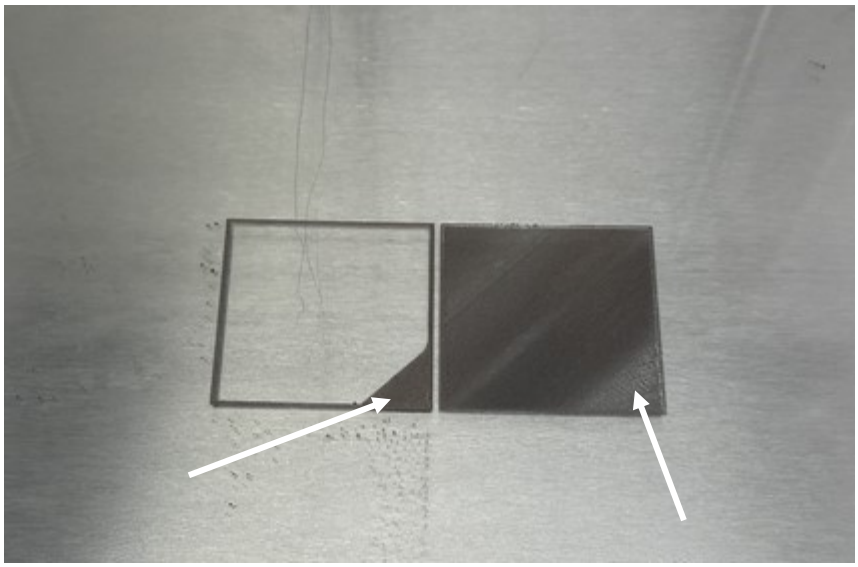

Figure 17: Electrifi Uncompleted Clogged Print

Another erroneous factor noted was that the nozzle size implemented was 0.25 mm rather than the recommended 0.4 mm standard nozzle. The 0.25 mm nozzle was utilized to keep consistent with the previously printed models that incorporated the identical nozzle size. Printing with Electrifi additionally clogged other filaments from being extruded due to the material fusing with the different thermoplastic material, then it hardened and ultimately clogged the nozzles. It was concluded that a different method was imperative to print the conductive filament at that small nozzle size.

From this research conducted above, the Protopasta filament was selected due to the ease of printing with a smaller 0.25 mm size nozzle, and because it demonstrated a lower resistance with greater conductive properties. This material consisted of an amorphous fused carbon called carbon black, which provided its electrical properties. The final four printed replicate electrodes were designed in SolidWorks, then exported to the Cura software where it was spliced, and eventually printed on the Ultimaker S5 Pro.

3.4 Dielectric Layer

This section provided an overview concerning the different materials tested for use in the dielectric layer of the parallel plate capacitor model with the dielectric layer of the capacitor utilized as an insulator. The different dielectric filaments modeled in this section included PLA, PP, and PC.

3.4.1 3D Printed Dielectric Layer

The proceeding step in the process was to incorporate SolidWorks to create a 55 x 55 mm square sample with four different thicknesses (1.5 mm, 1.0 mm, 0.5 mm, 0.25 mm). The model was then designed and implemented in correlation to these specific dimensions since the dielectric measured larger in length than the two conductive electrodes to eradicate the issue of any conductive material touching. These models were then exported to the Cura software where three samples of each thickness, for a total of twelve pieces, were printed on the same build plate. Three different types of FDM filament were then utilized for the Ultimaker; PLA, PP, and PC. An example of the dielectric CAD model was displayed in Figure 18, while Figure 19 displayed the Cura Model setup for the PLA samples.

.

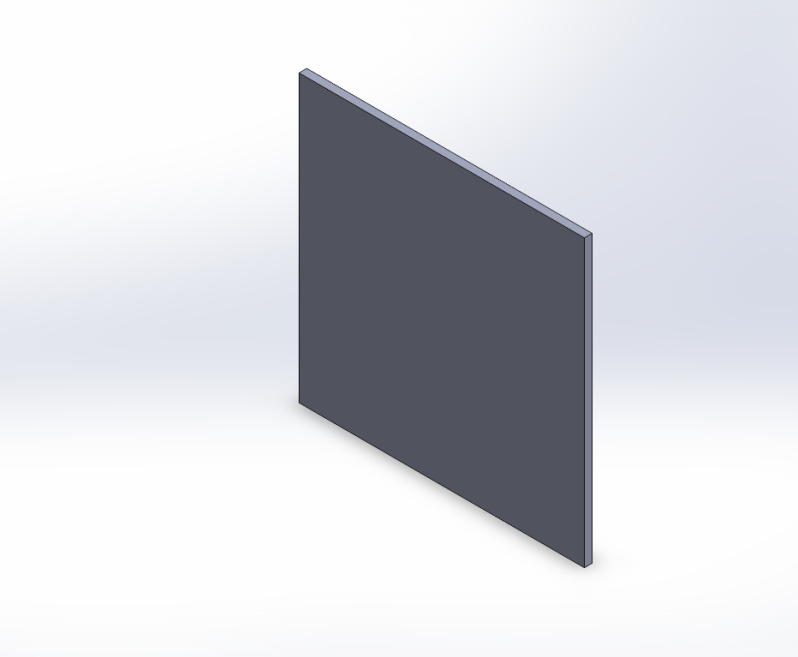

Figure 18: Dielectric CAD Isometric View (55 x 55 mm)

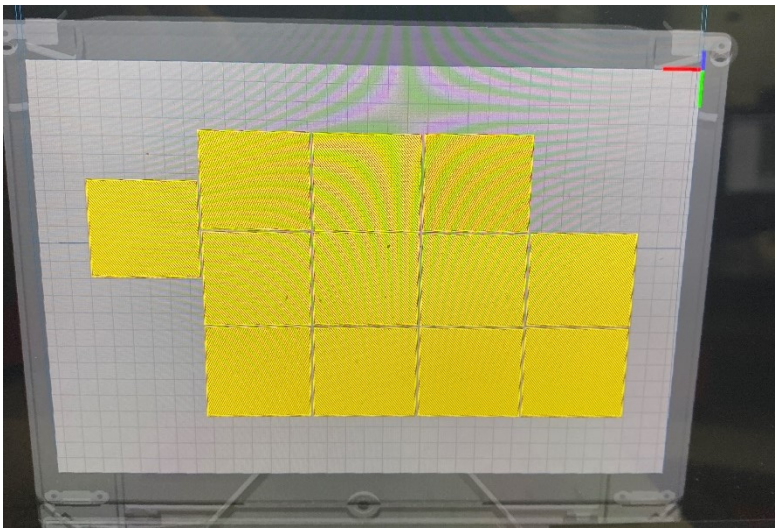

Figure 19: Example Cura Build Plate Design Screen (PLA)

3.4.2 3D Printed Dielectric Layer Settings

Each dielectric material encompassed varied default print settings which were displayed below in Table 6 (PLA), (PP), and (PC). These settings were recommendations provided by Cura software for the purpose of printing dielectric materials.

Table 6: PLA Printing Settings

Properties	PLA	PP	PC
Layer Height	0.1 mm	0.1 mm	0.1 mm
Infill Density	100%	100%	100%
Infill Pattern	Grid	Octagonal	Triangles
Printing Temperature	190 ℃	205 ℃	270℃
Build Plate Temperature	85 ℃	85℃	110℃
Print Speed	30 mm/s	25 mm/s	50 mm/s

The overall time frame consisted of remedying the different printing techniques utilized to create the Polycarbonate, Polypropylene properly, conductive filament samples, fine-tuning the printing methods, and finally testing the capacitors. One issue that occurred while printing PP and PC was the lack of adhesive property that bonded to the build plate. To solve this adhesion issue, the glue was utilized to ensure that the high printing temperatures for these certain filaments did not affect the first print layer adhesion itself. Another clarification that was used to rectify this error was the inclusion of brim material. Once the method was tested and successful, twelve samples that used each type of dielectric filament were printed with three different thicknesses S1, S2, and S3. The thicknesses, as previously described were 1.5 mm, 1.0 mm, 0.5 mm, 0.25 mm. The figure below displayed the completed samples for the PLA filament.

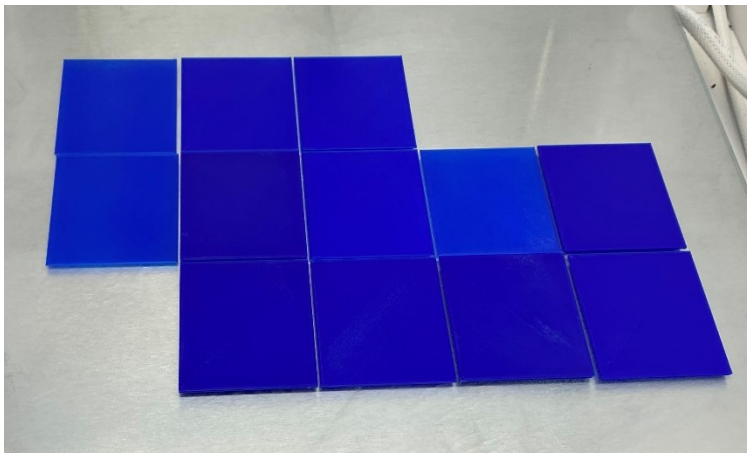

Figure 20: PLA Completed Samples on Ultimaker Build Plate
Volume 330 x 240 x 300 mm

3.5 Price Per Gram

In validation of the third objective of this research to determine if FDM is a low-cost-on-the fly option, the filament on the market was then evaluated and a price per gram was calculated. Each of the filament's prices are displayed below from the manufacturing websites in Table 7.

Table 7: Price of Filament

Filament Name	Cost Per Spool
Ultimaker blue PLA	$49.99 750 g [45]
Protopasta	$49.99 for 500 g [47]

From these values and then utilizing the gram estimator from the Cura software as displayed in Figure 21, the calculation for total cost per gram was evaluated as demonstrated in the sample equation (2) and calculations below.

Figure 21: Material Estimation

$$PPG = TP / TW \text{ [48]} \quad (2)$$

PPG- Price Per Gram

TP=Total Price

TW= Total Weight

$$PPG = \frac{\$49.99}{500g} = 0.1\left(\frac{\$}{g}\right) \textit{ Protopasta}$$

From this calculation, it was determined that the average cost for a fully-fused capacitor containing the volume of 55 x 55 x 1.5 mm was estimated to be $0.51 to fabricate. This price range emphasized that the use of FDM for 3D printed electronics provided a relatively cost-efficient solution as well as a durable option based on the thermoplastic material properties.

3.6 Apparatus

The following section provided an overall review of the various test instrumentation devices being used in this research. These devices included; multimeter, LCR meter and the EVAL AD5940ELCZ device.

3.6.1 Instrumentation

Over the course of this research, several different devices were implemented to measure certain characteristics and properties of the tested capacitors. The first device implemented was a simple multimeter (Model Astro AI DM6000AR). The multimeter device measured the resistance of the tested components by injecting a small current into the circuit, and then measured the voltage drop across the measured points. [49] When very low measurements were taken, then the (REL) button was used to "zero out" the resistance from the probes [50].

The second device utilized was the LCR meter; this model was a (B&K Precision 879B). The implementation of this meter was crucial since the data collected from the multimeter did not allow for varying test frequencies as described below. The LCR device was utilized with both regular probes that were included with the Multimeter meter described above and alligator clips that were provided with the LCR meter. The third device utilized to test the capacitance of the parallel plate capacitor was an EVAL AD5940ELCZ. The EVAL was specifically designed for "high precision analysis of electrochemical cells" [51]. This device was put into place to measure the impedance of the circuit, and then the capacitance was calculated that utilized the provided MATLAB code as displayed in the Appendix A.

3.6.2 Device Setup

This research incorporated two different setup methods as displayed in Figure 22. The first setup involved the use of 2 probes attached to the multimeter. This setup also involved vice clamps as pictured, with two wooden blocks to sandwich the dielectric

medium between the two electrodes. This setup was implemented for the multimeter measurements and the LCR measurements with the probes.

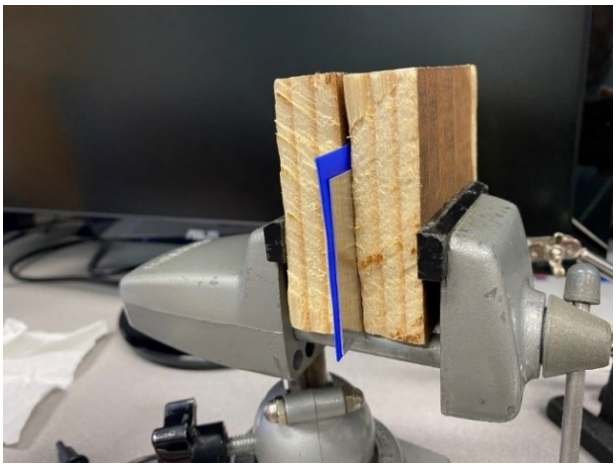

Figure 22: Vice Clamp Setup

The second setup included the alligator clips from the LCR meter as well as the connected alligator clips for the EVAL device. This setup, as pictured below, illustrated the two alligator clips connected to two pieces of paper, with one clip on either side of the electrodes that prevented the capacitor model from short circuiting. LCR with alligator clips and EVAL both utilized the previously described model to gain the attained measurements.

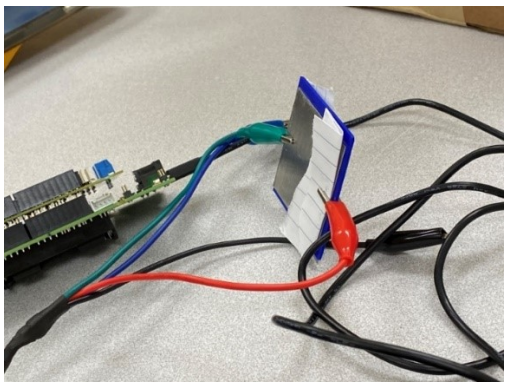

Figure 23: Alligator Clip Setup

Both test methods were repeated numerous times utilizing aluminum plate electrodes with different dielectric materials; Protopasta electrodes with dielectrics and the fully-fused capacitor. This research consisted of testing and printing conductive sandwich models with the Protopasta fused with the top and the bottom conductive plates in the parallel plate design. Then, the PLA was sandwiched in-between the model as the dielectric. A CAD model was developed and then converted to a .stl file that was sliced by the Cura Software for the Ultimaker printer as illustrated in Figure 24 below.

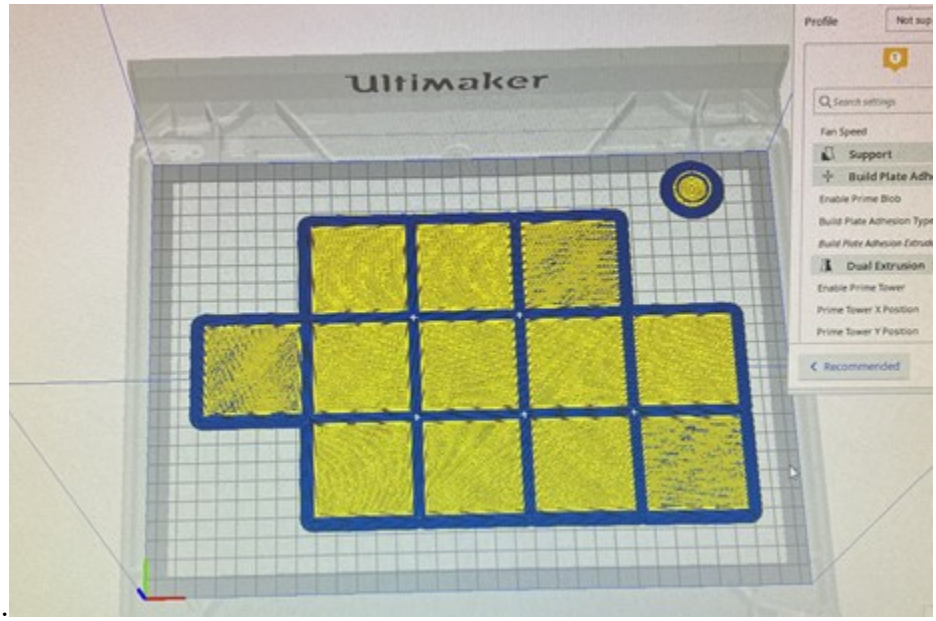

Figure 24: Cura Model of Twelve 3D Printed Fully-Fused Capacitors

The model included twelve different samples, each with varying dielectric thicknesses of the PLA print that utilized the dual extruder. The twelve models demonstrated three samples of each thickness (1.5 mm, 1.0 mm, 0.5 mm, 0.25 mm) while having kept the thickness of the printed conductive plate consistent with the previously used Al plates at 0.65 mm. The estimated timeframe for the first print was around 1 day and 17 hours to print. Unfortunately, the print gridlocked approximately 7 hours into the

print job due to the Protopasta material that became too brittle and developed microfractures in the filament itself as displayed in Figure 25.

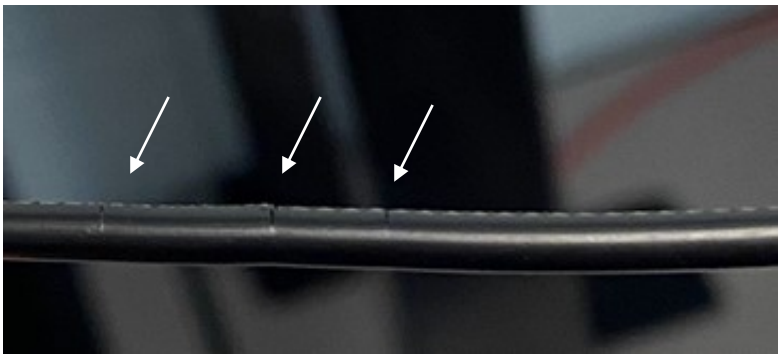

Figure 25: Microfractures in Conductive Protopasta Filament

These micro-fractures caused the material to break in the feeder and then ultimately gave the error of "no filament in the feeder." This issue was rectified by ordering new nozzles and Bowden tubes. It was discovered that the Bowden tubes, if not changed frequently, caused friction within the tubes, resulting in filament breakage.

Throughout the experimental process, it was noted that the 0.25 mm nozzle head clogged and would not allow any filament to be extruded from the nozzle itself. The clogging issue was resolved by the implementation of different methods and various procedures were conducted to unclog the nozzle. The first procedure was called the hot pull method. This method heated up the nozzle to a specific high temperature to melt the extra filament inside. Then, PLA filament was ultimately fed through the nozzle and was pulled to remove any filament build that may have occurred. Once this step was completed, a cold pull method was used, which decreased the nozzle temperature causing the filament

that was placed inside to harden, and then the filament was removed via a pair of tweezers. After a minimum of two cold pulls, the novel nozzle was then conducive for printing.

3.7 Fully Printed Capacitor

Another model designed in SolidWorks and transferred to Cura slicer was the fully printed capacitor model that utilized both extruders. The final dielectric integrated material for this model was the blue PLA that was previously tested. This material was incorporated due to its ease of printing without having a support brim, contrary the PP and PC. Also, when printed on top of the conductive material, the PLA had the best performance since both the PP and PC posed adhesion problems due to their material properties. Additionally, the PLA was also one of the most inexpensive filaments on the market. A total of twelve samples were created from the CAD models and transmitted to the Cura software.

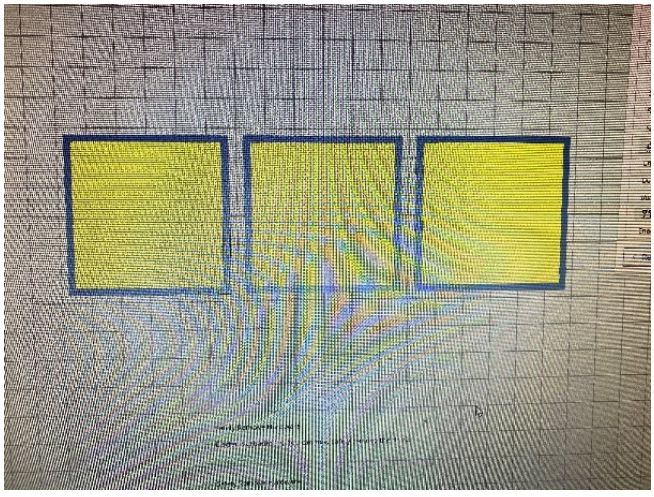

Figure 26: Cura Fully Printed Capacitor Model

Three samples of the same dielectric thickness were printed per build plate, as displayed below in the example figure. The conductive printed electrodes individually ranged around

0.65 mm as printed before. This model was different since each component was printed on top of the other simultaneously, rather than having sandwiched the models together after printing. The following figure displayed the completed fully-fused capacitor model with three samples on a build plate. The tower on the right side was integrated to keep the other print nozzle at a constant temperature so that the filament would not congeal and ultimately clog the nozzle.

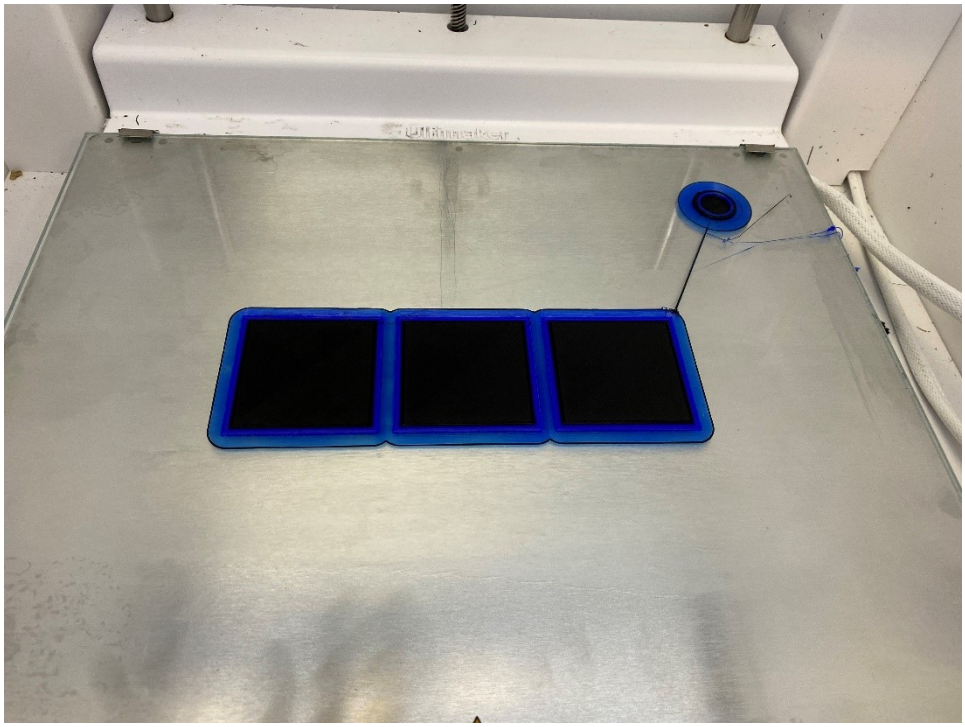

Figure 27: Example of Fully Printed Capacitor Fully-Fused Model (Blue: Dielectric Material (PLA), Black: Conductive Filament Protopasta)

CHAPTER 4

RESULTS AND DISCUSSION

The section below detailed the specific results of this study that utilized the different methods provided above. The three research objectives were investigated through the collected data below and conclusions were formulated based on the results of the plotted data.

4.1 Micrometer Measurements

The measurements below utilized the micrometer for the data collected. The micrometer was then used to determine the exact size of the different components being tested. These components included; aluminum and Protopasta electrodes, the different dielectric mediums PLA, PP, and PC. A digital micrometer was implemented throughout the experiment due to its high measurement accuracy.

4.1.1 Electrodes Measurements

The measurements for the specific electrodes, aluminum and Protopasta, were displayed in the data below.

4.1.1.1 Aluminum Plates Electrodes Measurements

Table 8 displayed the values measured that utilized a micrometer for the cut aluminum plate electrodes. As demonstrated by the measurements, the width and height

of the cut aluminum plates were not as accurate due to the human error involved in cutting the wrought aluminum sheet as described in the Procedures Section.

Table 8: Aluminum Plates Electrodes Measurements

Name	Thickness (mm)	Height (mm)	Width (mm)
Aluminum Plate 1	0.65	51	48.5
Aluminum Plate 2	0.65	49.5	51
Aluminum Plate 3	0.65	47.9	47.8
Aluminum Plate 4	0.65	50.6	48.2

4.1.1.2 Printed Protopasta Plates Electrodes Measurements

The table below displayed the measured data for the Protopasta printed electrode. It was exhibited through the data that being able to fully print the electrodes, while implementing the conductive filaments, resulted in more accurate and precise results. Being able to print the conductive print samples allowed for more accurate dimensions, mainly concerning the width and height of the samples.

Table 9: Printed Protopasta Plate Electrodes Measurements

Name	Thickness (mm)	Height (mm)	Width (mm)
Printed Proto-Pasta 1	0.65	50.2	50.6
Printed Proto-Pasta 2	0.65	50.2	50.5
Printed Proto-Pasta 3	0.65	50.3	50.2
Printed Proto-Pasta 4	0.65	50.2	50.4

The table displayed the results for the measured 3D printed dielectric medium as described above in the Methods Section. The data concluded that the same observations

could be drawn as before; being able to print the samples allowed for more accurate sample sizes than cutting the material.

4.1.2 Dielectric Medium Measurements

This section included the measurements for the different samples 1, 2, and 3 for the dielectric insulating materials.

4.1.2.1 PLA Dielectric Measurements

The table below described the PLA samples that were printed on the Ultimaker. This table demonstrated the issues that arose when material was printed with brim support material, for example, PP and PC. These samples were not as accurate regarding design dimensions as printing with PLA due to this extra support material cut off during the post-processing.

Table 10: PLA Measured Samples

Name	Thickness (mm)	Height (mm)	Width (mm)
PLA Sample 1	1.5	55.3	54.8
PLA Sample 2	1.5	54.9	55.2
PLA Sample 3	1.5	54.8	55
PLA Sample 1	1	54.9	54.8
PLA Sample 2	1.1	55.2	55
PLA Sample 3	1.1	54.9	55.2
PLA Sample 1	0.5	54.8	55.1
PLA Sample 2	0.5	54.9	55.1
PLA Sample 3	0.5	55	55.1
PLA Sample 1	0.25	54.9	54.8
PLA Sample 2	0.25	55	54.8
PLA Sample 3	0.25	54.8	55

The table below presented the measurements for the printed Polypropylene (PP) samples. The Polypropylene samples provided less accurate results as the PLA samples since the PLA samples did not require a brim to solve the adhesion problem to the build plate.

4.1.2.2 PP Dielectric Measurements

The table below described the PP samples that were printed on the Ultimaker. These measured values displayed discrepancies between the different prints of varied height and width due to the brim support material being cut away during post-processing. Although support material was cut from the samples, the PP and PC samples were still more accurate than the previous cut method for the aluminum electrodes samples.

Table 11: PP Measured Samples

Name	Thickness (mm)	Height (mm)	Width (mm)
PP Sample 1	1.4	54.7	55
PP Sample 2	1.4	54.8	54.8
PP Sample 3	1.5	55.5	55
PP Sample 1	0.9	54.8	55.2
PP Sample 2	0.9	54.7	54.6
PP Sample 3	0.9	55.5	55.2
PP Sample 1	0.4	54.9	55.2
PP Sample 2	0.5	55	55.5
PP Sample 3	0.5	55.2	55
PP Sample 1	0.25	54.8	55
PP Sample 2	0.25	55.4	55.2
PP Sample 3	0.25	55.1	56.2

4.1.2.3 PC Dielectric Measurements

Table 12 displayed the measurements for the printed Polycarbonate samples. These samples were also printed with a brim to help with the adhesion properties of bonding the material to the print bed. These measured values displayed variations between the different prints of varied height and width due to the brim support material being cut away during post-processing.

Table 12: PC Measured Samples

Name	Thickness (mm)	Height (mm)	Width (mm)
PC Sample 1	1.5	55.3	55.8
PC Sample 2	1.5	55.3	55.2
PC Sample 3	1.5	55.3	55.6
PC Sample 1	1	55.3	55.5
PC Sample 2	1	55.7	55.8
PC Sample 3	1	55.7	55.4
PC Sample 1	0.5	56.3	54.6
PC Sample 2	0.5	55.7	55.5
PC Sample 3	0.5	55.3	56.4
PC Sample 1	0.25	56.1	56.8
PC Sample 2	0.25	56.4	55.1
PC Sample 3	0.25	56.6	55.4

4.2 Device Measurements

The various sections below detailed the results obtained from each type of device and capacitor model. Based on the literature review, the frequency of a circuit did not affect the overall capacitance and the capacitance remained constant. However, due to thermal polymer properties and infill patterns, recent research findings confirmed that these materials themselves were affected by the different temperature changes, frequencies, and

speed of deformation [52]. This concept was plotted and illustrated through the different graphs at the varying frequencies 100 Hz, 120 Hz, 1 kHz, 10 kHz for the LCR meter. These were the tested frequency ranges; 1 kHz, 5kHz, 7.5 kHz, and 10 kHz for the EVAL meter. Each graph displayed the global average of the collected data. The process of having attained the averages was listed below.

1. Calculated averages for three samples at the same thickness. For example, (S1, S2, S3) at 1.5 mm. There would be a culmination of eight averages included in this step.
2. Calculated the averages of the previous step. There was a total of four averages collected for that step.
3. Graphed the global averages from above for each different dielectric material that was implemented.

In this thesis, there was a culmination of twenty-four different models per dielectric material for a total of seventy-two different parallel plate capacitors. Each capacitor model consisted of three samples of the same thickness (S1, S2, S3) that contained two sets of different aluminum plates. There were four different dielectric thicknesses (1.5 mm, 1.0 mm, 0.5 mm, and 0.25 mm). The dielectric medium thickness and the frequency were the only variables in this research. However, the electrodes plates remained constant at the estimated average of around 0.65 mm.

4.2.1 Multimeter: Aluminum Electrode

The table below displayed the calculated ideal capacitance of a parallel plate capacitor which used the dielectric permittivity of air. Equation 1 is utilized for these

calculations. These calculations are demonstrated as a base line for the following created capacitor results.

Table 13: Theoretical Capacitance for a 50 x 50 mm Parallel Plate Capacitor

Distance Thickness (mm)	Calculated Capacitance (pF)
1.5	14.8
1	22.1
0.5	44.3
0.25	88.5

Figure 28 displayed the plotted data for the total global average for each sample set. Each plot encompassed the different types of dielectrics used and varying dielectric thicknesses as well. Figure 28 displayed the multimeter measurements for the cut wrought aluminum electrodes samples. The highest capacitance from this data collected was PP 3D printed dielectric samples at around 143.3 pF. The second capacitance was the PLA printed dielectric sample and the PC sample. This section only included the plotted results for the aluminum plate electrodes model.

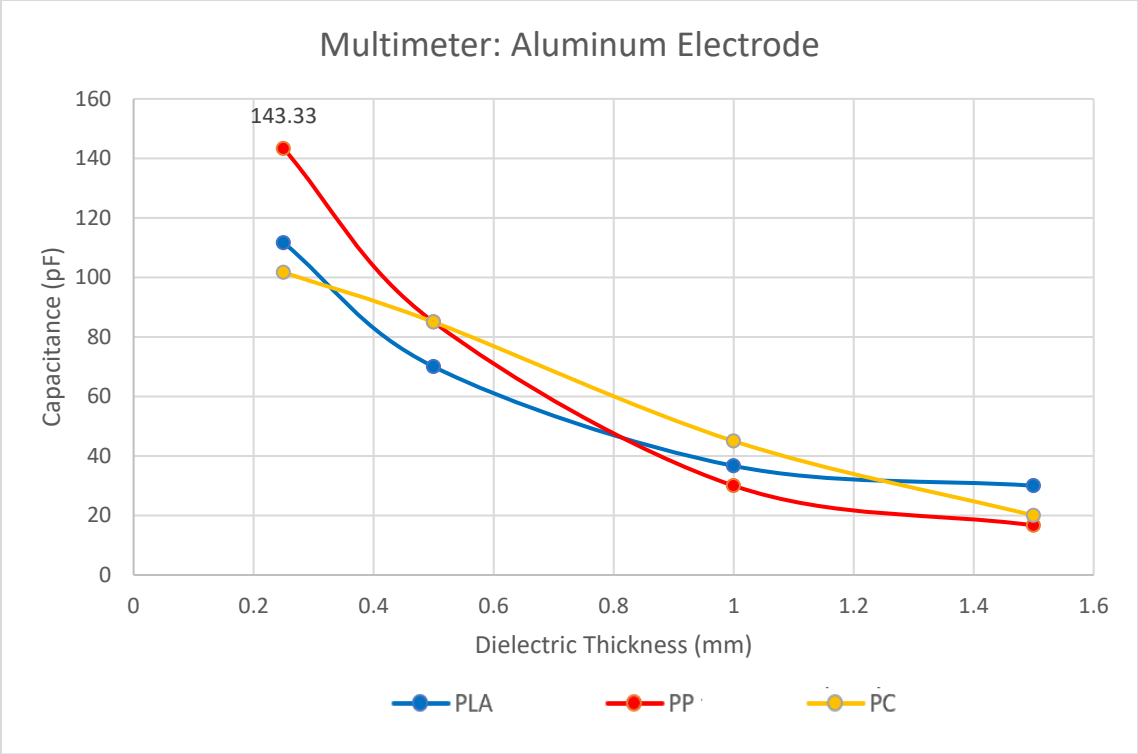

Figure 28: Multimeter Measurement: Aluminum Electrode

Figure 29 described the data for the 3D printed Protopasta plate electrodes with the different 3D printed dielectric samples. It was observed from the data that the PP sample still yielded the highest capacitance compared to the others; with the printed electrodes the capacitance of each sandwich model was increased, except for the PP samples which was around the same capacitance as the aluminum plate electrode samples.

4.2.2 Multimeter: Protopasta Electrode

This section below graphed the Protopasta Electrode data as measured with the multimeter. Three separate dielectric materials are measured PLA, PP, and PC.

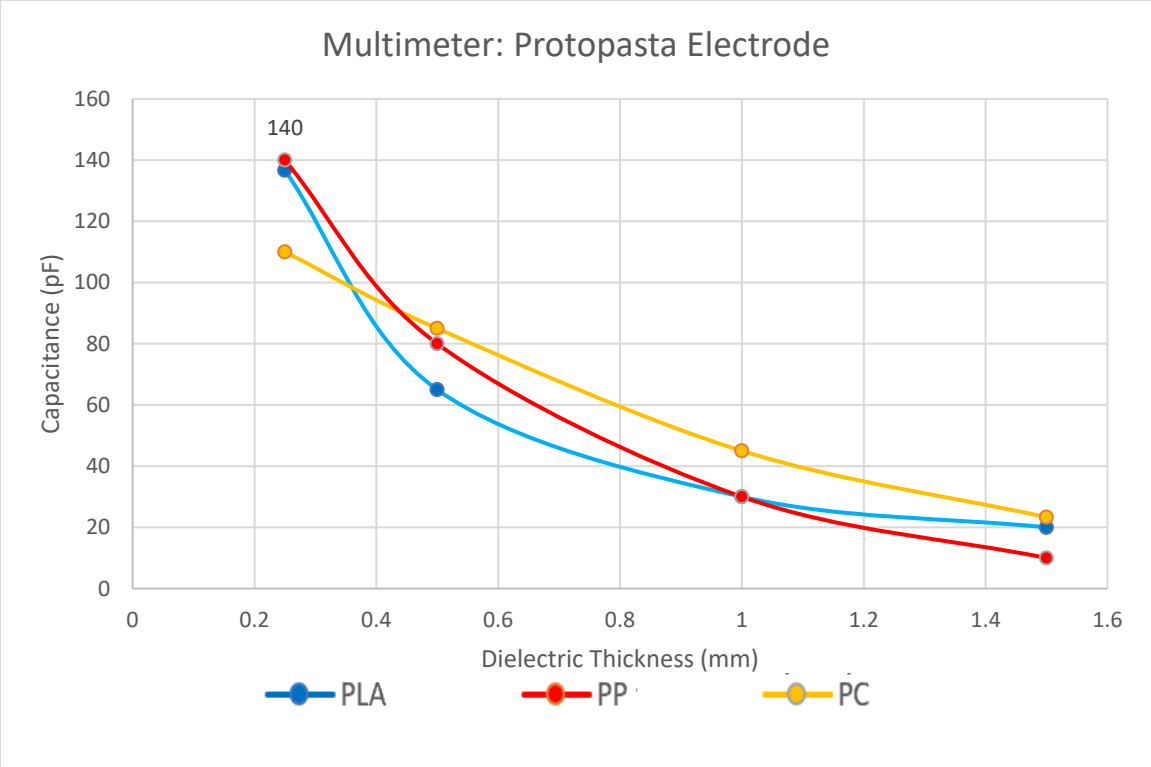

Figure 29: Multimeter Measurement: Protopasta Electrode

4.2.3 LCR with Probes: Aluminum Electrode

The results below for this subsection were measured utilizing the LCR meter described above in the Methods Section but included the implementation of the probes to have remained consistent with the multimeter measurements. The unique characteristics of the LCR measurements allowed for the data to be collected at an operating frequency for a typical capacitor model. The fixed frequencies included; 100 Hz, 120 Hz, 1 kHz, and 10 kHz. This section focused primarily on the plotted results for the aluminum plate electrodes model. In this section, the equations were formulated for percent increase and percent decrease for each dielectric material that began after the 100 Hz range.

Figure 30 displays the capacitance results at the given frequency of 100 Hz. The data below demonstrated that PP as the dielectric material still yielded the highest

capacitance compared to the other printed dielectrics. Another discrepancy between the multimeter measurements and the LCR measurements below was that the multimeter measurement had not allowed for change in frequency.

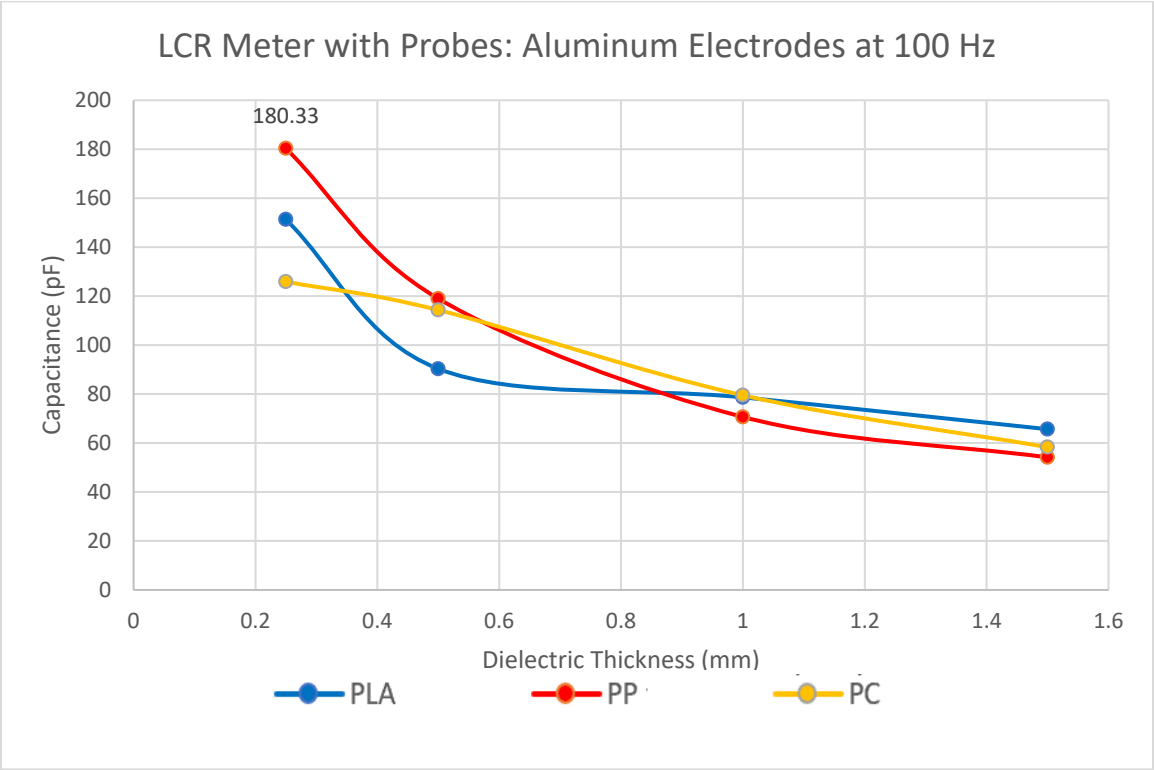

Figure 30: LCR with Probes Measurement: Aluminum Electrode at 100 Hz

Figure 31 displayed the results of the LCR meter with probes at 120 Hz where each of the following figures were increasing frequency. From this data, it was confirmed that when the frequency was increased, then the capacitance was decreased. The percent decreased for this model taken at the 0.25 mm dielectric thickness was PLA 1.54%, PP 0.46%, and PC increased slightly at 0.48%.

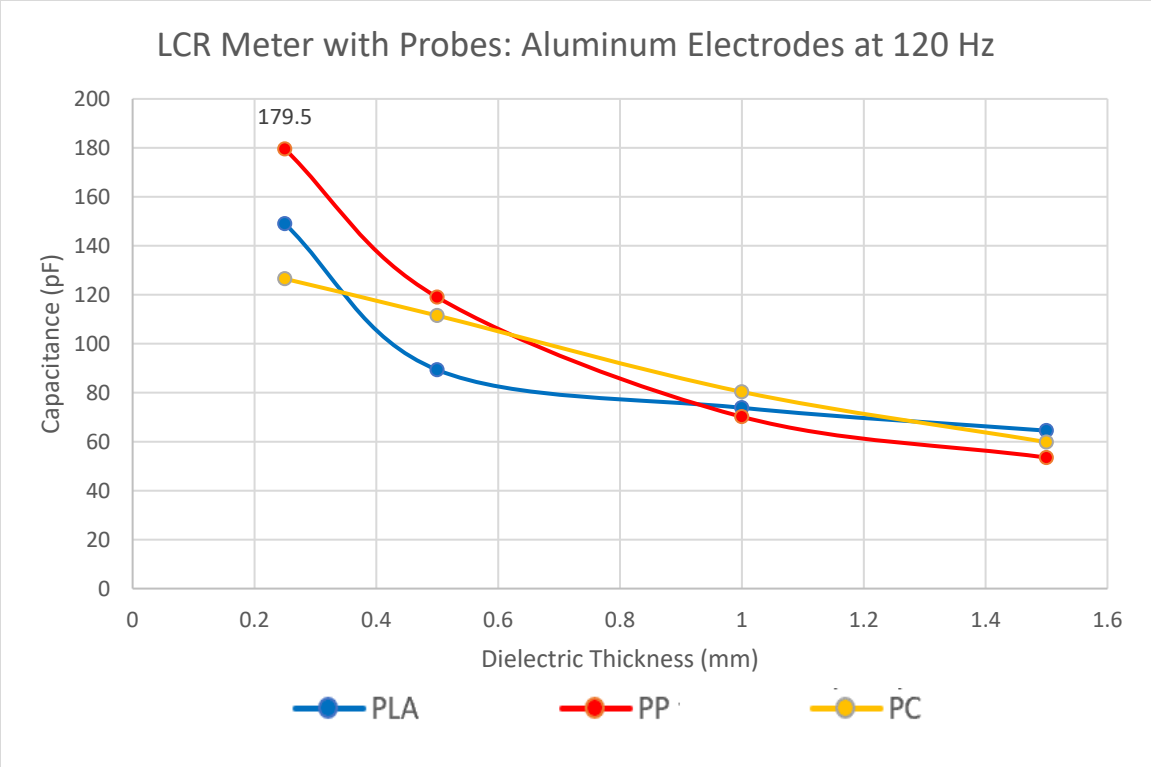

Figure 31: LCR with Probes Measurements: Aluminum Electrode at 120 Hz

Figure 32 displayed the capacitance of the aluminum plate electrode at the frequency of 1 kHz. The percent changes were as follows: PLA 3.53%, PP 3.69% and PC 0.08% decreased from the previous frequency.

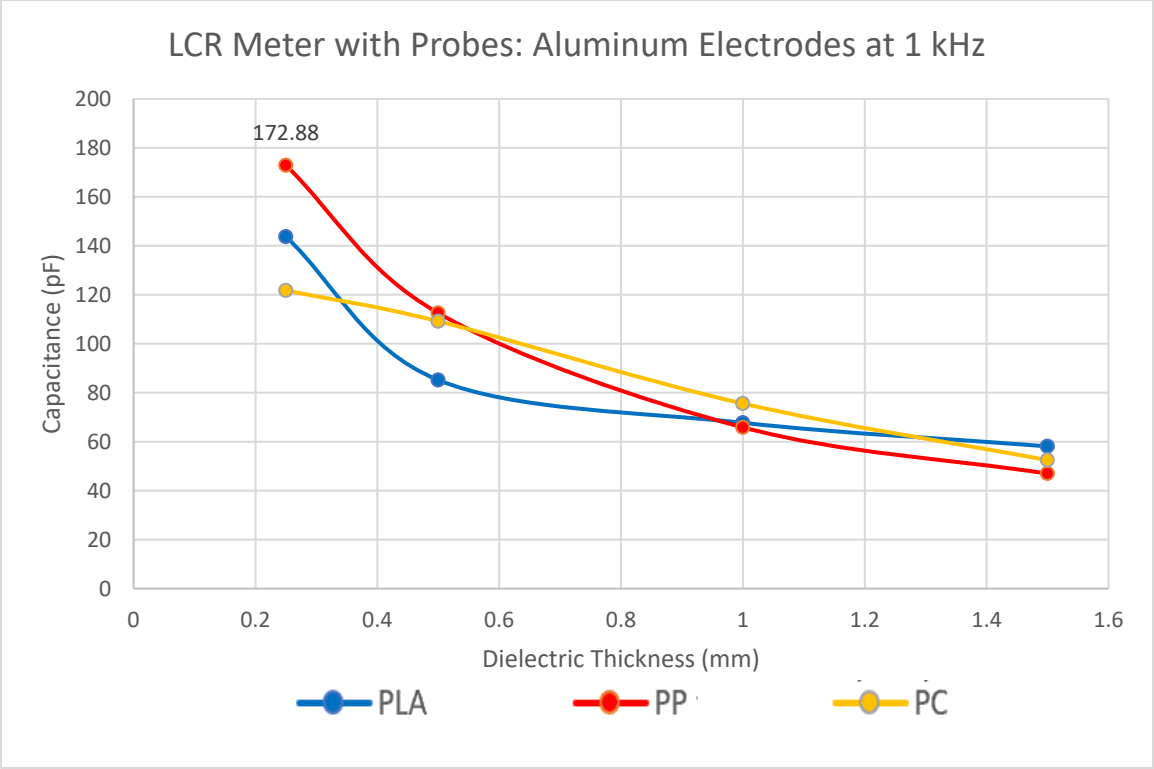

Figure 32: LCR with Probes Measurements: Aluminum Electrode at 1 kHz

Figure 33 displayed the results of the same capacitor model with the aluminum as the electrode at a higher frequency of 10 kHz. These data demonstrated the pattern of increase in frequency and decrease in capacitance. The percent decreases were PLA 2.35%, PP 1.41%, and PC 0.08% decreased from the previous frequency of 1kHz.

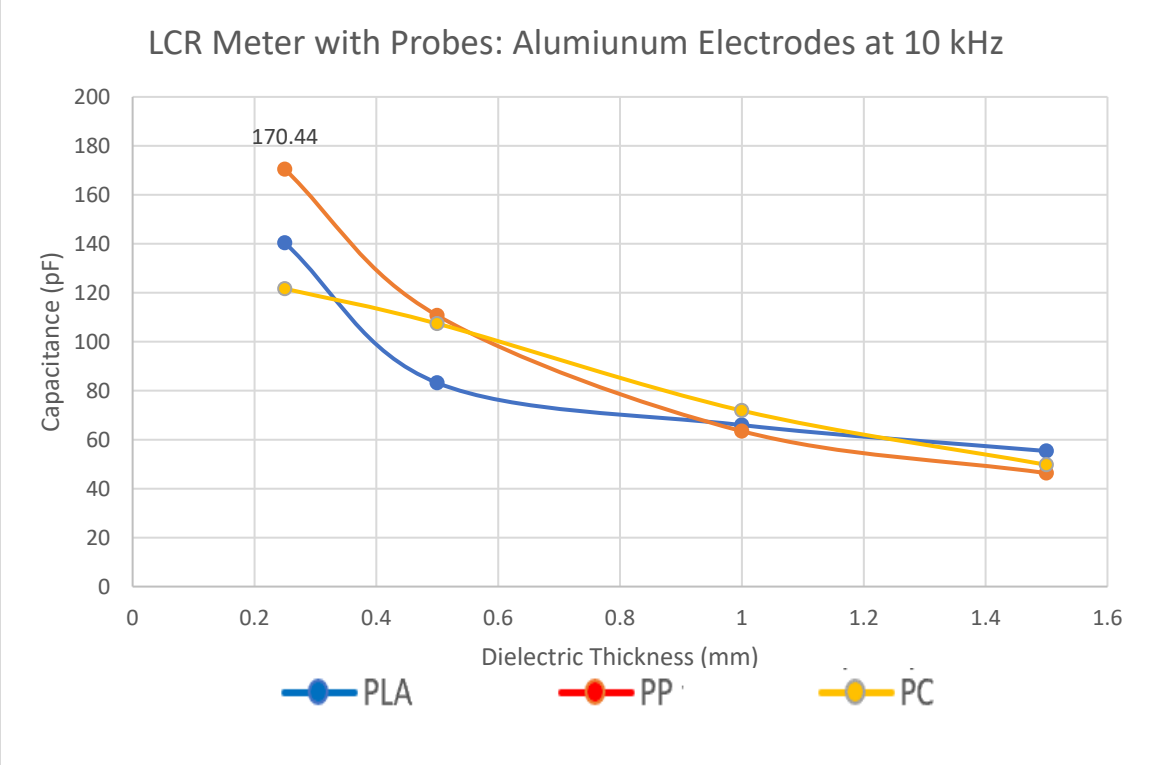

Figure 33: LCR with Probes Measurements: Aluminum Electrode at 10 kHz

4.2.4 LCR with Alligator Clips: Aluminum Electrode

This section included the various graphs for the LCR with Alligator Clips. This technique was utilized since the LCR meter original was supplied with alligator clips. The alligator clips were displayed in Figure 34. This section primarily included the plotted results for the aluminum plate electrodes model.

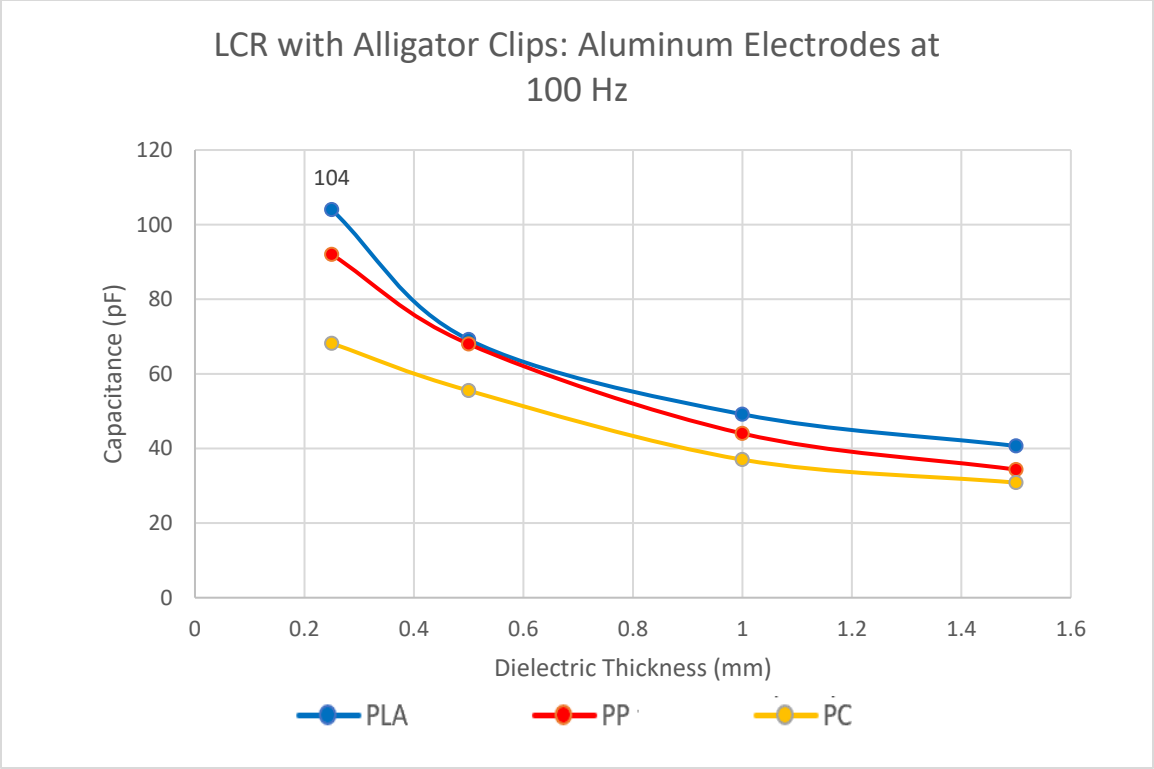

Figure 34: LCR with Alligator Clips Measurements: Aluminum Electrode at 100 Hz

Figure 35 displayed the capacitance at the frequency of 120 Hz with the aluminum electrode. The percent decreases were PLA 0.16%, PP 0.54%, and PC 0.98.

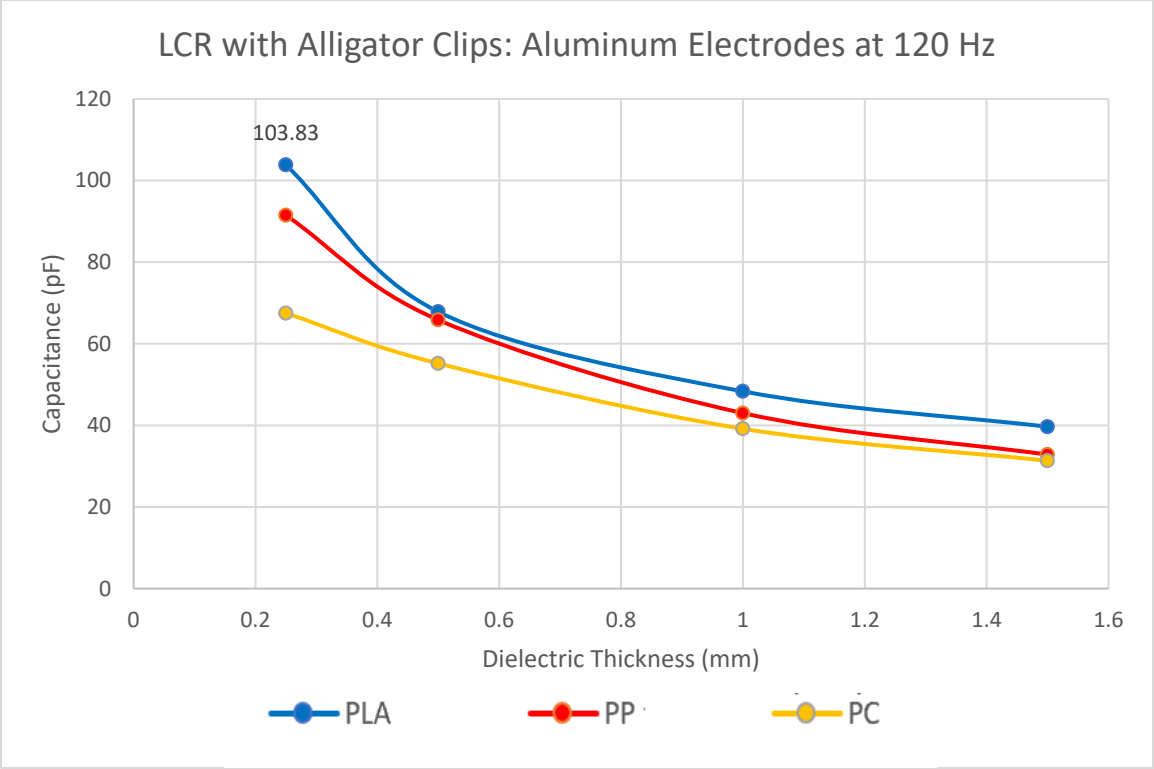

Figure 35: LCR with Alligator Clips Measurements: Aluminum Electrode at 120 Hz

Figure 36 depicted the same characteristics as the previous graph, which illustrated an increase in frequency while the capacitance of the parallel plate capacitor model decreased. This figure displayed the capacitance when the frequency was increased to 1 kHz. The percent decreases were PLA 6.37%, PP 2.90%, and PC 1.65%.

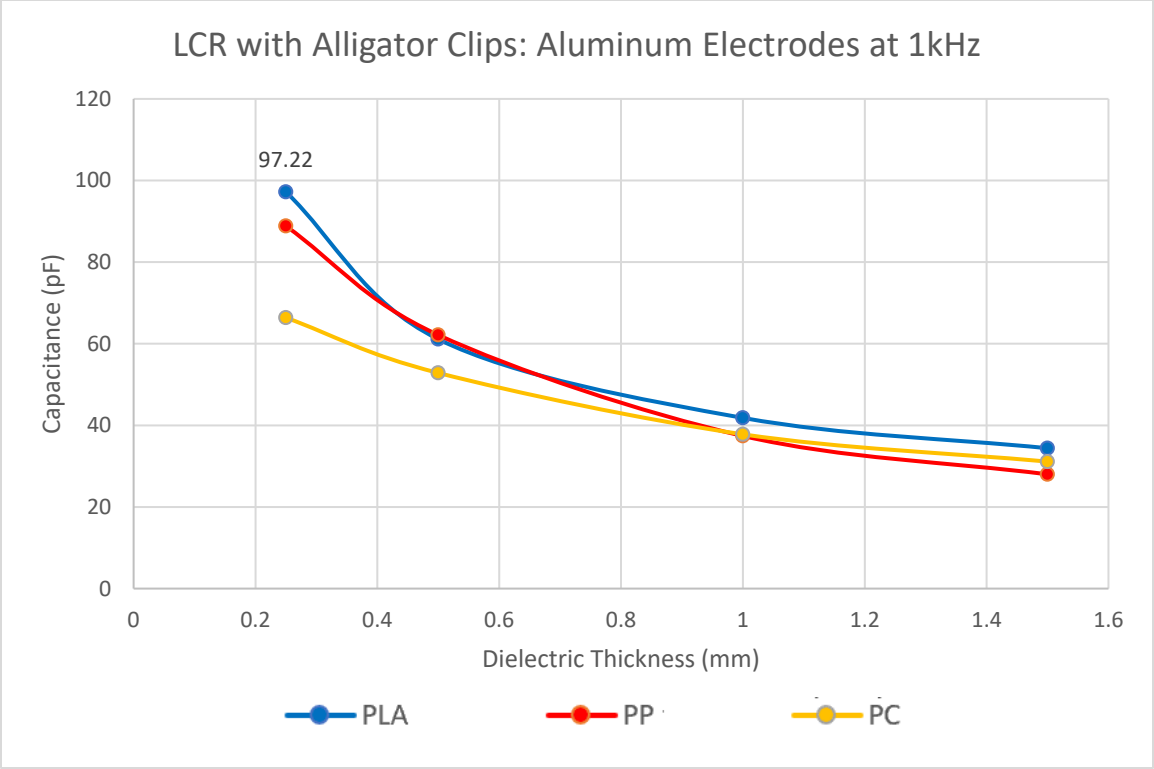

Figure 36: LCR with Alligator Clips Measurements: Aluminum Electrode at 1 kHz

Figure 37 displayed the capacitance measurements at the increased frequency of 10 kHz. The percent decreases were PLA 2.30%, PP 0.72%, and PC 1.10%. Still, PLA displayed the highest percent decrease.

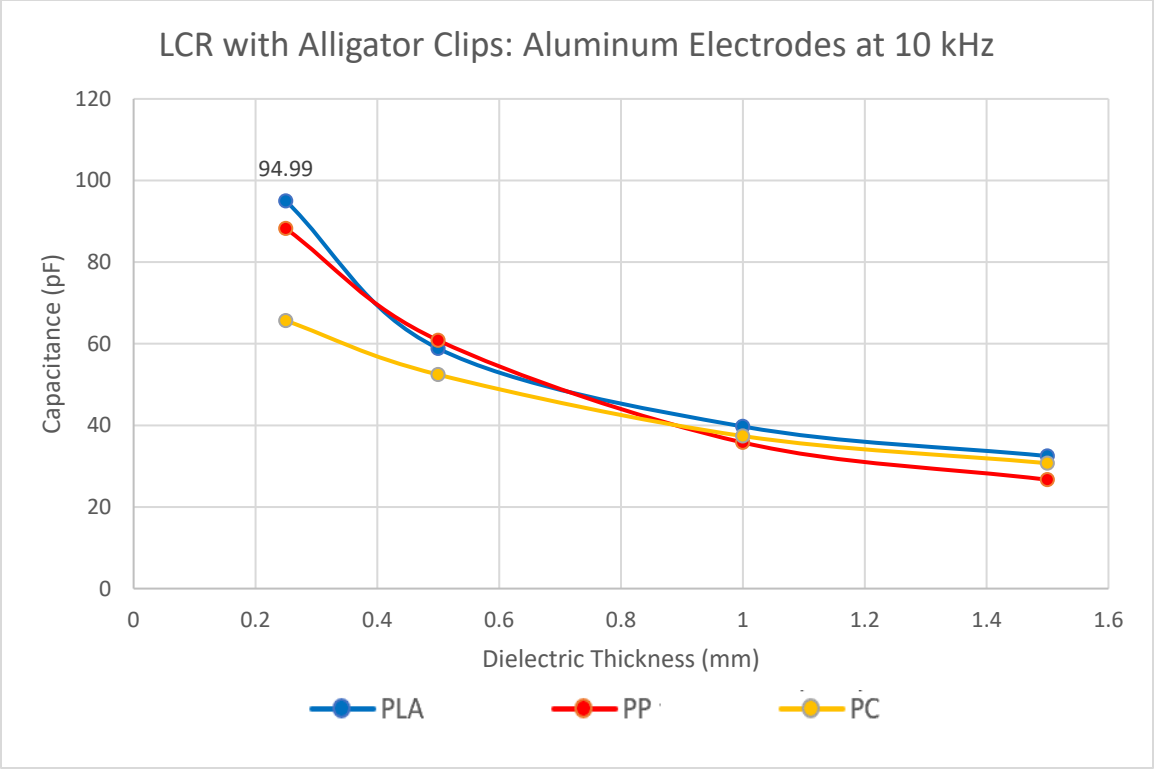

Figure 37: LCR with Alligator Clips Measurements: Aluminum Electrode at 10 kHz

4.2.5 EVAL: Aluminum Electrode

This section displayed the results for the third device implemented in this research. The device was unique since it allowed for a broad range of frequencies rather than the preprogrammed standard frequencies given off by the LCR device. The impedance of the models was measured at the frequencies of 1 kHz, 5 kHz, 7.5 kHz, and 10 kHz frequency range. The capacitance was calculated when having used the capacitance formula that was displayed below. The dielectric constant was also calculated using a formula displayed later in the Results Section. The results were measured using the EVAL meter at the various frequencies; 1 kHz, 5 kHz, 7.5 kHz, and 10 kHz. As the results demonstrated, some errors occurred when implementing this device. Compared to the previous results, the increase in frequency also showed a decrease in capacitance. Contrary to these previous findings, the

results for the EVAL measurements using the aluminum plate electrodes did not display this same pattern. Each measurement from the EVAL was taken at the 200-point interval. This discrepancy was due to the different discharge and charge cycles of each different electrode and dielectric material being used. The percent decrease was still calculated as in the previous section, but in some cases the percent increase was calculated instead due to an increase in the results rather than a decrease.

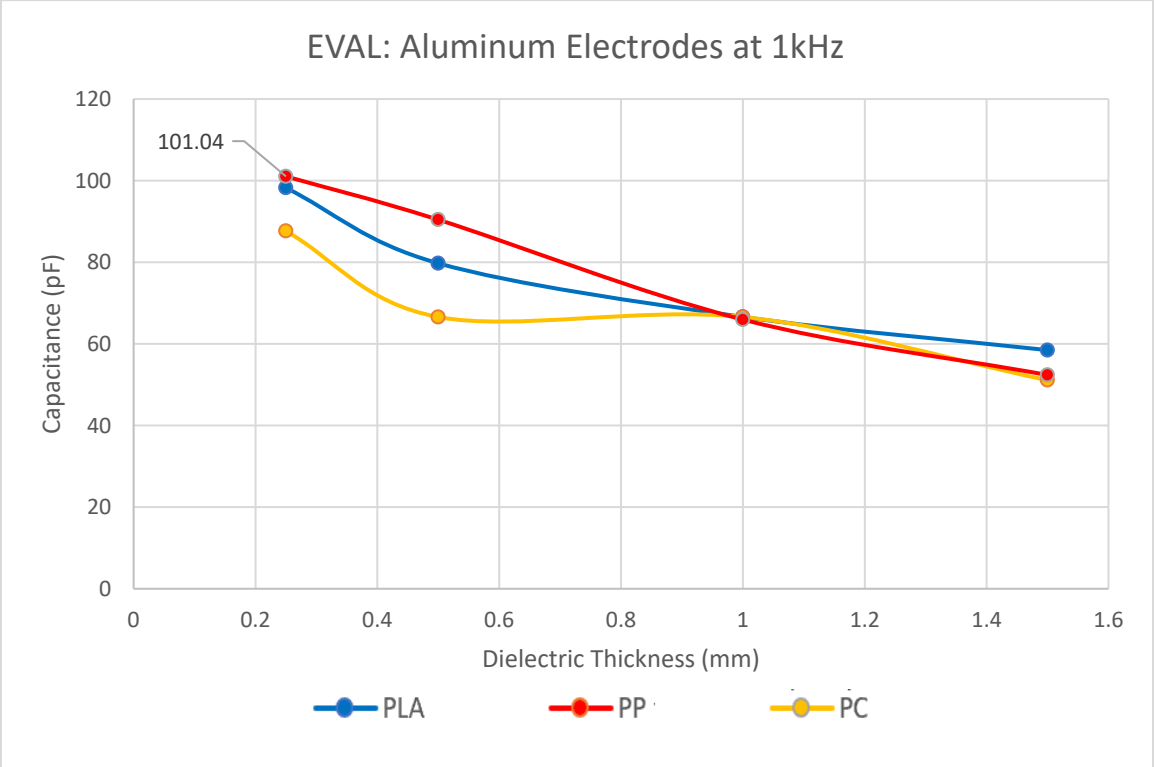

Figure 38: EVAL: Aluminum Electrodes at 1kHz

The graph displayed the capacitance at the given frequency of 5 kHz. As noted above, there was a slight variation between the previous data graphs and the EVAL graphs with aluminum electrodes. In Figure 39 below, the highest capacitance recorded was approximately around 107.29 pF, which was an increase compared to the previous 101.04

pF measurement. The percent increase PLA was 1.62%, PP 6.18%, and PC had a percent decrease of 0.18%. PP material had the highest percent change based on frequency compared to PLA.

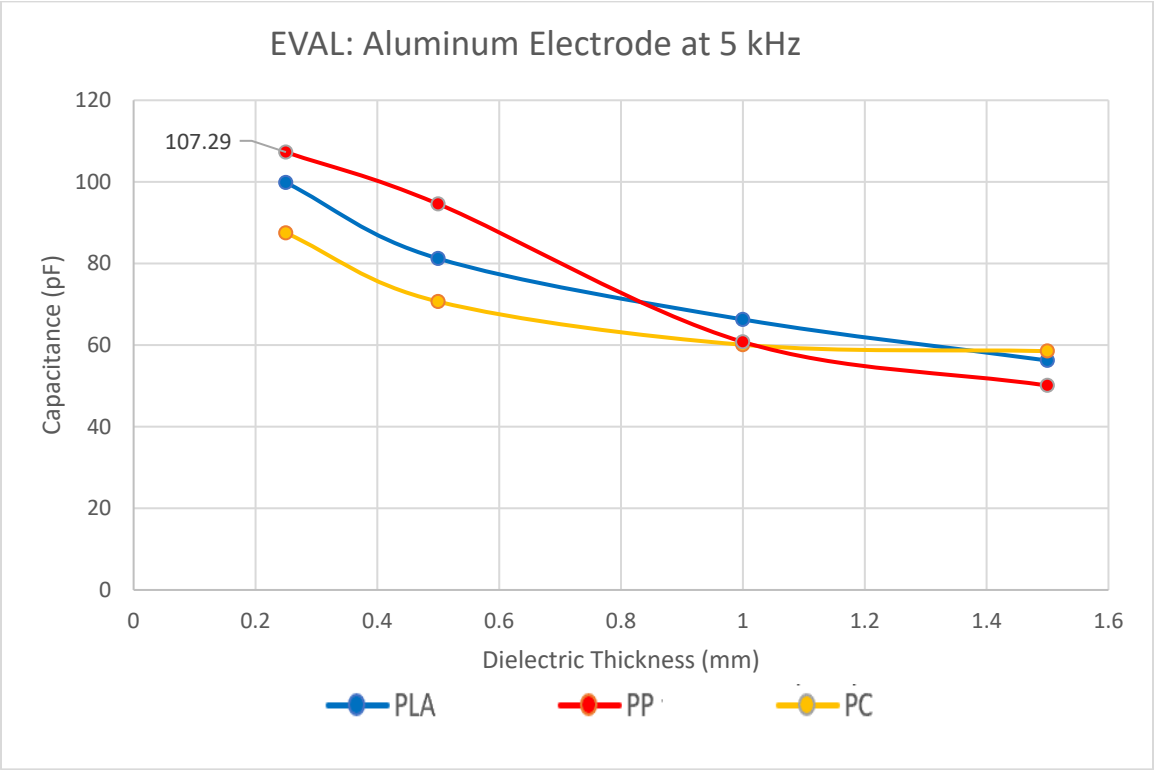

Figure 39: EVAL: Aluminum Electrode at 5 kHz

Figure 40 displayed the data at an increased frequency of 7.5 kHz. The percent increases were PLA 4.05%, PP 6.39%, and PC 1.81%. In that collection of data, PP still represented the highest amount of percent change based on the graphs.

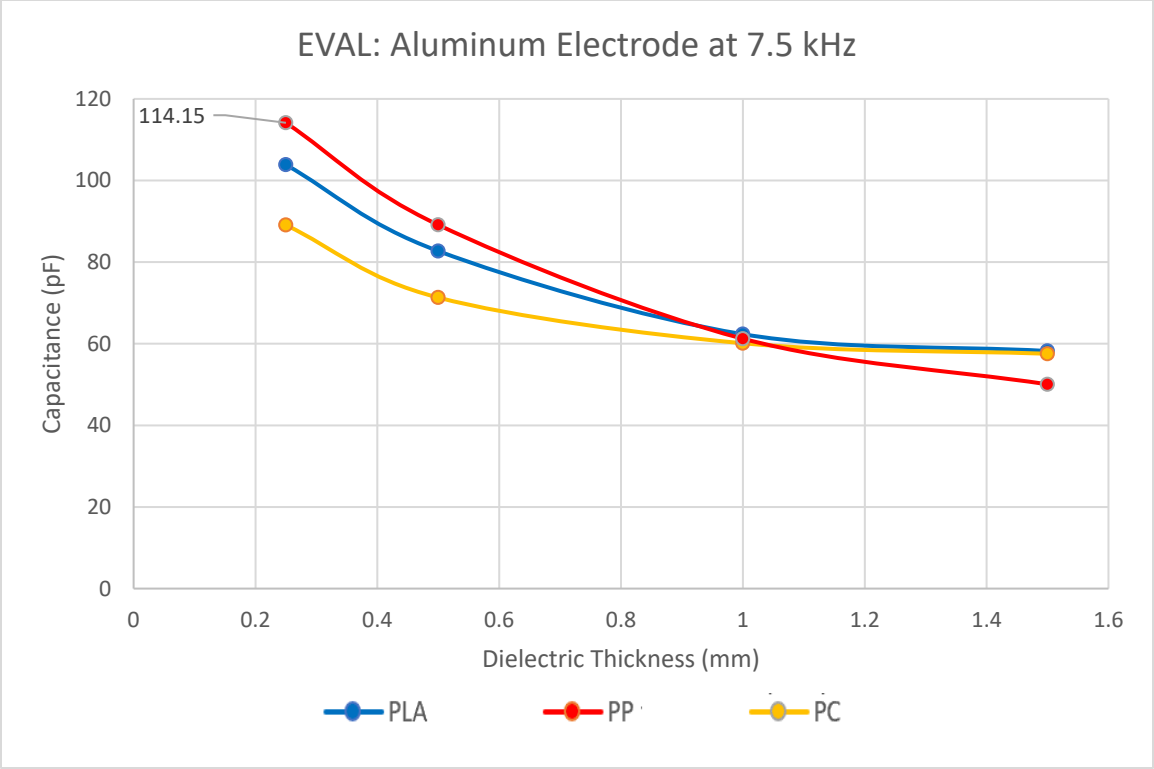

Figure 40: EVAL: Aluminum Electrode at 7.5 kHz

Figure 41 displayed the EVAL collected data at the increased frequency of 10 kHz. The percentages were PLA 2.22%, PP 1.71%, where PC displayed a percent decrease of 0.56%. PLA in that case experienced the highest amount of percentage change.

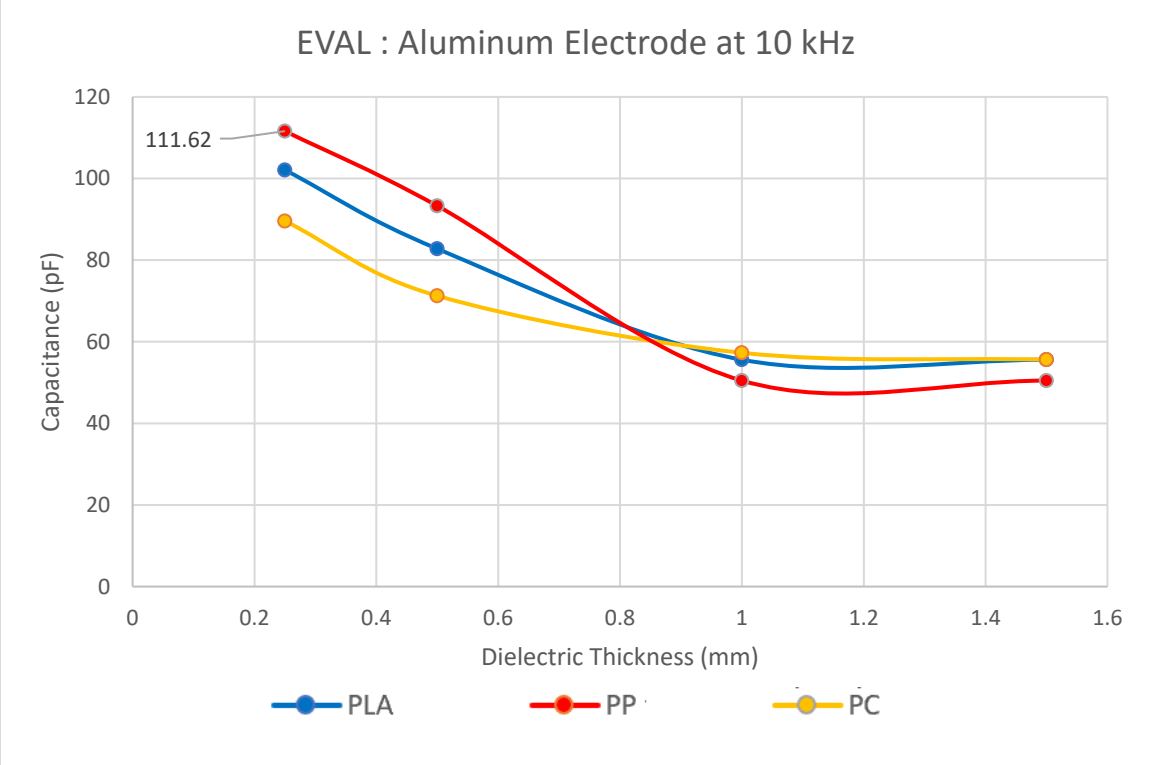

Figure 41: EVAL Measurements: Aluminum Electrode at 10 kHz

4.2.6 Observations Aluminum Electrode

The aluminum electrode was utilized as the control capacitor for this research. These capacitors results were compared to the theoretical calculated capacitor with the dielectric permittivity constant of air. The multimeter was implemented for this comparison since the devices demonstrated a fixed low frequency that was unable to be changed. The increase in capacitance can account for the differences in the dielectric constants. The dielectric constant of air was around 1, based on the surrounding literature, while the dielectric constant for PLA which was used as the dielectric below was around 2.7. These expected results are produced in the table below.

Table 14: Calculated Capacitance vs Aluminum Plate Electrodes Capacitance

Distance Thickness (mm)	Calculated Theoretical Capacitance with Air (pF)	Aluminum Plate Electrodes Capacitance with PLA (pF)
1.5	14.757	40.67
1	22.135	49.17
0.5	44.271	69.17
0.25	88.542	104

Some other observations included in the table emphasized that as the dielectric thickness was decreased, then the overall capacitance of the capacitance was increased. Also, when the frequency was increased, then the overall capacitance was decreased. In terms of which dielectric displayed the highest capacitance, the thermoplastics PP had the highest with PLA as the second highest capacitance.

4.2.7 LCR Meter with Probes: Protopasta Electrodes

In this section, a fully 3D printed electrode was utilized in place of the cut aluminum plate electrode. The same tests were run that implemented the same devices as before. The first subsection consisted of the multimeter method.

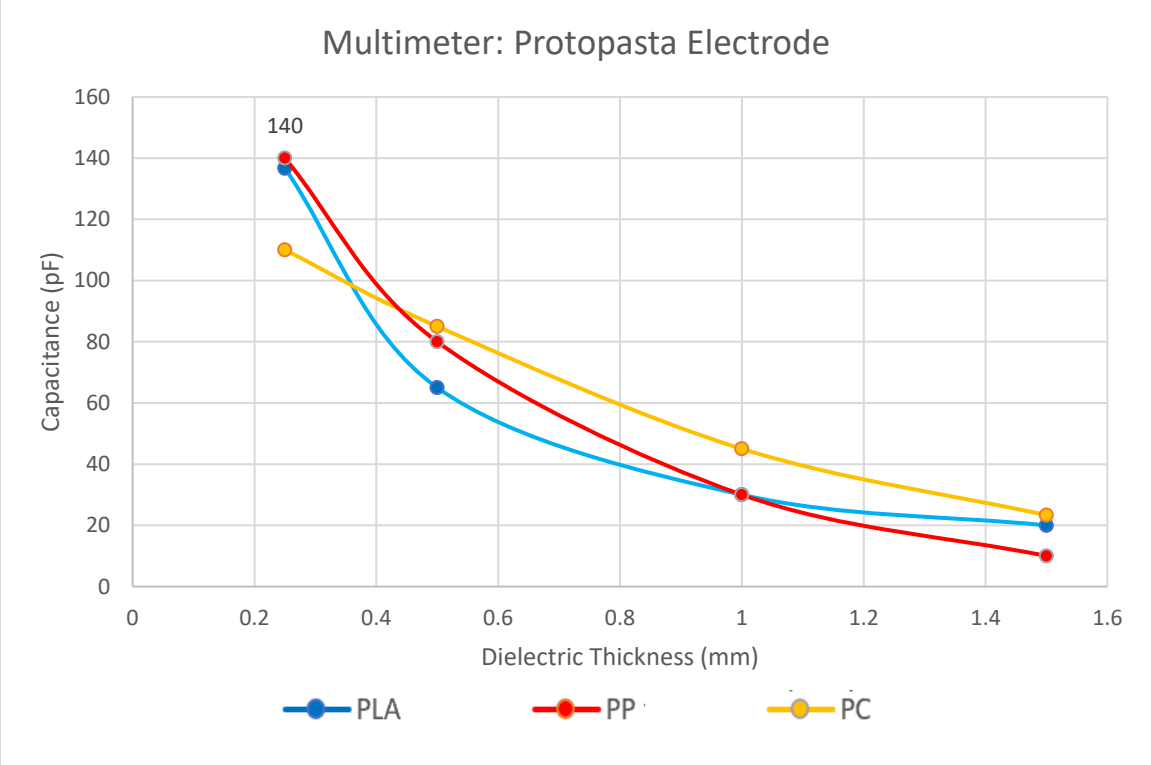

Figure 42: Multimeter Measurement: Protopasta Electrode

4.2.8 LCR Meter with Probes: Protopasta Electrodes

Figure 43 included the measurements for the LCR with Probes at 100 Hz, 120 Hz, 1 kHz, and 10 kHz frequencies. These tests followed the same previous pattern that when frequency increased, then the capacitance decreased. The percent changes of each material were displayed below similar to the previous section.

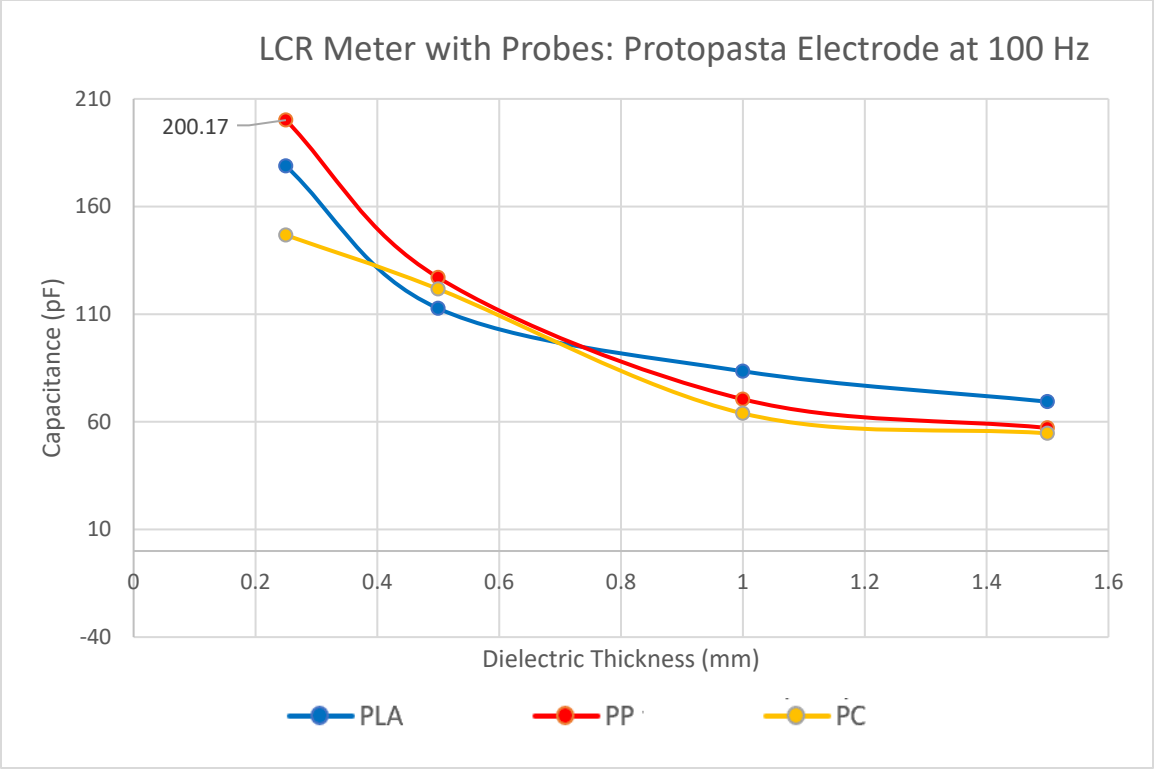

Figure 43: LCR Meter with Probes: Protopasta Electrode at 100 Hz

Figure 44 displayed the total capacitance of each model with different dielectric materials and thicknesses as before. The percent changes were PLA 0.19% decrease, PP 1.25% decrease and PC percent increase at 0.54%. PP in that case yielded the highest percent decrease.

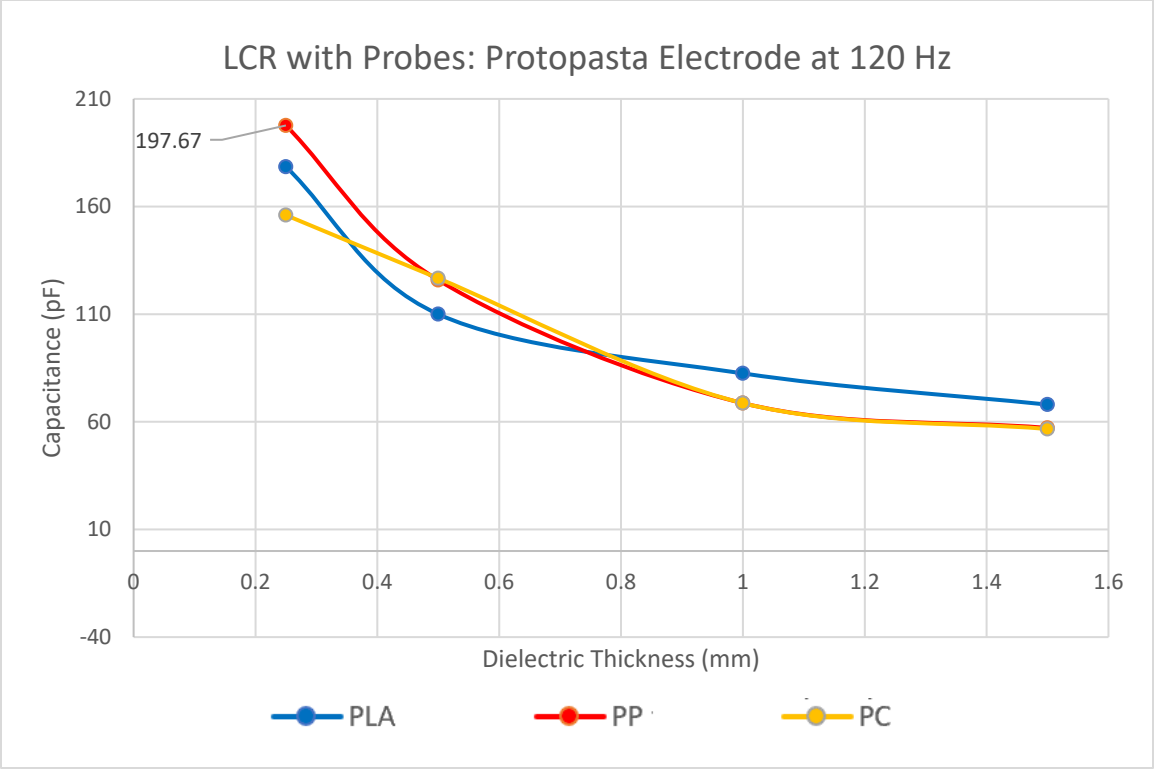

Figure 44: LCR Meter with Probes: Protopasta Electrode at 120 Hz

Figure 45 displayed the increased frequency of the capacitor with the different dielectric mediums. The different percentage changes were PLA 5.52% decrease, PP 5.09% decrease, and PC 5.95% decrease. The PC and PLA yielded the highest percent calculated percent decrease.

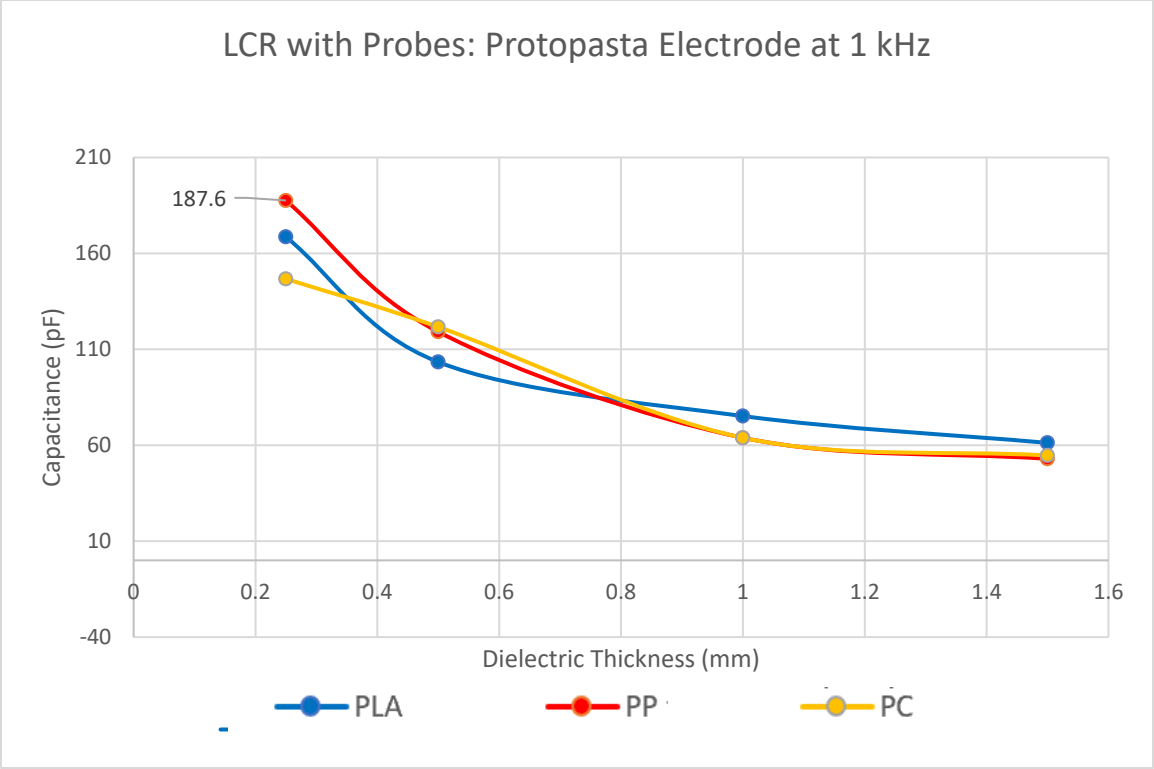

Figure 45: LCR Meter with Probes: Protopasta Electrode at 1 kHz

Figure 46 displayed the capacitance as the frequency increased. The percent changes were PLA 5.95% decrease, PP 1.62% decrease, and PC at 2.39% decrease. The data represents that PLA had the highest percent change at that specific frequency.

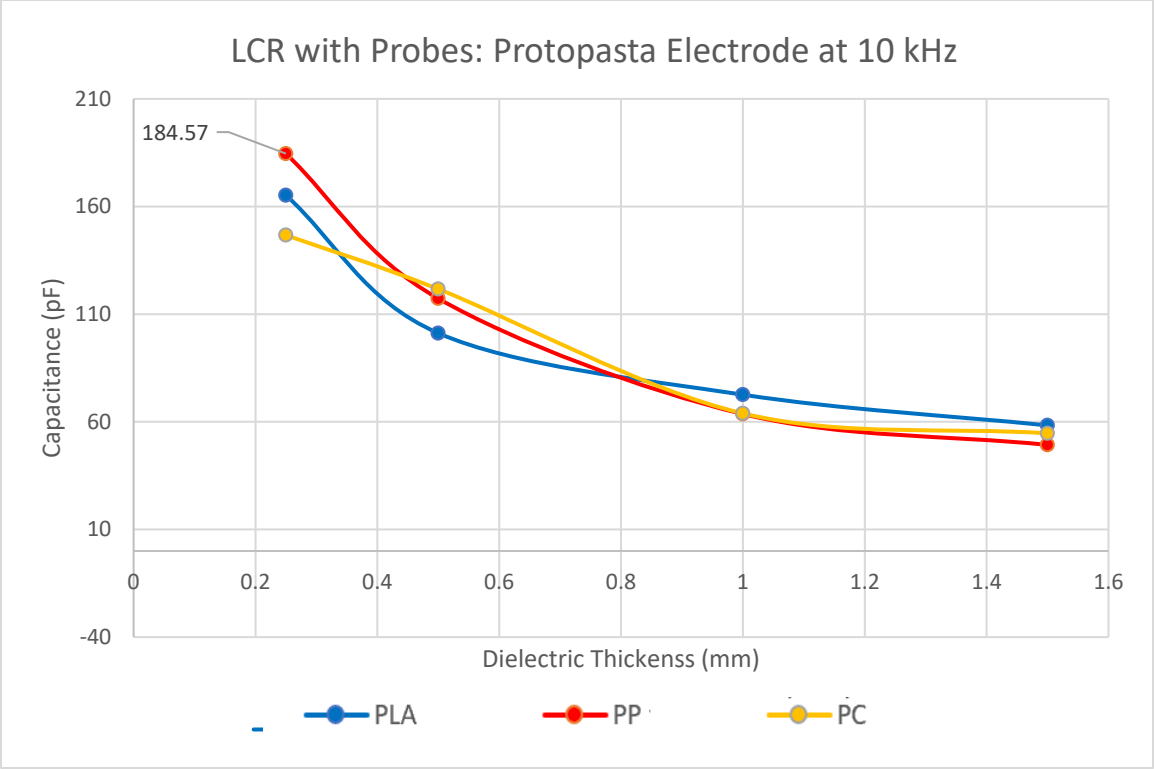

Figure 46: LCR Meter with Probes: Protopasta Electrode at 10 kHz

4.2.9 LCR Meter with Alligator Clips: Protopasta Electrode

This section implemented the same LCR meter as the previous section, which replaced the probes with the provided alligator clips. The aluminum electrode plates were also interchanged for the printed Protopasta plates. The calculated percent change was displayed below for each frequency range; 100 Hz 120 Hz, 1kHz, and 10 kHz.

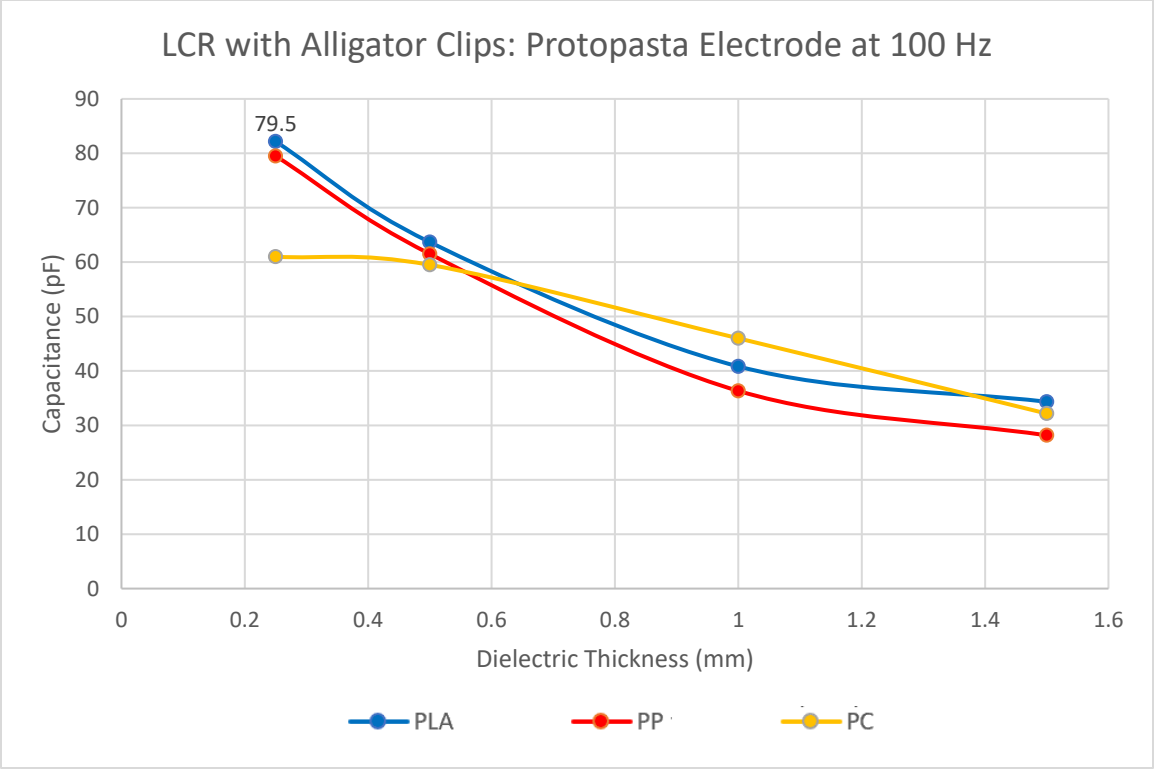

Figure 47: LCR Meter with Alligator Clips: Measurements: Protopasta Electrode at 100 Hz

Figure 48 displayed the results for capacitance at the increased frequency of 120 Hz compared to the previous frequency of 100 Hz. The percent changes were PLA 0.81% decrease, PP 1.64% decrease, and PC 0.80% decrease. PP demonstrated the highest amount of percent change based on the results below.

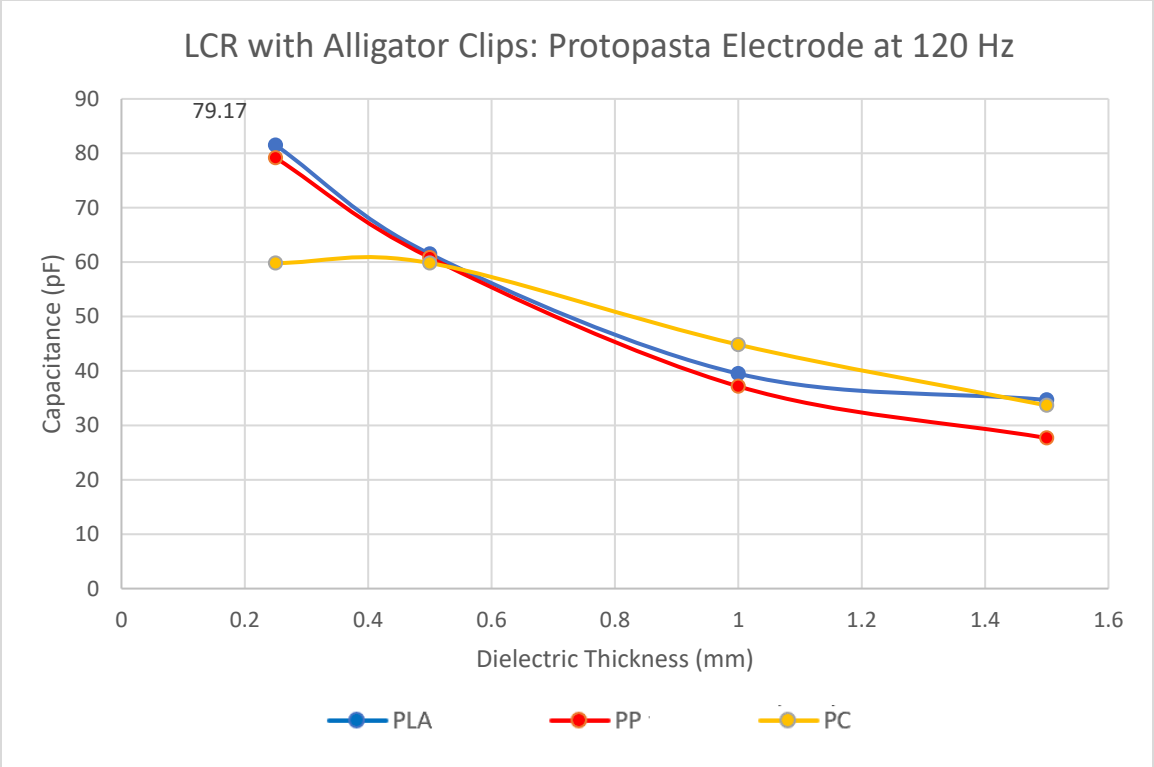

Figure 48: LCR Meter with Alligator Clips: Measurements: Protopasta Electrode at 120 Hz

The following graph displays the capacitance of the models where the frequency was increased to 1 kHz. The percent changes were PLA 1.64% decrease, PP 2.82% decrease, and PC 1.06% decrease. PP in this frequency range ultimately represented the highest percent change.

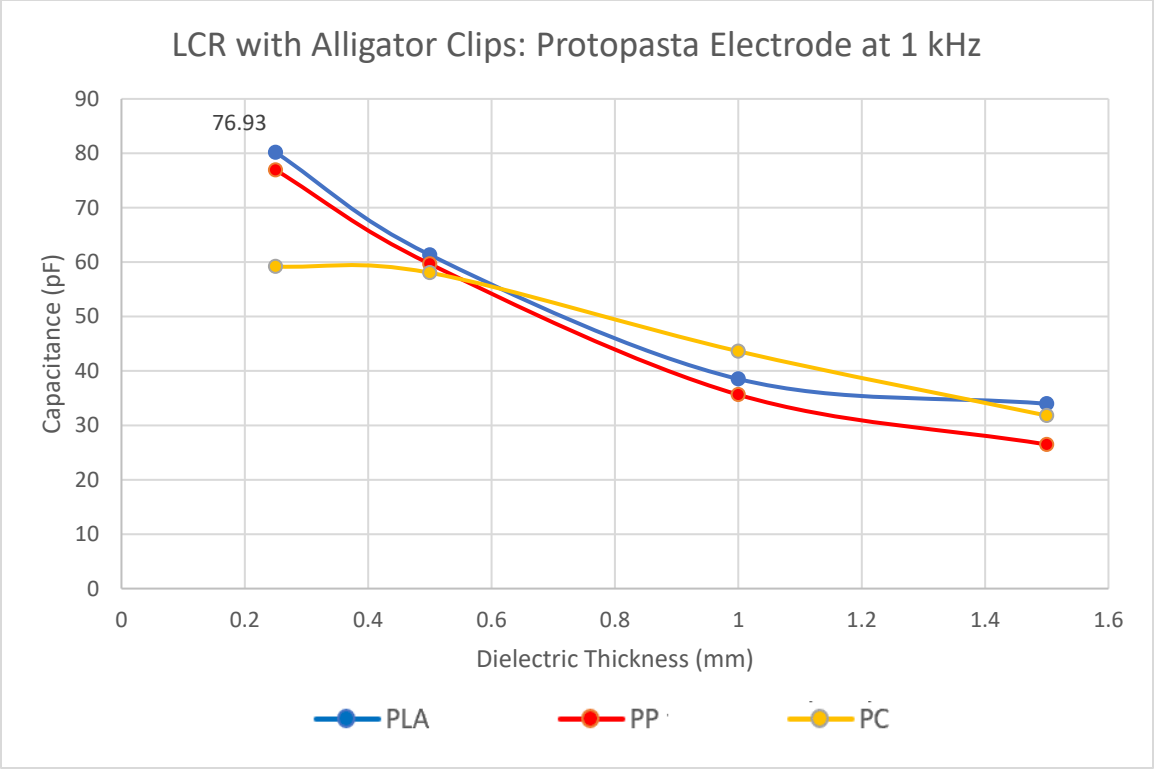

Figure 49: LCR Meter with Alligator Clips: Protopasta Electrode at 1 kHz

The percent changes were PLA 0.80% decrease, PP 0.45% decrease, and PC 0.36% decrease. PLA in this frequency range yielded the highest percent change.

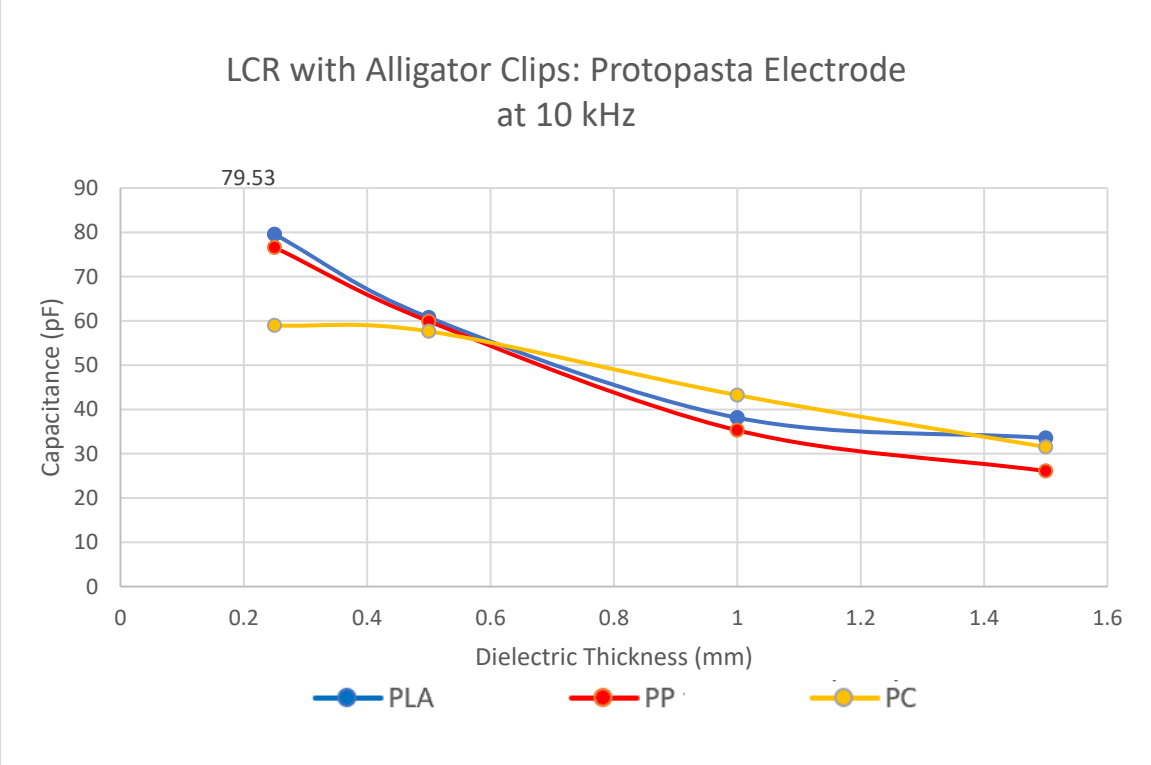

Figure 50: LCR Meter with Alligator Clips: Protopasta Electrode at 10 Hz

4.2.10 EVAL: Protopasta Electrodes

The following culmination of tests involved the operation of the EVAL at the test frequencies of 1 kHz, 5 kHz, 7.5 kHz, and 10 kHz. The results were depicted below. Then, the printed Protopasta was replaced as the electrode for each capacitor model. The percent change was also calculated as in the previous sections.

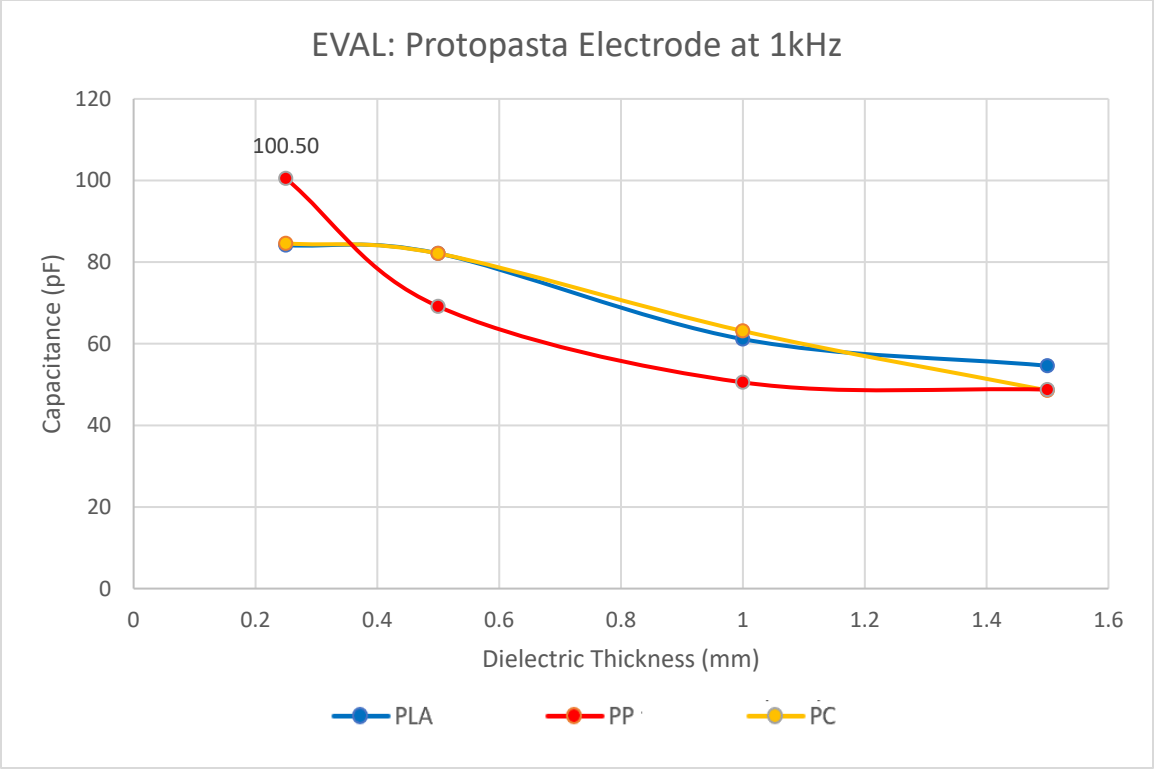

Figure 51: EVAL: Measurements: Protopasta Electrode at 1 kHz

Figure 52 represents the collected data as the frequency increased from 1 kHz to 5 kHz. The percent changes for the data were PLA 0.61% decrease, PP 0.36% decrease, and PC 3.69% decrease. PP yielded the highest percent change based on the provided data.

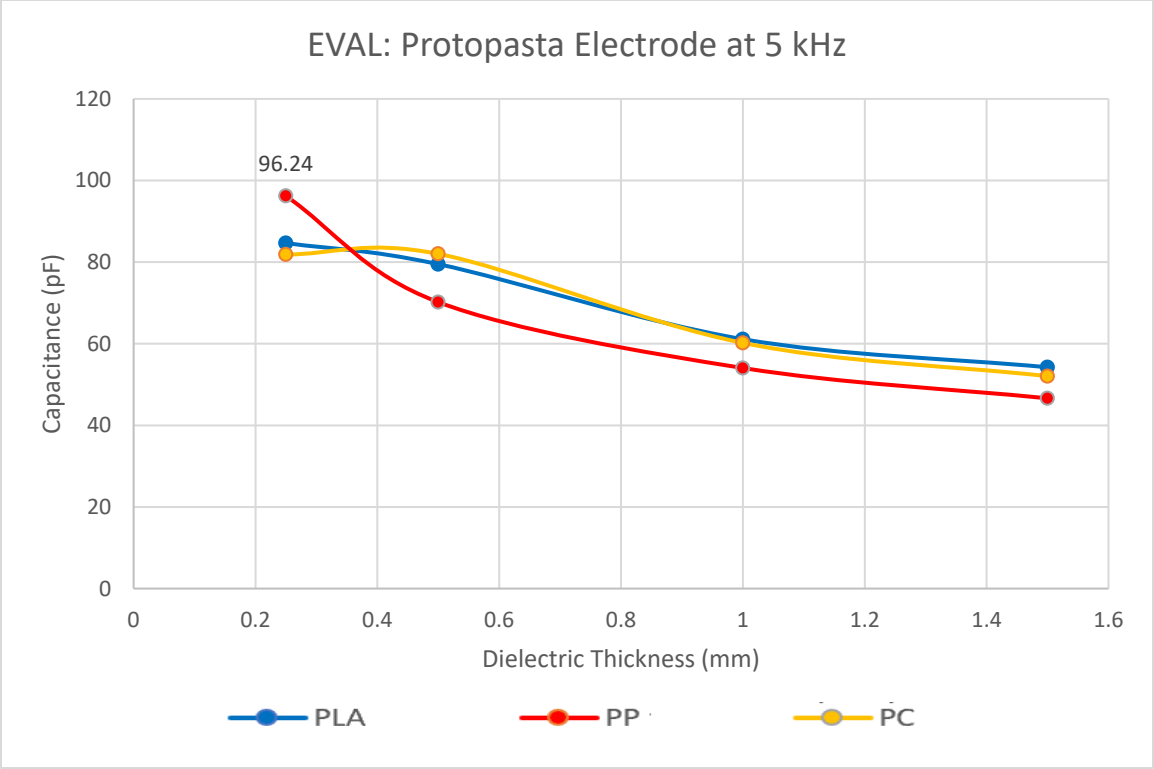

Figure 52: EVAL: Measurements: Protopasta Electrode at 5 kHz

Figure 53 represents the collected data at the frequency of 7.5 kHz. The percent changes were PLA 5.43% increase, PP 1.10% increase, and PC 4.71% increase. PLA demonstrated the highest percent change overall.

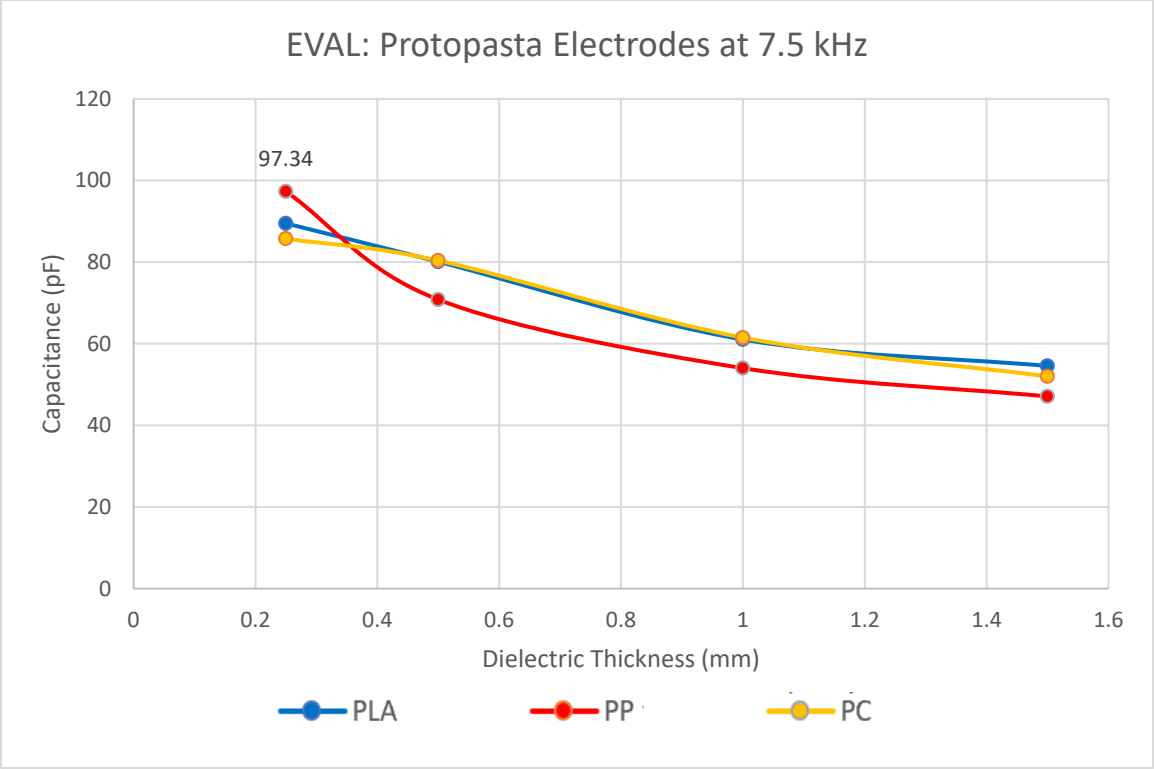

Figure 53: EVAL: Measurements: Protopasta Electrode at 7.5 Hz

The next figure displays the increase at the frequency of 10 kHz. The percent changes were PLA 0.85% decrease, PP 0.35% increase, and PC 3.74% increase. PC in this case demonstrated the highest percent change, although PLA was the only dielectric material that decreased its capacitance as frequency increased.

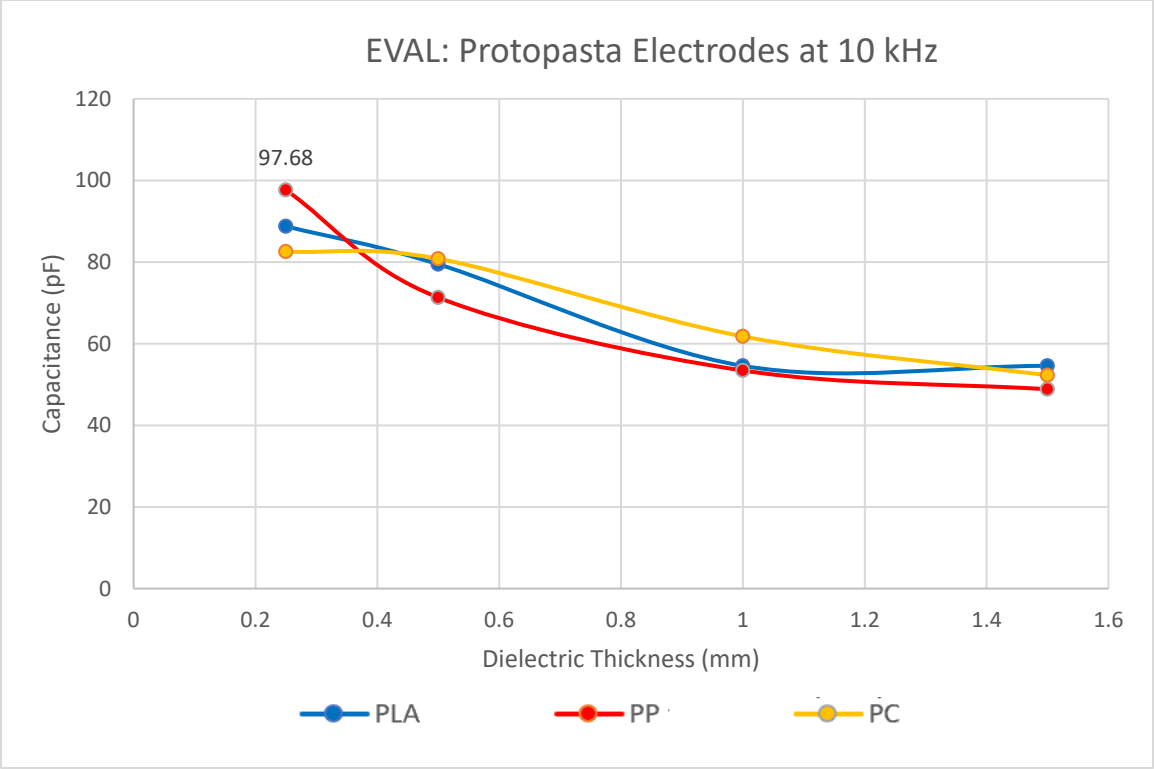

Figure 54: EVAL Measurements: Protopasta Electrode at 10 kHz

4.2.11 Observations Protopasta Electrode

The Protopasta electrode was a 3D printed electrode compared to the previous aluminum plate electrode measured. This capacitor exhibited different capacitance than the aluminum electrode and in some of the measurements above yielded a higher overall capacitance. The device that displayed the most consistent and similar results throughout was the LCR meter with the alligator clips. This method allowed various frequencies 100Hz, 120Hz, 1kHz, and 10 kHz. This comparison below was at the lowest frequency tested, 100 Hz; this frequency provided the highest capacitance values. For the results displayed with the LCR with alligator clips on the aluminum plates, The results were expected since the aluminum plate was made of pure conductive material.

On the other hand, the Protopasta is a fused thermoplastic material with additives of black carbon deposits. Therefore, it was not fully conductive when compared to aluminum.

Table 15: Aluminum Plate Capacitor vs Protopasta Electrode

Distance Thickness (mm)	Aluminum Plate Capacitor Capacitance (pF)	Protopasta Electrode Capacitor Capacitance (pF)
1.5	40.67	34.33
1	49.17	40.83
0.5	69.17	63.67
0.25	104	82.17

Some other observations concluded that as the dielectric thickness decreased, then the overall capacitance of the capacitor was increased. Also, when the frequency was increased, then the overall capacitance was decreased. In terms of which dielectric displayed the highest capacitance, the thermoplastics PP yielded the highest with PLA as the second.

4.2.12 Multimeter Results: Aluminum Electrodes, Protopasta Electrodes and Protopasta Fully-Fused Capacitor Model with PLA

The following sections exhibited the use of a fully printed capacitor compared to the previous capacitor models. The electrodes were printed with Protopasta, and the selected dielectric was PLA based on its ease of operation, print properties, and adhesion to other printed materials. The results emphasized that the inclusion of a parallel plate capacitor almost doubled the overall capacitance.

4.2.13 Multimeter Aluminum Electrode with PLA

The next three graphs below presented the comparison between the aluminum electrode with PLA (Figure 55) to the Protopasta printed electrodes and PLA (Figure 56) to the fully printed model (Figure 57).

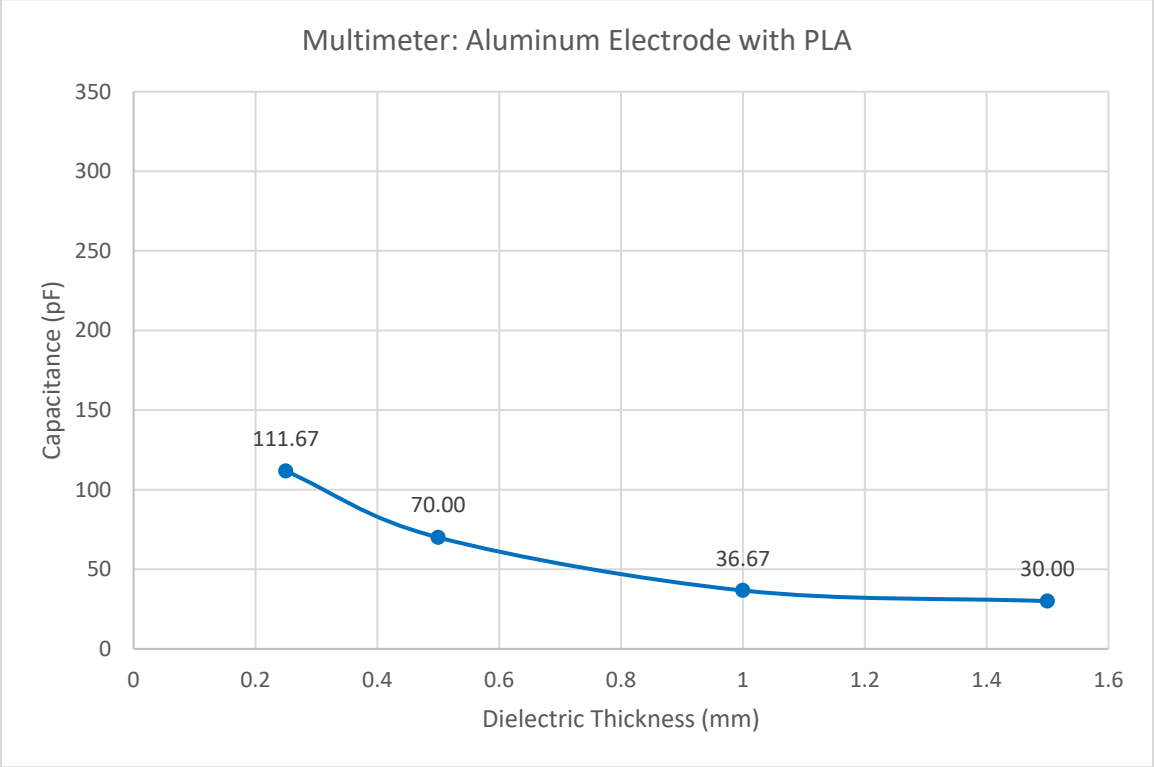

Figure 55: Multimeter: Aluminum Electrode Capacitor

As the data displayed below, the printed Protopasta electrode yielded higher capacitance than the capacitor with the aluminum plates.

4.2.14 Multimeter Protopasta Electrodes with PLA

The data below displayed the multimeter results with the Protopasta electrode capacitor model. The highest capacitance value at 136.67 was compared to the aluminum electrode at 111.67 pF.

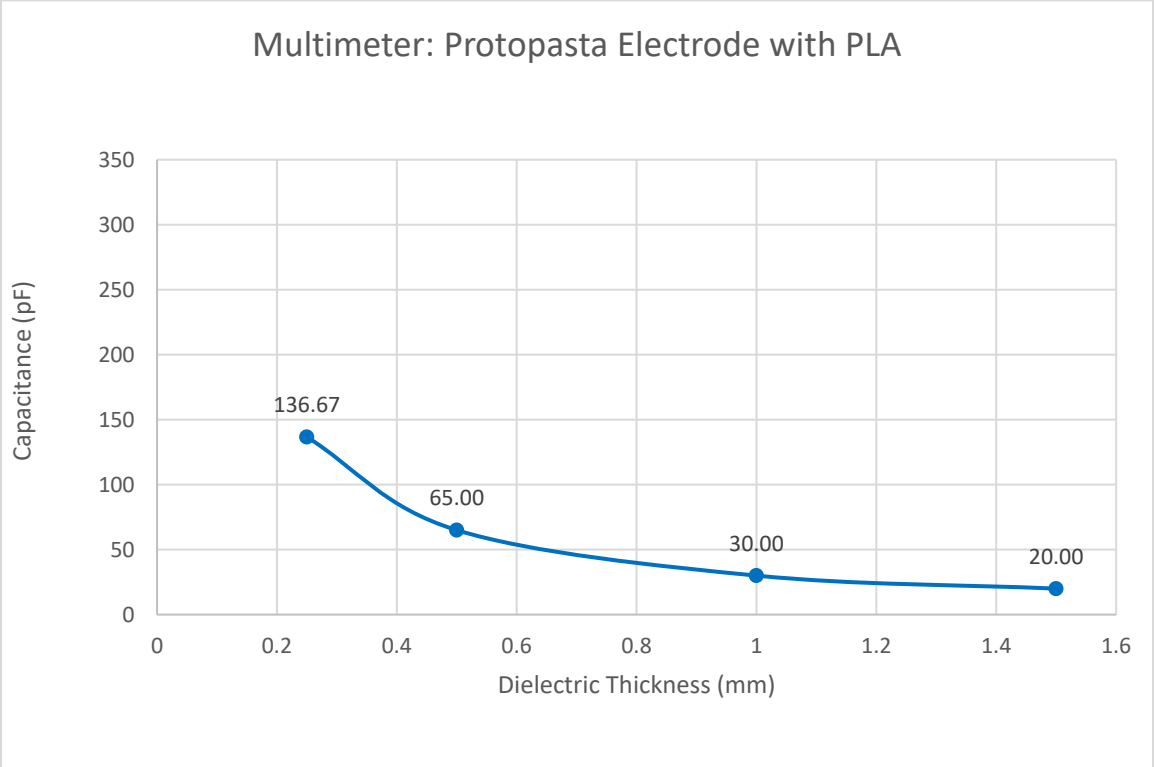

Figure 56: Multimeter: Protopasta Electrode with PLA

4.2.15 Fully-Fused Printed Protopasta with PLA

The figure below displayed the results for the dual extruder 3D printed capacitor. As the figure illustrated, the overall capacitance was almost doubled to 296.67 pF compared to 136.67 pF for the previous capacitor model.

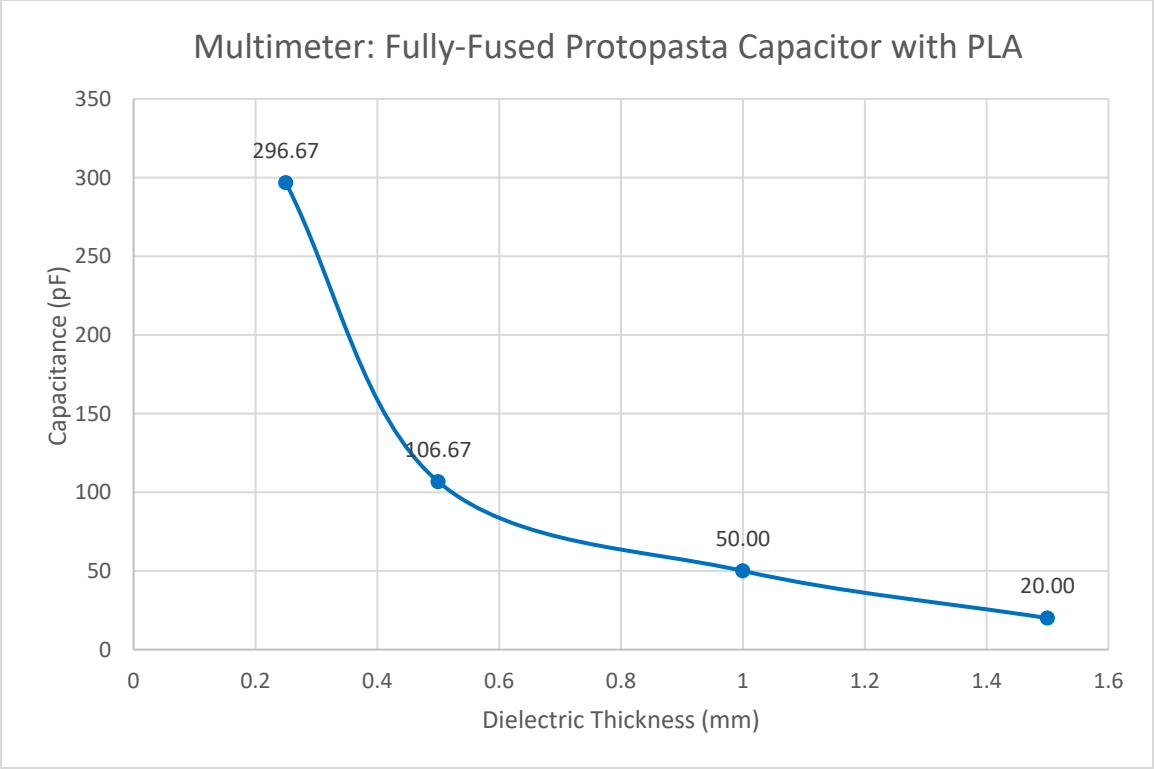

Figure 57: Multimeter: Fully-Fused Protopasta Capacitor with PLA

From Figure 58, it was observed that first being able to print with the Electrode with the Protopasta filament increased its capacitance compared to the wrought cut aluminum electrode model.

4.2.16 LCR with Probes Fully Printed Capacitor Fully-Fused Model

This section consisted of the same fully-fused capacitor model with PLA that implemented the dual extrusion capabilities. The yielded highest capacitance value at the dielectric thickness of 0.25 mm was 348.67 pF.

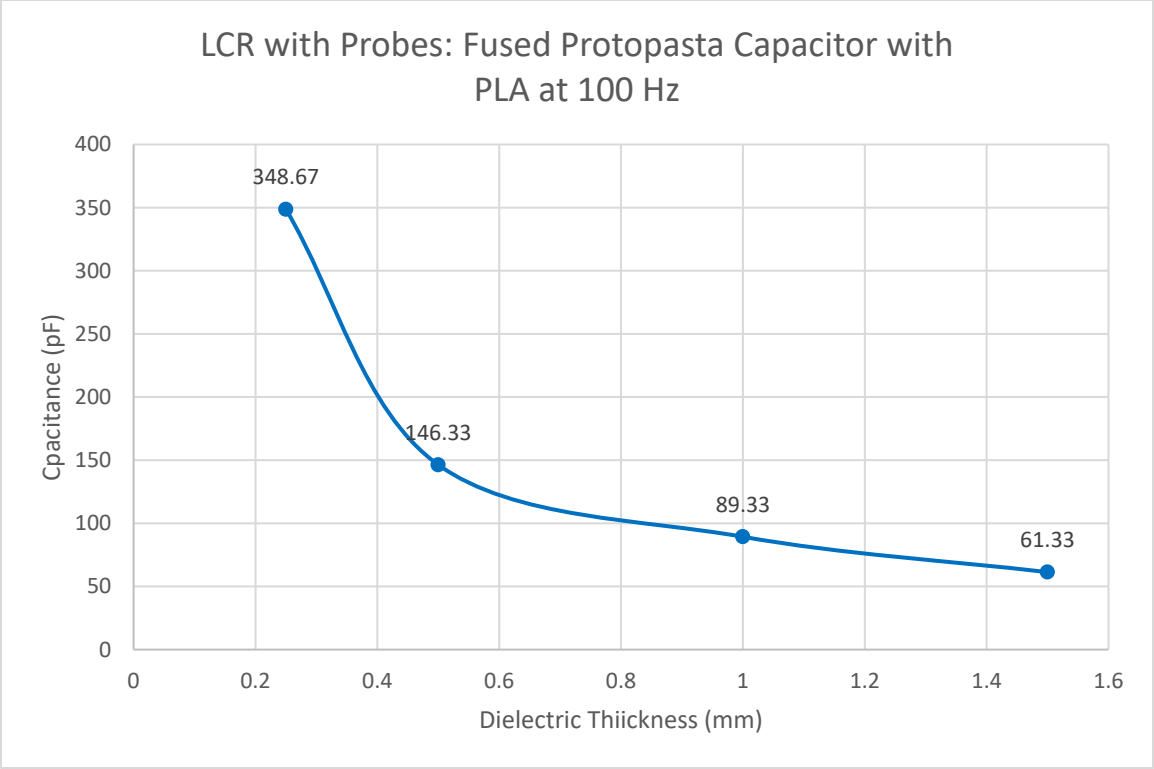

Figure 58: LCR with Probes: Fused Protopasta Capacitor with PLA at 100 Hz

Figure 59 displayed the same printed capacitor model with PLA as the dielectric at the frequency of 120 Hz. The percent change was 2.84% decrease as the frequency was increased.

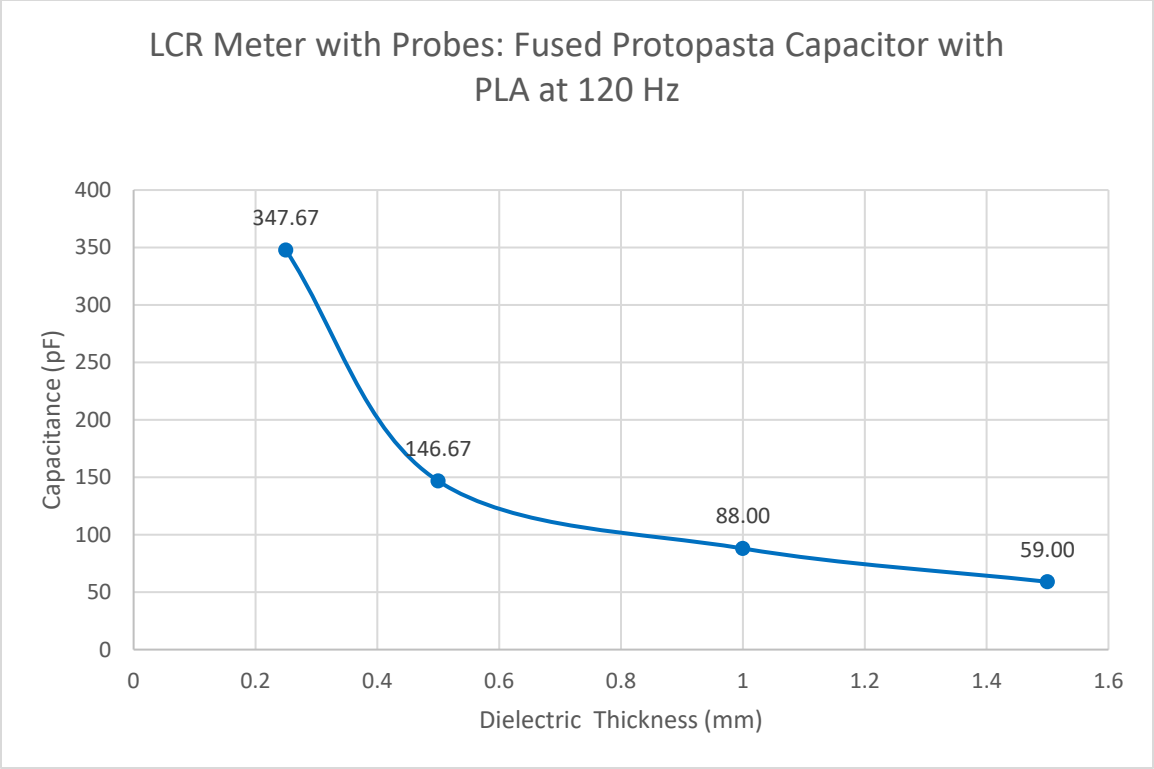

Figure 59: LCR with Probes: Fused Protopasta Capacitor with PLA at 120 Hz

Figure 60 displays the model at the increased frequency of 1 kHz. The percent change for the PLA model was an approximate 1.91% decrease from 347.67 to 337.80 pF.

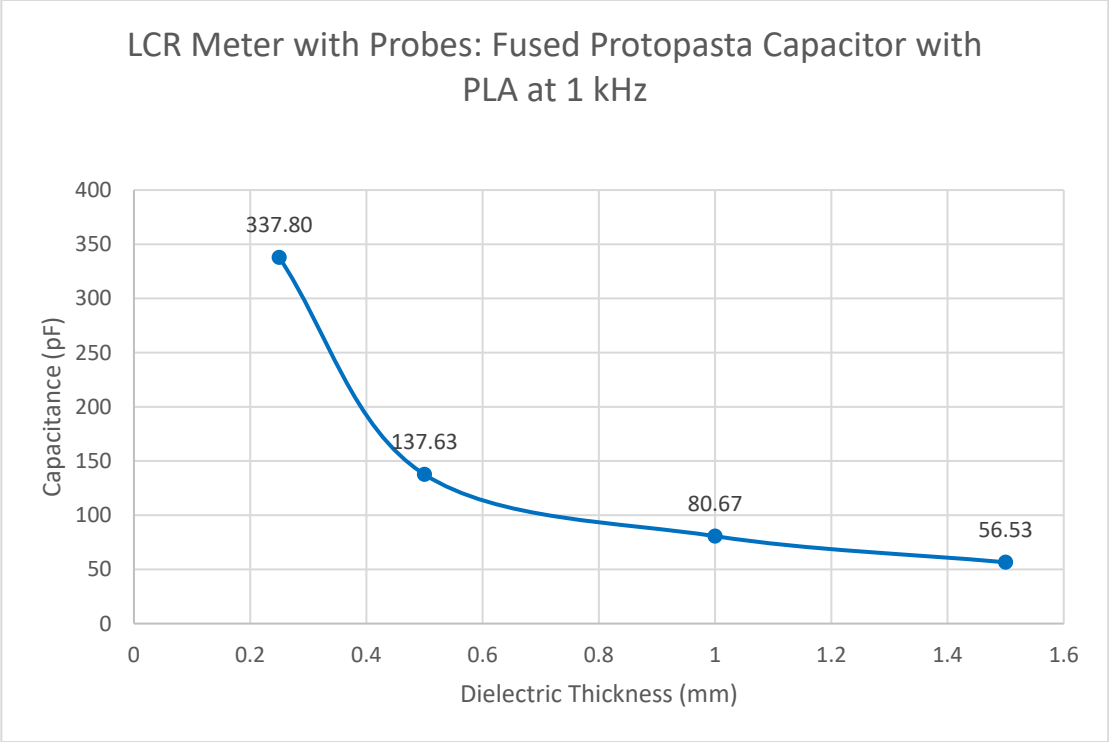

Figure 60: LCR with Probes: Fused Protopasta Capacitor with PLA at 100 Hz

Figure 61: LCR with Probes: displays the capacitance of the model at the increased 10 kHz frequency.

The percentage change was an estimated 1.66% for the model with the PLA dielectric medium.

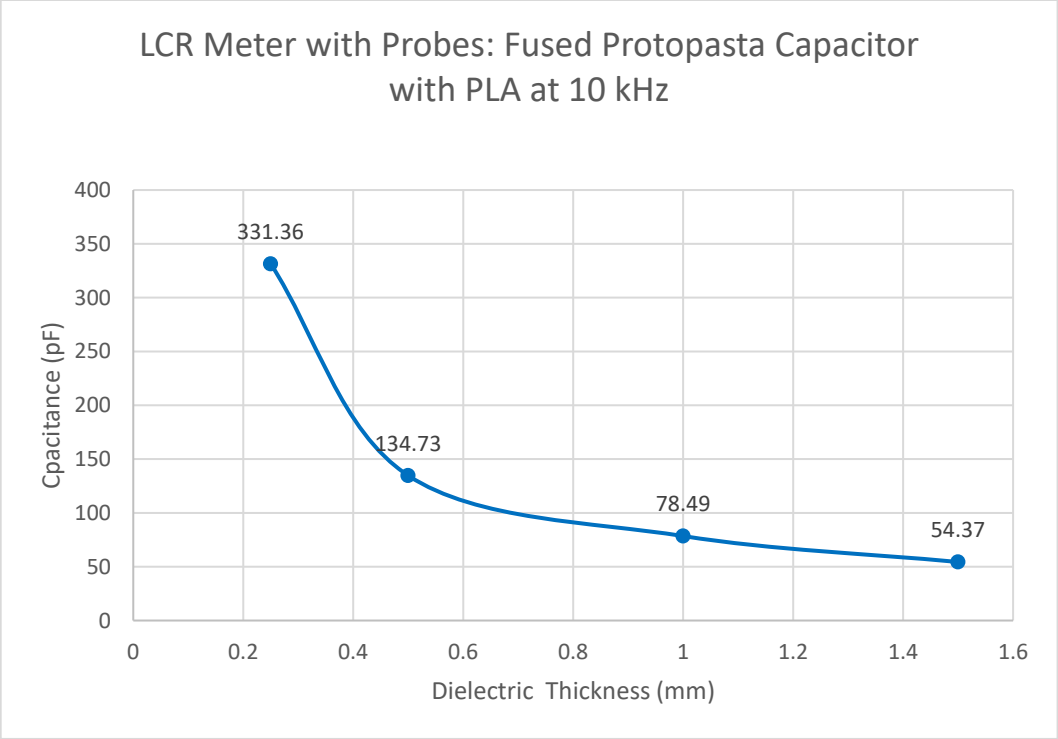

Figure 61: LCR with Probes: Fused Protopasta Capacitor with PLA at 100 Hz

4.2.17 LCR with Alligator Clips Protopasta Fully-Fused Model

The next figures below display the results for the different fully-fused models that utilized the LCR Meter with alligator clips instead of the probes. The percent decrease was also calculated as the previous sections.

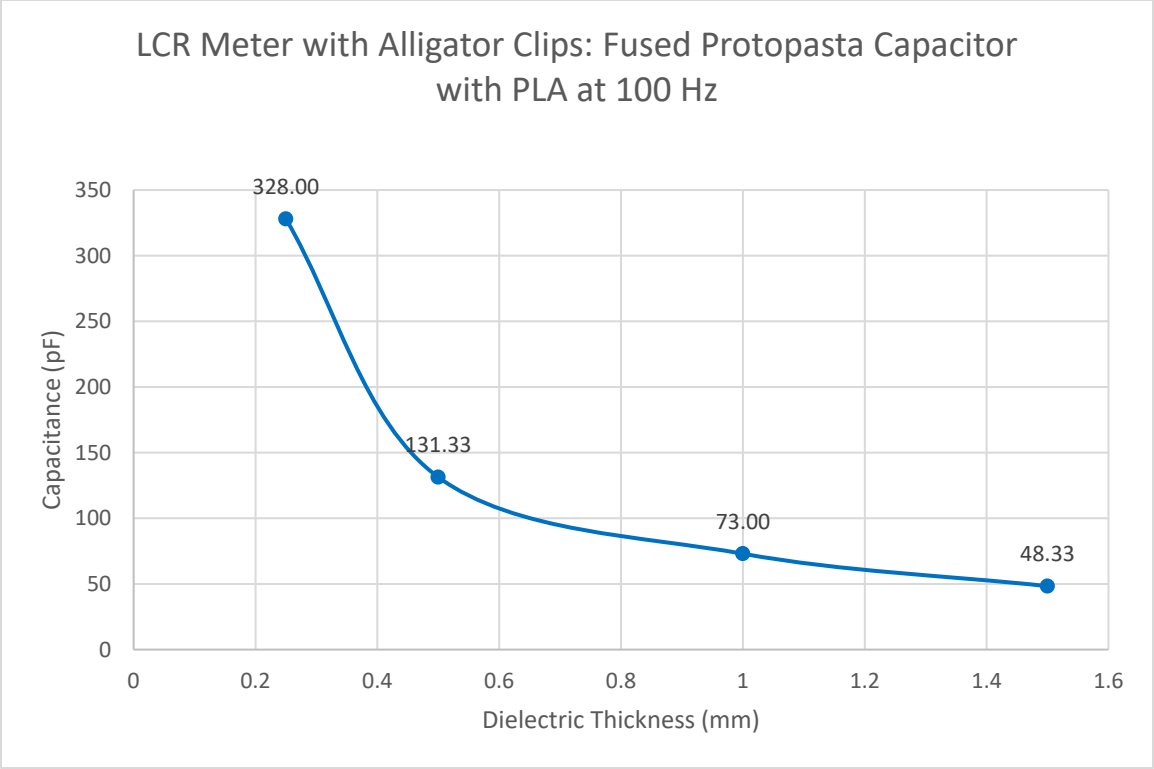

Figure 62: LCR with Alligator Clips: Fused Protopasta Capacitor with PLA at 100 Hz

Figure 63 displays the capacitance for the fully-fused model at 120 Hz. The decreased percent change yielded 0.31 %.

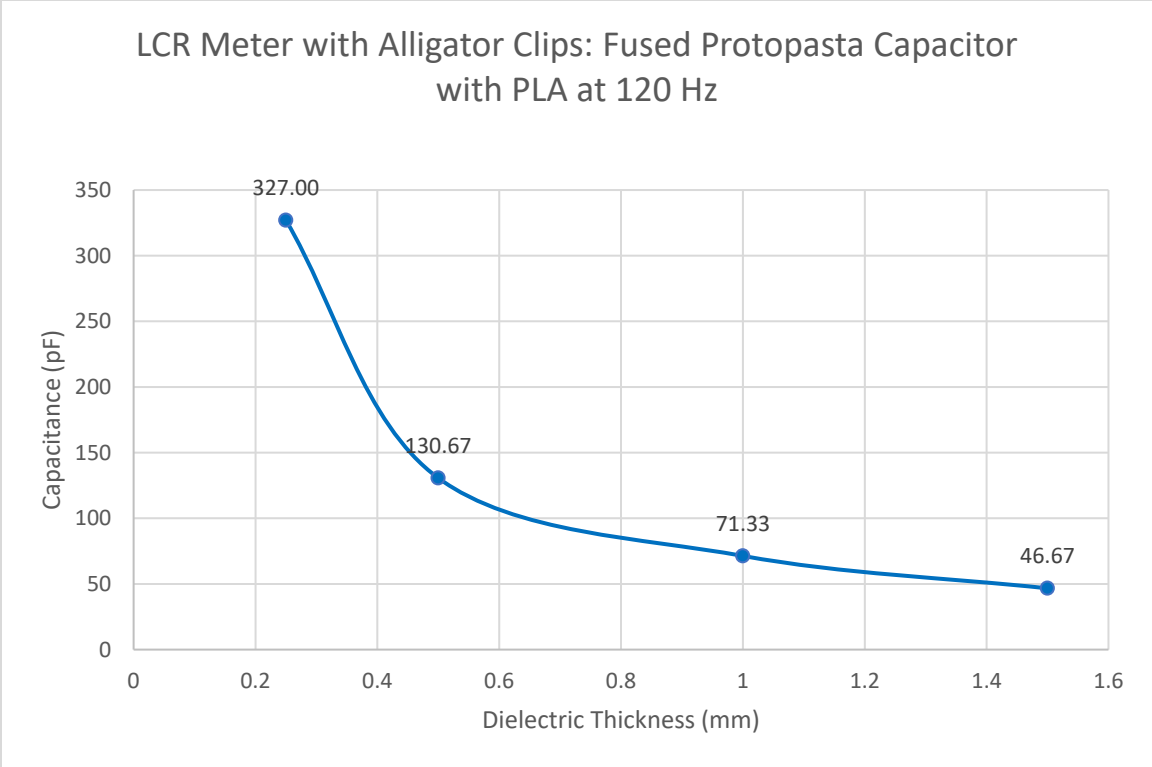

Figure 63: LCR with Alligator Clips: Protopasta Fully-Fused Model with PLA at 120 Hz

Figure 64 displays the capacitance for the fully-fused model at 1 kHz. The decreased percent change yielded 0.30 %.

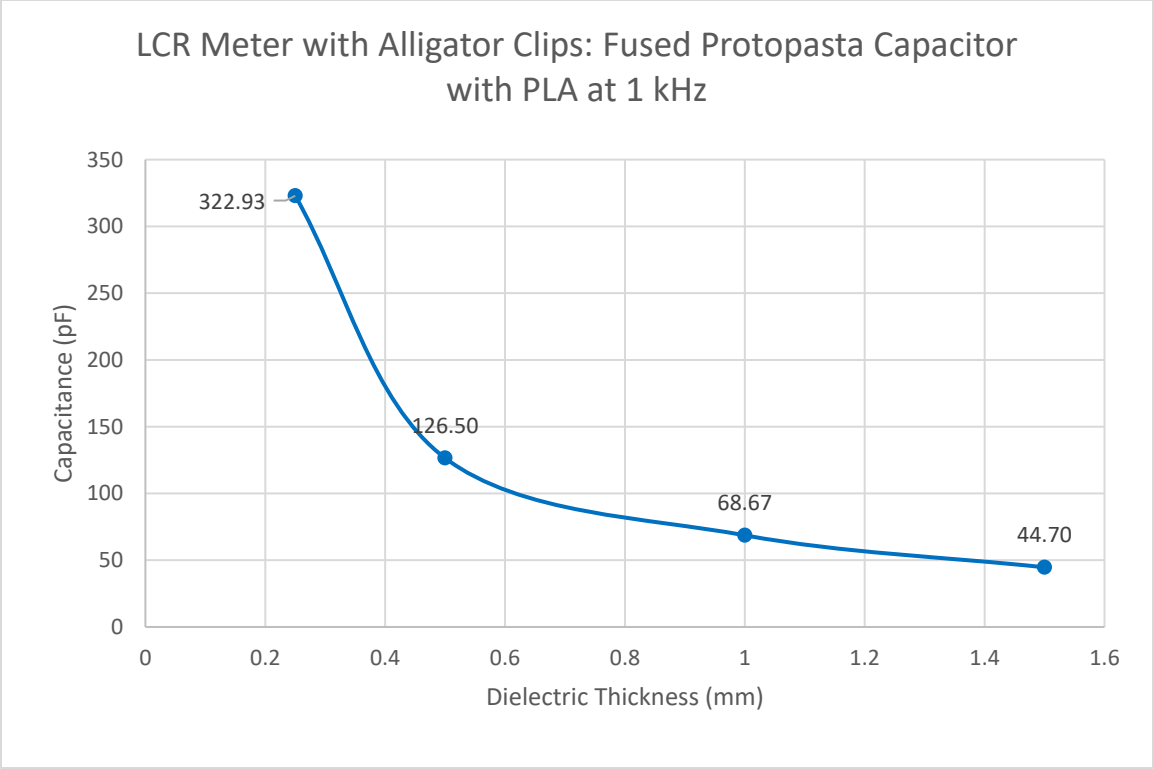

Figure 64: LCR with Alligator Clips: Fused Protopasta Capacitor with PLA at 1 kHz

The Figure 65 displays the fully-fused Protopasta capacitor at the frequency of 10 kHz. The percent decrease for that range from the previous frequency yielded 1.17%.

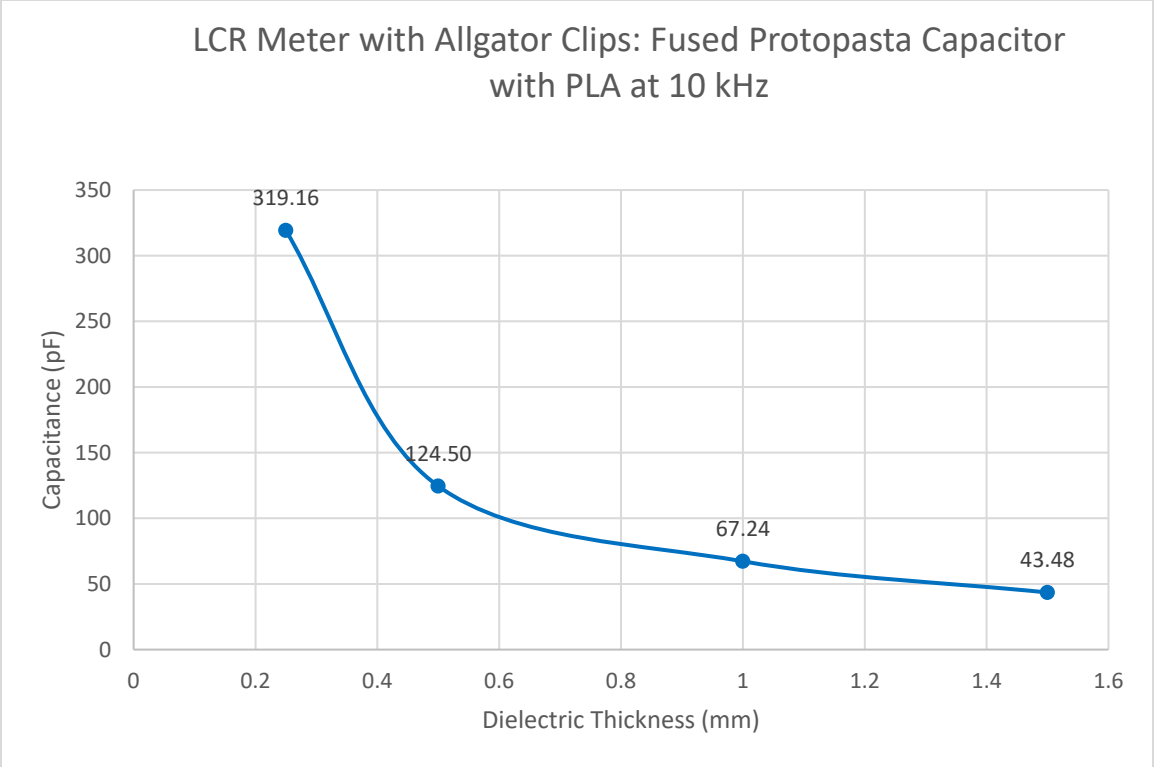

Figure 65: LCR with Alligator Clips: Protopasta Fully-Fused Model with PLA at 10 kHz

4.2.18 EVAL- Protopasta Fully-Fused with PLA

The following graphs displayed the capacitance measurements with the EVAL for the printed fully-fused Protopasta capacitor with PLA. The figure below displayed the capacitor with PLA at 1kHz.

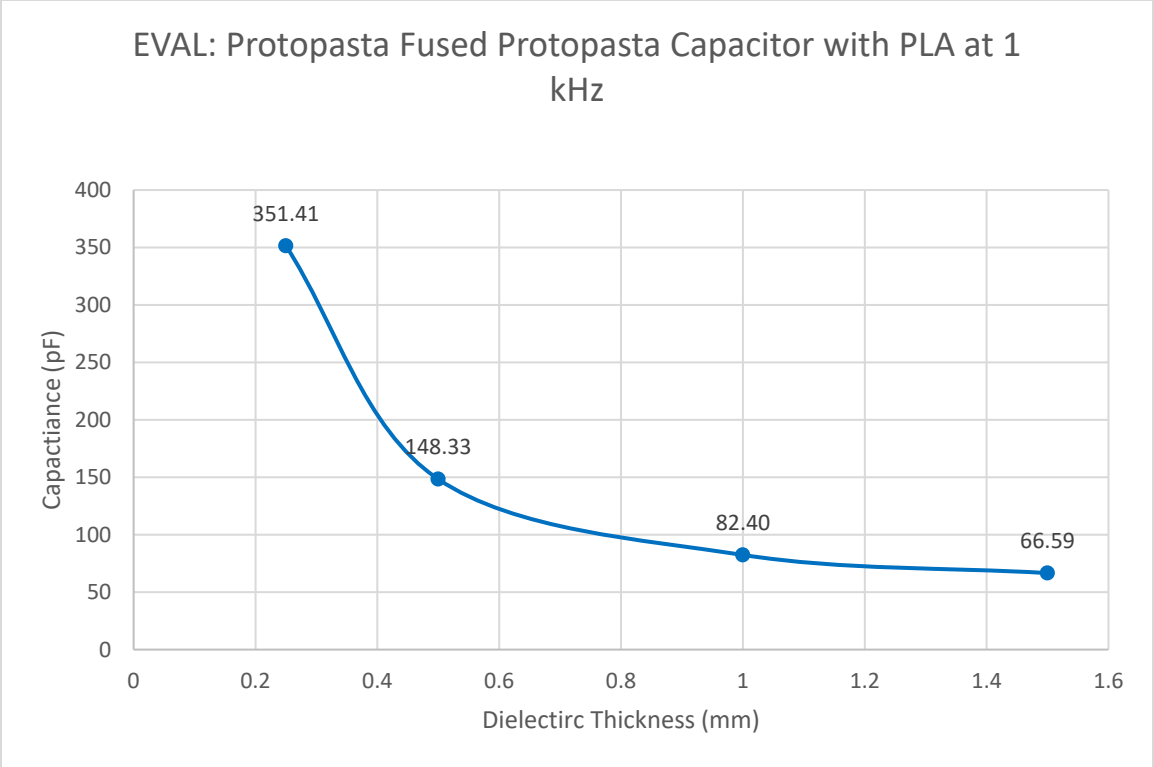

Figure 66: EVAL: Fused Protopasta Capacitor with PLA at 1 kHz

Figure 67 displayed the results at 5 kHz. The decreased percent change from the previous graph was 0.18%.

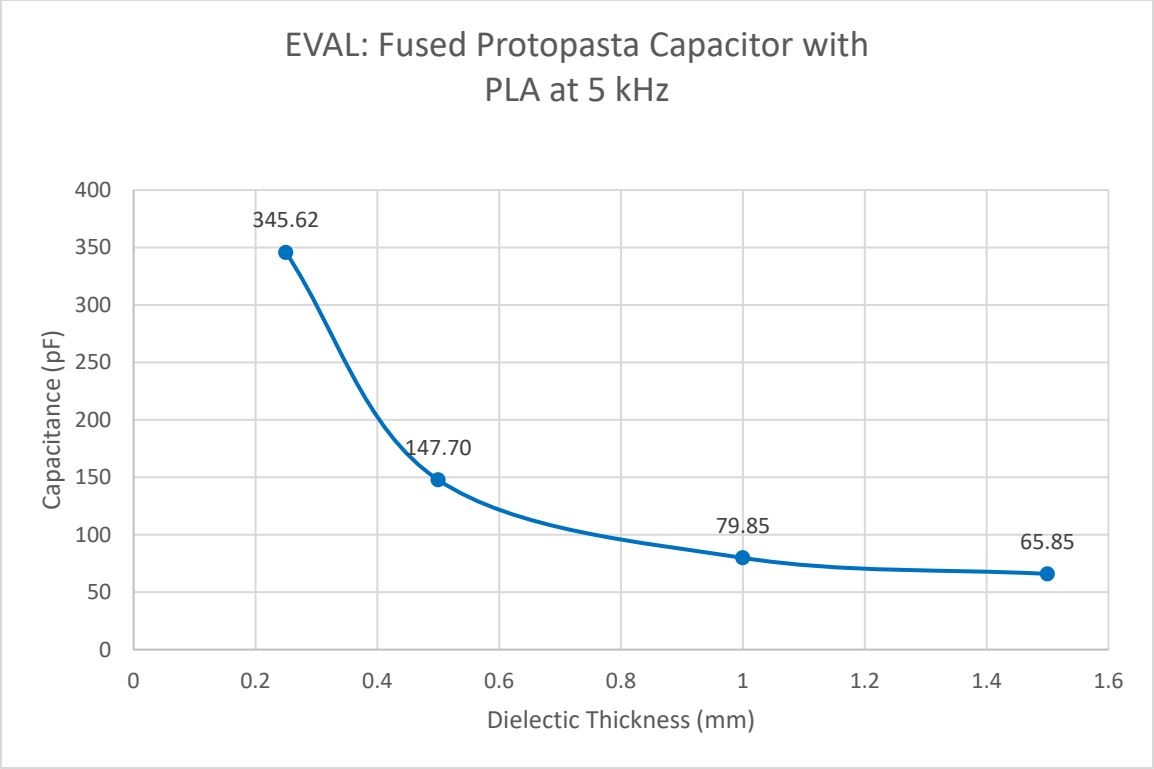

Figure 67: EVAL: Fused Protopasta Capacitor with PLA at 5 kHz

Figure 68 displayed the measurement results for the EVAL at the increased frequency of 7.5 kHz.

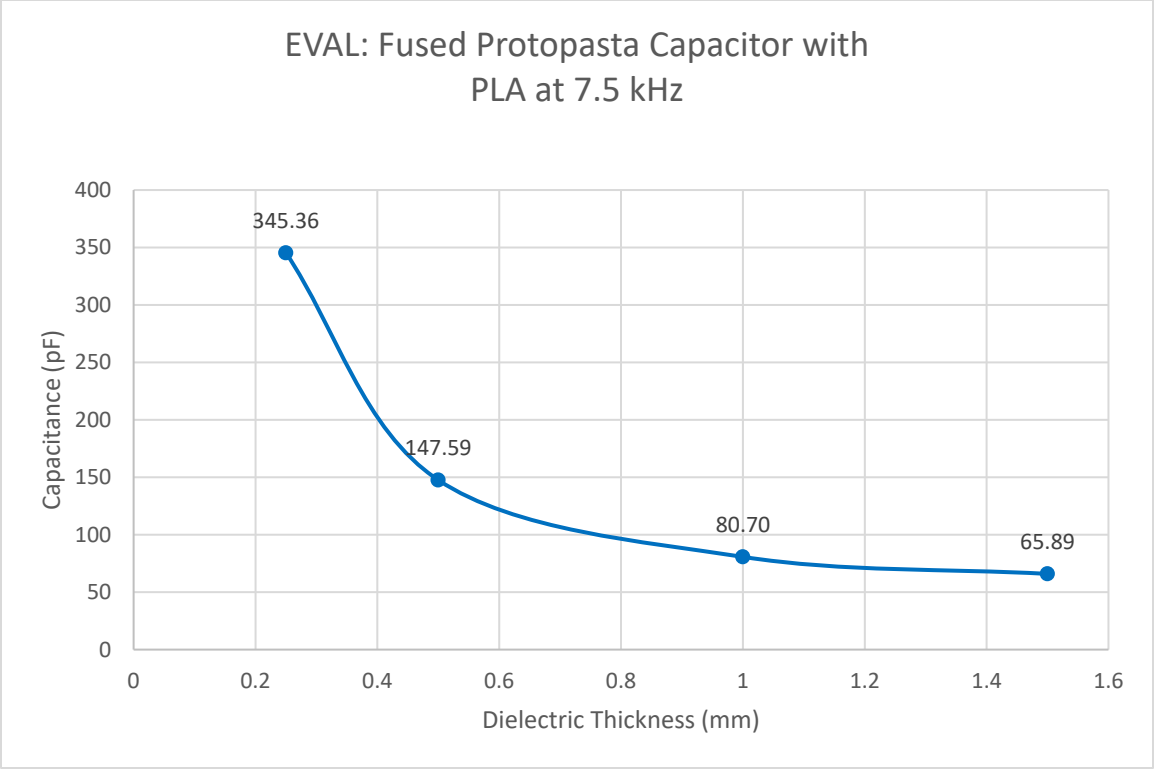

Figure 68: EVAL: Fused Protopasta Capacitor with PLA at 7.5 kHz

Figure 69 displayed the measurement results for the EVAL at the increased frequency of 10 kHz.

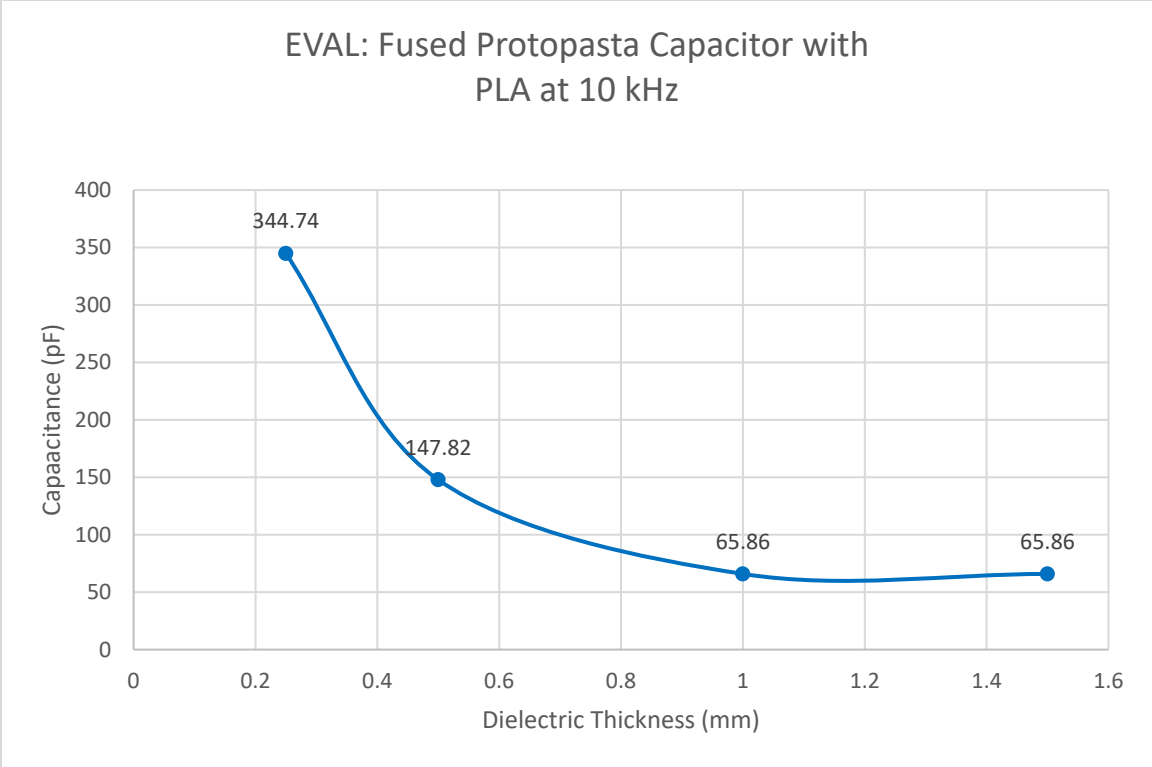

Figure 69: EVAL: Fused Protopasta Capacitor with PLA at 10 kHz

The fully-fused Protopasta capacitor was a 3D printed capacitor for which both the dielectric and conductive electrodes were fabricated .This capacitor exhibited three to four times overall higher capacitance than the printed capacitors with either aluminum or Protopasta electrodes. The measurement device that yielded the most consistent and similar results throughout was the LCR meter inclusive with the alligator clips. This method allowed testing at the frequencies of 100Hz, 120Hz, 1kHz, and 10 kHz. The comparison displayed in table 16 depicted the lowest frequency tested, 100 Hz; this frequency provided the highest capacitance values for the results displayed with the LCR meter and alligator clips for the aluminum electrode assembled capacitor.

Table 16 : Aluminum Plate Capacitor, Protopasta Plate Capacitor, and Fused Protopasta Capacitor

Dielectric Thickness (mm)	Aluminum Plate Capacitor Capacitance (pF)	Protopasta Electrode Capacitor Capacitance (pF)	Fused Protopasta Electrode Capacitor Capacitance (pF)
1.5	40.67	34.33	48.33
1	49.17	40.83	73.00
0.5	69.17	63.67	131.33
0.25	104	82.17	328.00

Table 17 depicted the highest capacitance with the use of various measurement devices. There are three different capacitor models exhibited in the table; aluminum, Protopasta, and the fused 3D printed capacitor model. The highest capacitor model was the fused 3D printed capacitor which displayed three to four times the capacitance of the regular aluminum and Protopasta model. This data demonstrated that at the lower frequency of 100 Hz, the capacitor models displayed the highest capacitance except for the fused model when measured with the EVAL device.

Table 17: Highest Capacitance Compared to Different Measurement Devices with PLA as the Dielectric (0.25 mm)

Method	Electrode Material	Maximum Capacitance	Frequency (Hz)
Multimeter	Aluminum	111.67	N/A
Multimeter	Protopasta	136.67	N/A
Multimeter	Fused 3D printed Capacitor	296.67	N/A
LCR with Probes	Aluminum	151.33	100.00
LCR with Probes	Protopasta	178.83	100.00
LCR with Probes	Fused 3D printed Capacitor	348.67	100.00
LCR with Alligator Clips	Aluminum	104.00	100.00
LCR with Alligator Clips	Protopasta	79.50	100.00
LCR with Alligator Clips	Fused 3D printed Capacitor	328.00	100.00
EVAL	Aluminum	103.86	7500.00
EVAL	Protopasta	89.50	7500.00
EVAL	Fused 3D printed Capacitor	351.41	1000.00

Figure 70 below depicted that when frequency was increased, then the capacitance also decreased. As displayed below, the average capacitance at 100 Hz yielded the highest result at 351.41 pF while the lowest capacitance ranged from 10 kHz at 344.74 pF.

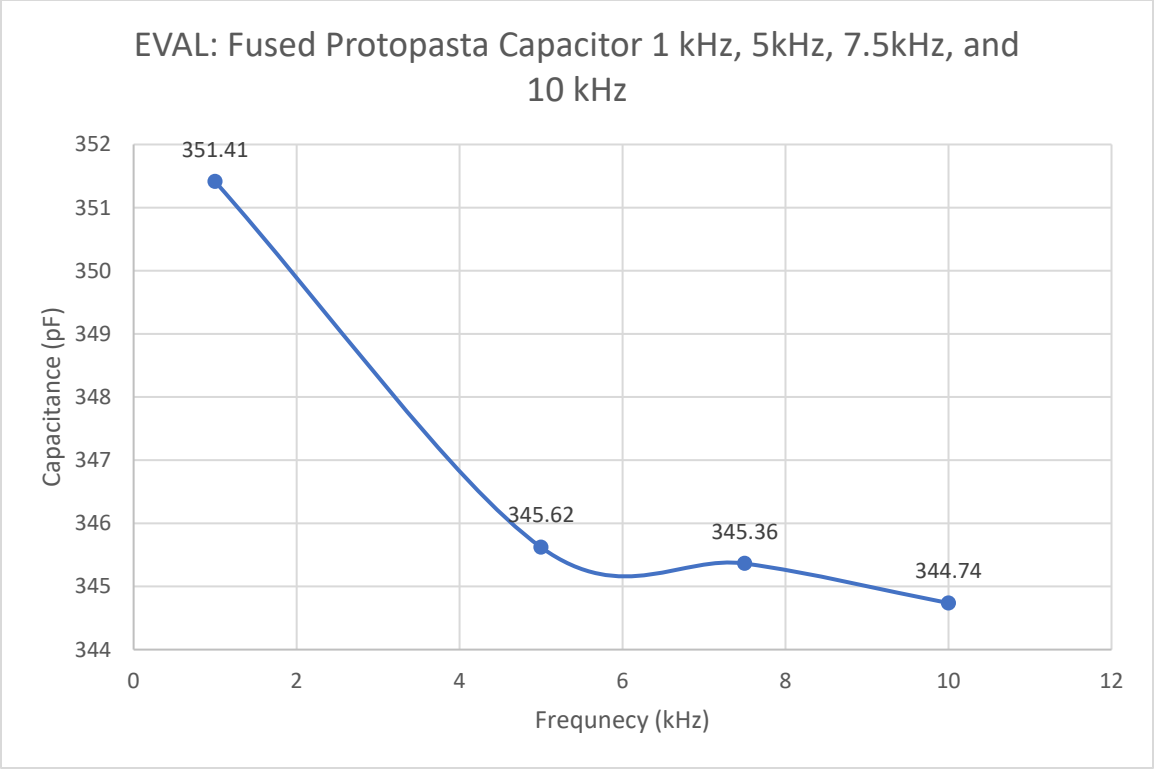

Figure 70: Fused Protopasta Capacitor 1 kHz, 5kHz, 7.5kHz, and 10 kHz

The overall results from this section indicate that when the frequency was increased, the maximum capacitance decreased. Furthermore, the data exhibited that the 3D printed fully-fused capacitor almost quadrupled the capacitance compared to the regular parallel plate capacitor models.

The initial test measurement used for this capacitor was based on the dimensions for testing the dielectric constant for a diameter size sample of 5 cm or 50 mm [44]. However, this article did not calculate the overall capacitance with white PLA based on the measured dielectric constant for a 1 mm sample and dielectric constant of 3.2. An ideal capacitance could still be calculated. From this data, the overall capacitance for this sample is displayed below. The capacitance for this measurement was approximately 55.6 pF.

$$C = \frac{\varepsilon * A * k}{d} = \frac{8.85 * 10^{-12} * 1963.5 * 3.2}{1} = 55.6\, pF$$

This value was equivalent to the ideal capacitance at the dielectric thickness of 1 mm. The overall total capacitance of this ideal model using the literature values for the dielectric material was lower than the measured capacitance for the fully-fused capacitor model. The fully-fused capacitor created and tested in this thesis was 73.00 pF with the LCR meter attached to the alligator clips at 100 Hz. This was a percent increase of 31.295%. Then, utilizing the same calculation as before for the dielectric thickness of 0.5 mm, the capacitance was calculated. This result is displayed below.

$$C = \frac{\varepsilon * A * k}{d} = \frac{8.85 * 10^{-12} * 1963.5 * 3.11}{0.5} = 108\, pF$$

This 108 pF was less than the measured capacitance of 131.33 pF of the created fully-fused capacitor at the same dielectric thickness. This was a percent increase of 23.45%. The highest increase in capacitance occurred when the dielectric material was printed at a thickness of 0.25 mm. However, this article only measured the dielectric of PLA at the thickness size of 1 mm and 0.5 mm. Using the same calculation as noted before, while also utilizing the dielectric constant with the dielectric thickness at 0.25 mm, the ideal capacitance was computed using the EVAL device in this research as provided below.

$$C = \frac{\varepsilon * A * k}{d} = \frac{8.85 * 10^{-12} * 1963.5 * 1.20}{0.25} = 83.4\, pF$$

This calculated capacitance at 83.4 pF was then compared to the capacitance of the fully-fused capacitor at 328.00 pF for the capacitor with a dielectric thickness of 0.25 mm. This is a percent increase of 253.448%. If the ideal capacitance was calculated using the dielectric values found in this thesis research as displayed below, then the calculated ideal capacitance of 50 x 50 mm squares would be approximately 106 pF compared to the fully-fused model at the same dielectric thickness using the EVAL device which was used to determine the dielectric constant at 1 kHz. The capacitance value at that desired thickness was 351.41 pF. This is a calculated percent increase of 231.519%.

$$C = \frac{\varepsilon * A * k}{d} = \frac{8.85 * 10^{-12} * 2500 * 1.20}{0.25} = 106\, pF$$

Even if the dielectric constant from the research article [44] for the higher dielectric constant of 3.2 was used with a thickness of 0.25 mm which was calculated below, the fully fused model at the thickness of same 0.25 mm overall capacitance was greater.

$$C = \frac{\varepsilon * A * k}{d} = \frac{8.85 * 10^{-12} * 1963.5 * 3.2}{0.25} = 223\, pF$$

According to the expected results as displayed in this thesis, when the dielectric thickness of material was increased, then the overall dielectric constant was also increased. The fully fused capacitor that was created and tested in this thesis yielded an overall capacitance of 328.00 pF, which was one of the lower measurements with the LCR using alligator clips compared to the EVAL at 1kHz which was 351.41 pF. This yielded an

overall percent increase of 47.09%, or in the case of the EVAL measurement at 1 kHz, which was a 57.58% increase.

4.3 Results-Dielectric Constant

The dielectric constant measurement was calculated by the EVAL device. This device measured the impedance of the model, then the capacitance was calculated in MATLAB. Figure 71 displayed the sample code that was utilized after it was used to calculate the capacitance and the dielectric constant. The capacitance was calculated by the formula below. This formula considered that the resistance was negligible, and the magnitude was the value Xc which was the capacitive reactance of the capacitor.

$$C = \left(\frac{1}{2*\pi} * f * mg\right) \tag{4}$$

This equation was derived from the formula for reactance which is depicted below.

$$X_c = \frac{1}{2*\pi*C} \tag{5}$$

$$X_c = mg \tag{6}$$

```
%% 1kHz and 1.5 mm

C_1_1_5= (1/(2*pi*f_1*mg_1_1_5))

k_1_1_5=C_1_1_5*d_1_5/(E0*A)

%% 1kHz and 1.00 mm

C_1_1_0= (1/((2*pi)*f_1*mg_1_1_0))

k_1_1_0=((C_1_1_0*d_1_0)/(E0*A))

%% 1 kHz and 0.5 mm

C_1_0_5= (1/((2*pi)*f_1*mg_1_0_5))

k_1_0_5=((C_1_0_5*d_0_5)/(E0*A))

%% 1kHz and 0.25 mm

C_1_025= (1/((2*pi)*f_1*mg_1_0_25))

k_1_025=((C_1_025*d_0_25)/(E0*A))

```

Figure 71: Sample MATLAB Code for Calculation of Dielectric Constant

The dielectric constant was calculated by the formula above and the sample outputs were displayed in the figure below.

```
C_1_1_5 =

   5.1126e-11


k_1_1_5 =

    3.4645


C_1_1_0 =

   6.4604e-11


k_1_1_0 =

    2.9186
```

Figure 72: Example MATLAB Outputs for Capacitance and Dielectric Constant

Figure 73 exhibited the data for the variations of dielectric thickness at increasing frequencies (1kHz, 5kHz, 7.5 kHz, 10 kHz). The data depicted demonstrated that by increasing the dielectric thickness, then the overall dielectric constant was also increased.

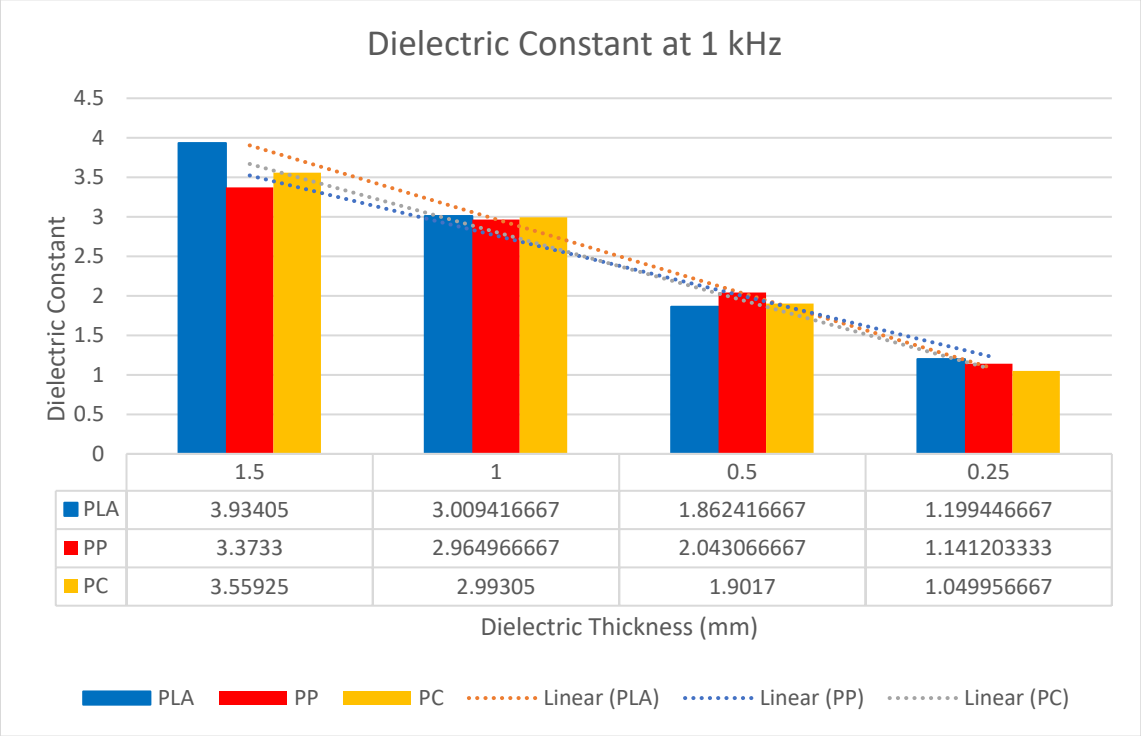

Figure 73: Derived Dielectric Constant at 1 kHz

Figure 74 depicted the dielectric constant at an increased frequency of 5 kHz. When the frequency was increased based on the data, then the overall dielectric proportionally increased. The figure below depicted the same pattern as before; when the dielectric thickness was increased, then the overall dielectric constant increased.

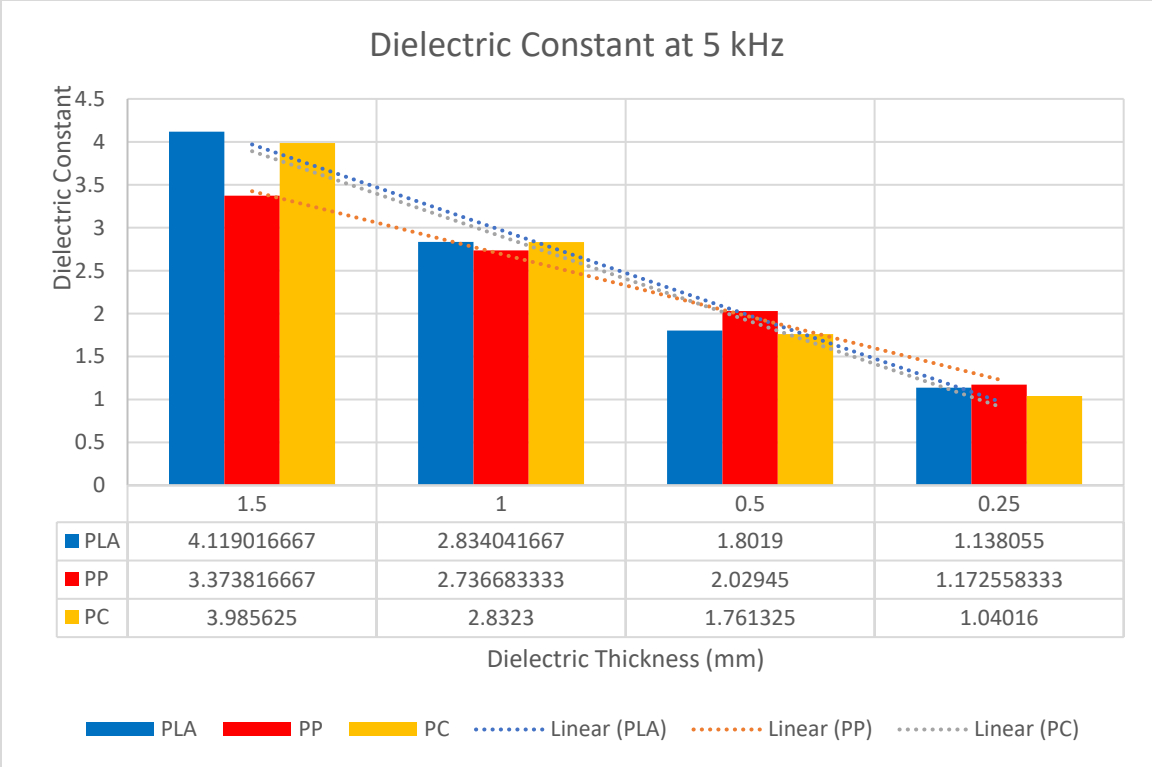

Figure 74: Derived Dielectric Constant 5 kHz

Figure 75 exhibits the dielectric constant results at the increased frequency of 7.5 kHz. The figure below depicted the same pattern as before; when the dielectric thickness was increased, then the overall dielectric constant increased.

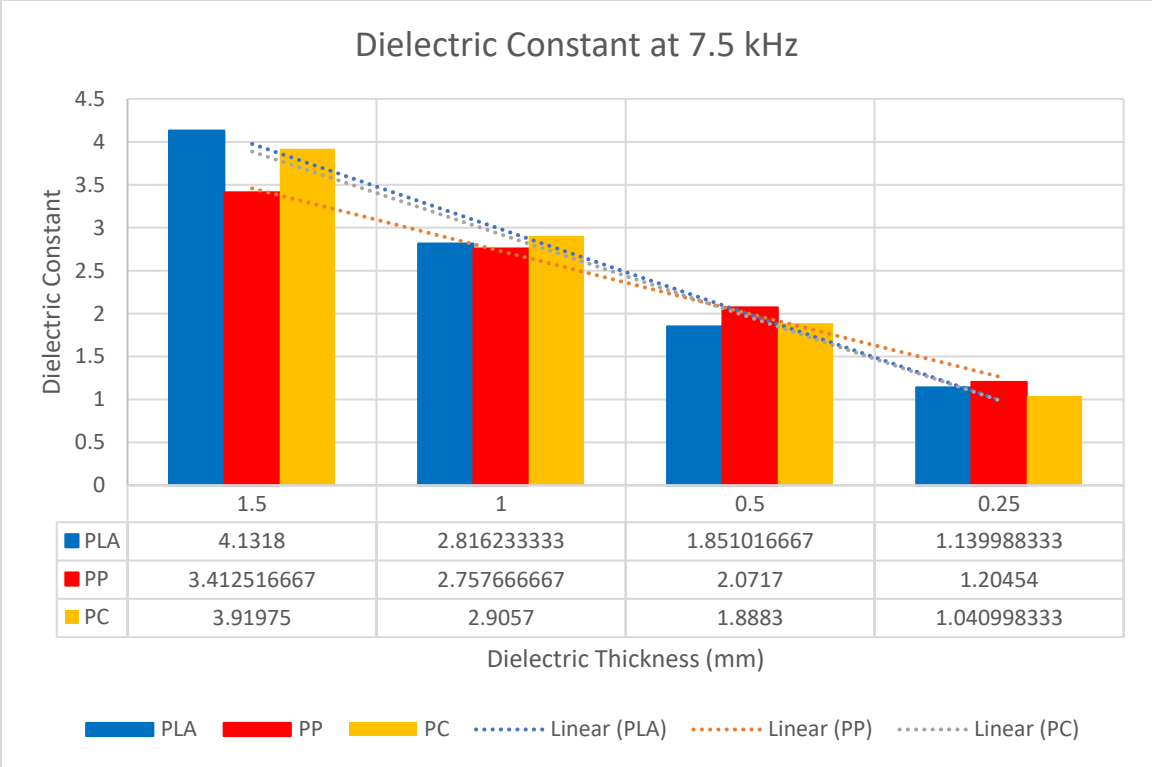

Figure 75: Derived Dielectric Constant 7.5 kHz

Figure 76 displays the dielectric constant at the frequency of 10 kHz. The figure below depicted the same pattern as before; when the dielectric thickness was increased, then the overall dielectric constant increased.

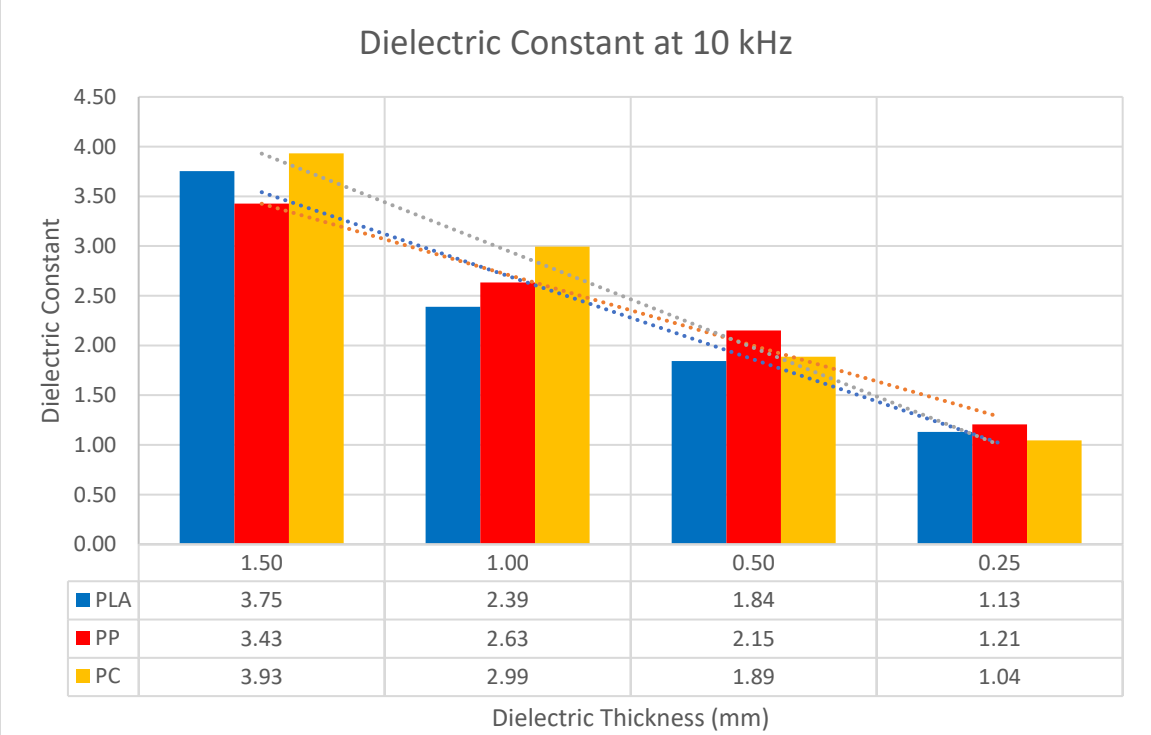

Figure 76: Derived Dielectric Constant at 10 kHz

The data collected was in the range of the values found in the research. The reported dielectric constant was at 2.7 for a 3 mm sample. One discrepancy between the literature values and the data exhibited above was that the dielectric measurements were taken at different frequencies. The previous values in the research were measured at the high frequencies at the 1 MHz level. The method utilized in the previous literature was printed at a disk shape of 54 mm with a thickness of 3 mm using an 0.4 mm nozzle at the frequency of 1 MHz [53]. As exhibited through the recent bar graphs above, the increased dielectric material thickness also increased the overall dielectric constant. These results displayed that when the frequency was increased, then the overall dielectric constant decreased for the thermoplastic PLA material.

CHAPTER 5

CONCLUSION AND FUTURE WORK

5.1 Conclusion

The first major contribution of this research was the design and fabrication of a fully-fused 3D printed capacitor using a simultaneous dual extrusion process with conductive and dielectric filaments. The overall capacitance of a fused 3D printed capacitor displayed three to four times compared to the traditional aluminum parallel plate capacitor. This fully-fused 3D printed capacitor, which implemented Protopasta conductive filament for the electrodes and PLA as a dielectric, yielded the highest overall capacitance when measured at 100 Hz. The LCR meter measured the overall capacitance with alligator clips to be 348.67 pF compared with the aluminum parallel plate capacitor at 151.33 pF, which illustrates an increase of 215.39% using the 3D printed fabrication technique.

The second significant contribution of this research was the utilization of a high-resolution 0.25 mm nozzle and the exploration of printing different conductive materials with this novel size. Preliminary print jobs with Electrifi conductive filament resulted in problems associated with clogging the print nozzle. However, Protopasta conductive filament was successfully extruded through the reduced nozzle size of 0.25 mm. A multimeter was used to measure the resistance of the printed material. Several other conductive filaments (marketed as antibacterial) were tested in the development of a fully-fused 3D printed capacitor. However, it was found that these filaments did not print

accurately with the 0.25 mm print nozzle, nor did they contain enough conductive material for use in the design of an electrode.

The third contribution was the measurement and calculation of the dielectric constant of different thermoplastics at various low-range frequencies since the values found in the literature were at a higher range from 1MHz-100MHz. This research yielded the dielectric constants of each material PLA, PP, and PC at the frequencies of 1 kHz, 5 kHz, 7.5 kHz, and 10 kHz. As expected, the results demonstrated that as the dielectric thickness increased, the dielectric constant also increased.

The fourth contribution of this research was the analysis of the percent change in the dielectric constant for several common FDM polymer filament materials at different frequencies. PLA and PP yielded the highest percent change when averaged across all measured frequencies. This indicates that these materials that could be implemented for the design of tunable 3D printed capacitors that have operating requirements over a diverse range of frequencies.

5.2 Future Work

This research demonstrates the successful design and fabrication of a fully-fused 3D printed capacitor through low-cost, dual-extrusion FDM fabrication methods. However, there are still many issues that remain before this technology could be commercialized. First, the overall footprint of the fully-fused 3D printed capacitor needs to be decreased, as this capacitor is significantly larger compared to other capacitors on the market today. However, this 3D printed capacitor allows for flexibility and durability based upon the properties of the thermoplastic filament materials.

Future work should include resolving the nozzle-clogging issues experienced when printing with Electrifi conductive filament. The material properties published by the manufacturer of Electrifi indicate a significantly higher conductivity when compared to Protopasta. As a result, it is anticipated that the measured capacitance in a fully-fused 3D printed capacitor would be substantially higher using the Electrifi conductive filament. Another benefit of printing with Electrifi over Protopasta is that Electrifi material is more flexible. Further experimentation on how the different nozzle diameters affect the overall electrical properties of a fully-fused 3D printed capacitor can be explored as well.

Another feature to be researched in the future that concerns a capacitor's quality is the (Equivalent Series Resistance). This is the "sum of in-phase AC resistance of a capacitor and implemented to rate a capacitor's quality" [54]. A calculated ideal capacitance would have a loss which is equivalent to an ESR of zero. The LCR meter that was implemented in this thesis can be utilized to also measure the loss tangent of the capacitance to truly exhibit if this capacitor can work in an electrical circuit properly.

Furthermore, another benefit of 3D printing are its capabilities of being able to print complex structures and geometries. Also, the capacitor design of an interdigitated capacitor is a plausible future topic. This opens the door for future testing knowing that possibly increasing the print z-direction increases the capacitance, while printing multiple fingers and interconnected parts increases the capacitance as well. One question explored in future research could be "how does changing the print orientation affect the final resistance?" The question regarding print orientation is conceived based on the datasheet provided by Protopasta below. Due to time constraints, this question could not be answered using the test samples printed.

REFERENCES

[1] "3D Printed Electronics - Aerosol Jet Technology - Optomec", *Optomec*, 2021. [Online].

[2] B. Vayre, F. Vignat and F. Villeneuve, "Designing for Additive Manufacturing", *Procedia CIRP*, vol. 3, pp. 632-637, 2012. Available: 10.1016/j.procir.2012.07.108.

[3] "Additive Manufacturing vs 3D Printing | GE Additive", *Ge.com*, 2021. [Online].: [Accessed: 10- Apr- 2021].

[4] K. Snikhovska, "Seven Types of 3D Printers - Different printing and extruder technologies", *Pen and Plastic*, 2021. [Online].

[5] "Designifying | 3d Printing 3D Scanning services provider Companies Gurgaon Delhi", *Designifying.com*, 2021. [Online].

[6] I. Yadroitsev, P. Bertrand and I. Smurov, "Parametric analysis of the selective laser melting process", *Applied Surface Science*, vol. 253, no. 19, pp. 8064-8069, 2007. Available: 10.1016/j.apsusc.2007.02.088.

[7] K. Snikhovska, "Seven Types of 3D Printers - Different printing and extruder technologies", *Pen and Plastic*, 2021. [Online].

[8] "Types of 3D Printers: Complete Guide - SLA, DLP, FDM, SLS, SLM, EBM, LOM, BJ, MJ Printing", *3D Insider*, 2021. [Online].

[9] D. Jafari and W. Wits, "The utilization of selective laser melting technology on heat transfer devices for thermal energy conversion applications: A review", *Renewable and Sustainable Energy Reviews*, vol. 91, pp. 420-442, 2018. Available: 10.1016/j.rser.2018.03.109.

[10] "The Ultimate Guide to Stereolithography (SLA) 3D Printing", *Formlabs*, 2021. [Online].

[11] N. Ltd., "Top Multi-Layer 3D-Printer AME Manufacturing Company | Nano Dimension", *Nano-di.com*, 2021. [Online].

[12] Sukeshini A., M., Meisenkothen, F., Gardner, P. and Reitz, T., 2013. Aerosol Jet® Printing of functionally graded SOFC anode interlayer and microstructural investigation by low voltage scanning electron microscopy. *Journal of Power Sources*, 224, pp.295-303.

[13] "3D Printed Electronics - Aerosol Jet Technology - Optomec", *Optomec*, 2021. [Online]. Available: https://optomec.com/printed-electronics/aerosol-jet-technology/.

[14] "What is SLA 3D Printing? -Pros & Cons | Maker Freedom", *Maker Freedom*, 2021. [Online].

[15] "How to design parts for SLA 3D printing | Hubs", *Hubs.com*, 2021. [Online].

[16] P. Flowers, C. Reyes, S. Ye, M. Kim and B. Wiley, "3D printing electronic components and circuits with conductive thermoplastic filament", *Additive Manufacturing*, vol. 18, pp. 156-163, 2017. Available: 10.1016/j.addma.2017.10.002.

[17] E. Grames, "What is FDM 3D Printing? – Simply Explained", *All3DP*, 2021. [Online].

[18] "3D Printing Resolution: High or Low?", *Additivemanufacturing.media*, 2021. [Online].

[19] X. Aeby, R. van Dommelen and D. Briand École Polytechnique Fédérale de Lausanne, "Fully FDM 3D Printed flexible Capacitive and Resistive Transducers", 2019.

[20] "Capacitors - Engineering and Technology History Wiki", *Ethw.org*, 2021. [Online].

[21] "What Are Applications of Capacitors?", *Lifewire*, 2021. [Online].

[22] A. Nishino, "Capacitors: operating principles, current market and technical trends", *Journal of Power Sources*, vol. 60, no. 2, pp. 137-147, 1996. Available: 10.1016/s0378-7753(96)80003-6.

[23] "Capacitor Market Size, Share 2021, Trend, Industry Update, Global Market Player, Top Researcher, Future Demand, Strategic Planning, Revenue, Forecast To 2025", *Wboc.com*, 2021. [Online].

[24] M. Inc., "The role of a Capacitor in Electronic Components? | Matsusada Precision", *Matsusada Precision*, 2021. [Online].

[25] "Lumen Learning – Simple Book Production", Courses.lumenlearning.com, 2021. [Online].

[26] "Lumen Learning – Simple Book Production", Courses.lumenlearning.com, 2021. [Online].

[27] J. Celaya, C. Kulkarni, S. Saha, G. Biswas and K. Goebel, "Accelerated aging in electrolytic capacitors for prognostics", *2012 Proceedings Annual Reliability and Maintainability Symposium*, 2012. Available: 10.1109/rams.2012.6175486.

[28] Mica Capacitor Construction, Working and Its Applications", *ElProCus - Electronic Projects for Engineering Students*, 2021. [Online].

[29] "Chapter 2: Film Capacitor", *EE Power*, 2021. [Online].

[30] A. Shaik, "Electronics Tutorial, Basic Physics, Online Tests, Computer Basics, Concepts of Physics", *Physics-and-radio-electronics.com*, 2021. [Online].

[31] I. Celland and R. Price, "Polymer Film Capacitor", 2011.

[32] "Paper Capacitor : Construction, Types, Working & Its Advantages", *ElProCus - Electronic Projects for Engineering Students*, 2021. [Online].

[33] "What Is Non-polarized Capacitor", *Apogeeweb*, 2021.

[34] G. Gudavalli and T. Dhakal, "Simple Parallel-Plate Capacitors to High–Energy Density Future Supercapacitors", *Emerging Materials for Energy Conversion and Storage*, pp. 247-301, 2018. Available: 10.1016/b978-0-12-813794-9.00008-9.

[35] "Ceramic Capacitor Market Size 2021 - Top 3 Reason For Industry to Grow at High CAGR, Growth Factors, Industry Demand and Forecast to 2026 |Major companies : Murata, Samsung Electro, TDK Corporation [Reports Page No 119]", *Wicz.com*, 2021. [Online].

[36] "Capacitor & Types Of Capacitors | Fixed, Variable, Polar & Non-Polar", *ELECTRICAL TECHNOLOGY*, 2021. [Online].

[37] "Energy Stored in Capacitors | Physics II", *Courses.lumenlearning.com*, 2021. [Online]. Available: https://courses.lumenlearning.com/austincc-physics2/chapter/19-7-energy-stored-in-capacitors/.

[38] "Energy Stored in Capacitors | Physics II", *Courses.lumenlearning.com*, 2021. [Online].

[39] X. Chen, R. Paul and L. Dai, "Carbon-based supercapacitors for efficient energy storage", *National Science Review*, vol. 4, no. 3, pp. 453-489, 2017. Available: 10.1093/nsr/nwx009.

[40] P. Flowers, C. Reyes, S. Ye, M. Kim and B. Wiley, "3D printing electronic components and circuits with conductive thermoplastic filament", *Additive Manufacturing*, vol. 18, pp. 156-163, 2017. Available: 10.1016/j.addma.2017.10.002.

[41] "D-Bot Core-XY 3D Printer by spauda01", *Thingiverse.com*, 2021. [Online].

[42] X. Aeby, R. van Dommelen and D. Briand École Polytechnique Fédérale de Lausanne, "Fully FDM 3D Printed flexible Capacitive and Resistive Transducers", 2019.

[43] Fused Filament Fabrication of Electronic Circuits and Components with Conductive Thermoplastics", *International Research Journal of Engineering and Technology*, 2021.

[44] P. Veselý, E. Horynová, T. Tichý and O. Šefl, "Study of electrical properties of 3D printed objects", 2018.

[45] "Ultimaker S5 Pro Bundle: 3D print with always-on productivity", *ultimaker.com*, 2021. [Online].

[46] "FAQs | Multi3D", *Multi3D*, 2021. [Online].

[47] “Conductive PLA", *ProtoPlant, makers of Proto-pasta*, 2021. [Online]

[48] [22] "Price Per Gram Calculator - Calculator Academy", *Calculator Academy*, 2021. [Online].

[49] T. Reed, "Multimeter Measurements Explained", *Evaluationengineering.com*, 2021.

[50] "How to Measure Resistance with a Digital Multimeter", *Fluke.com*, 2021. [Online].

[51] "EVAL-AD5940ELCZ Evaluation Board | Analog Devices", *Analog.com*, 2021. [Online].

[52] T. Tezel, G. Atlıhan, V. Kovan and E. Topal, "Effect of Printing Orientation Angle of 3D Printed PLA Thin Beams on The Natural Frequency", 2019.

[53] "Ultimaker PLA material: Highly versatile, easy to print", *ultimaker.com*, 2021.

[54] &. 878B, "Model 879B, 40,000 Count Dual Display Handheld LCR Meters - B&K Precision", *Bkprecision.com*, 2021. [Online

APPENDIX A

MATLAB Code

```
%% Frequency Dielectric constant measurement
close all;
clc;
clear all;

% Define
A=0.0025;
E0=8.85418782 *10^(-12);
f_1=1000;
f_5=5000;
f_7_5=7500;
f_10=10000;

d_1_5=0.0015;
d_1_0=0.001;
d_0_5=0.0005;
d_0_25=0.00025;

%Define mg (magnitude)
mg_1_1_5=
mg_5_1_5=
mg_7_5_1_5=
mg_10_1_5=

mg_1_1_0=
mg_5_1_0=
mg_7_5_1_0=
mg_10_1_0=

mg_1_0_5=
mg_5_0_5=
mg_7_5_0_5=
mg_10_0_5=

mg_1_0_25=
mg_5_0_25=
mg_7_5_0_25=
mg_10_0_25=
```

```
mg_1_0_25=
mg_5_0_25=
mg_7_5_0_25=
mg_10_0_25=


%% 1kHz and 1.5 mm

C_1_1_5= (1/(2*pi*f_1*mg_1_1_5))

k_1_1_5=C_1_1_5*d_1_5/(E0*A)

%% 1kHz and 1.00 mm

C_1_1_0= (1/((2*pi)*f_1*mg_1_1_0))

k_1_1_0=((C_1_1_0*d_1_0)/(E0*A))

%% 1 kHz and 0.5 mm

C_1_0_5= (1/((2*pi)*f_1*mg_1_0_5))

k_1_0_5=((C_1_0_5*d_0_5)/(E0*A))

%% 1kHz and 0.25 mm

C_1_025= (1/((2*pi)*f_1*mg_1_0_25))

k_1_025=((C_1_025*d_0_25)/(E0*A))


%% 5kHz and 1.5mm Frequency Dielectric constant measurement

C_5_1_5= (1/((2*pi)*f_5*mg_5_1_5))

k_5_1_5=((C_5_1_5*d_1_5)/(E0*A))

%% 5kHz and 1.00 mm

C_5_1_0= (1/((2*pi)*f_5*mg_5_1_0))

k_5_1_0=((C_5_1_0*d_1_0)/(E0*A))

%% 5 kHz and 0.5mm
```

```
C_5_0_5= (1/((2*pi)*f_5*mg_5_0_5))

k_5_0_5=((C_5_0_5*d_0_5)/(E0*A))

%% 5kHz and 0.25mm

C_5_025= (1/((2*pi)*f_5*mg_5_0_25))

k_5_025=((C_5_025*d_0_25)/(E0*A))

%% 7.5kHz and 1.5mm Frequency Dielectric constant measurement

C_7_5_1_5= (1/((2*pi)*f_7_5*mg_7_5_1_5))

k_7_5_1_5=((C_7_5_1_5*d_1_5)/(E0*A))

%% 7.5kHz and 1.00 mm

C_7_5_1_0= (1/((2*pi)*f_7_5*mg_7_5_1_0))

k_7_5_1_0=((C_7_5_1_0*d_1_0)/(E0*A))

%% 7.5 kHz and 0.5mm

C_7_5_0_5= (1/((2*pi)*f_7_5*mg_7_5_0_5))

k_7_5_0_5=((C_7_5_0_5*d_0_5)/(E0*A))

%% 7.5kHz and 0.25mm

C_7_5_025= (1/((2*pi)*f_7_5*mg_7_5_0_25))

k_7_5_025=((C_7_5_025*d_0_25)/(E0*A))


%% 10kHz and 1.5mm

C_10_1_5= (1/((2*pi)*f_10*mg_10_1_5))

k_10_1_5=((C_10_1_5*d_1_5)/(E0*A))

%% 10kHz and 1.0mm

C_10_1_0= (1/((2*pi)*f_10*mg_10_1_0))
```

```
k_10_1_0=((C_10_1_0*d_1_0)/(E0*A))

%% 10kHz and 0.5mm

C_10_0_5= (1/((2*pi)*f_10*mg_10_0_5))

k_10_0_5=((C_10_0_5*d_0_5)/(E0*A))

%% 10kHz and 0.25mm

C_10_0_25= (1/((2*pi)*f_10*mg_10_0_25))

k_10_0_25=C_10_0_25*d_0_25/(E0*A)
```